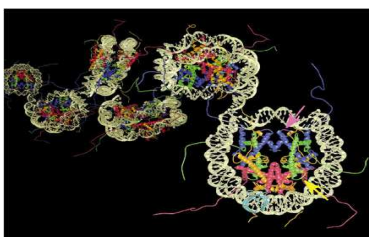




“Design, Synthesis and Biological Evaluation  
of Novel Small Molecules as Modulators of Epigenetic Targets”



**Tutor**  
**Prof. Antonello Mai**

**Coordinatore**  
**Prof. Marco Tripodi**

**Docente guida**  
**Prof. Antonello Mai**

**Dottorando**

**Maria Tardugno**

**Dottorato di Ricerca in Scienze Pasteuriane**

**XXIV CICLO**

---

*PhD course in Pasteurian Sciences, XXIV cycle, Rome, 29th February, 2012*

## Index

Index.....	I
Introduction .....	1
1. HDACs, the big family .....	3
1.1 HDAC inhibitors.....	5
1.2. A long lasting story.....	6
2. SIRTUINS, the “energy road”.....	11
2.1. SIRT1, a busy target.....	12
2.2. The “handy-enzyme” SIRT2 and the emergent SIRT3.....	13
2.3 SIRT modulators .....	14
2.3.1. SIRT activators.....	15
2.3.2. SIRT inhibitors.....	15
3. HDMs, the histone demethylases .....	16
3.1. LSD1 and LSD2.....	16
3.1.1. Biological role of LSD1: HOTAIR interaction .....	19
3.1.2. Biological role of LSD1: BLIMP-1 interaction.....	20
3.1.3. Biological role of LSD1: SNAIL-1 interaction .....	20
3.2. LSD1-2, inhibitors.....	22
4. New frontiers in Epigenetics .....	24
4.1. Introduction and biological activity of Rufomycin B.....	26
5. New cynamil containing HDAC inhibitors .....	28
5.1. Chemistry .....	30
5.2. Results and discussion.....	35
5.2.1. Enzyme Inhibitory Assays. Maize HD1-B and HD1-A Enzymes.....	35
5.2.2. Human Recombinant HDAC1 and HDAC4 Assays. ....	36
5.2.3. Molecular Modeling and Docking Studies.....	42
5.2.4. Effects on Acetylation Level of Histone (Histone H3) and Non-Histone ( $\alpha$ -Tubulin) Substrates. p21 Induction.....	46
5.2.5. Cell Cycle Analysis, Apoptosis Induction, Granulocytic.....	48
5.3. Materials and methods .....	52
5.3.1. Experimental section. ....	53
5.3.1.1. Chemistry. ....	53
5.3.1.1.1. <i>General Procedure for the Synthesis of Ethyl 3-(4-Acylaminophenyl)-2-propenoates (5a-n). Ethyl 3-[4-(2-Phenylbutyryl)aminophenyl]-2-propenoate (5c).</i> .....	53

5.3.1.1.2. General Procedure for the Synthesis of 3-(4-Acylaminophenyl)-2-propenoic Acids (6a-n). 3-[4-(2-Phenyl-4-pentenylamino)phenyl]-2-propenoic Acid (6f):.....	54
5.3.1.1.3. General Procedure for the Synthesis of the 3-(4-Acylaminophenyl)-N-hydroxy-2-propenamides (1a-n) and the 3-[4-(Arylalkylamino)phenyl]-N-hydroxy-2-propenamides (3a-o). 3-[4-(2,3-Diphenylpropionyl)aminophenyl]-N-hydroxy-2-propenamide (1h).....	54
5.3.1.1.4. General Procedure for the Synthesis of the N-(2-Aminophenyl)-3-(4-acylaminophenyl)-2-propenamides (2a-l) and the N-(2-Aminophenyl)-3-[4-(arylalkylamino)phenyl]acrylamide (4a-o). N-(2-Aminophenyl)-3-[4-(quinolin-2-ylmethylamino)phenyl]acrylamide (4n).....	55
5.3.1.1.5. General Procedure for the Synthesis of Ethyl 3-[4-(Arylmethylamino)phenyl]-2-propenoates (7a-o). Ethyl 3-[4-(Benzofuran-2-ylmethylamino)phenyl]-2-propenoate (7k).....	55
5.3.1.1.6. General Procedure for the Synthesis of 3-[4-(Arylalkylamino)phenyl]-2-propenoic Acids (8a-o). 3-[4-(3-Pyridylmethylamino)phenyl]-2-propenoic acid (8h).....	56
5.3.1.2. Enantiomer Separations.....	56
5.3.1.3. Homology Models, Molecular Modeling and Docking Studies.....	58
5.3.1.4. Biological assays.....	59
5.3.1.4.1. In Vitro Maize HD1-B and HD1-A Enzyme Inhibition.....	59
5.3.1.4.2. Human Recombinant HDAC1 and HDAC4 Assays).....	60
5.3.1.4.3. Cellular Assays. Cell Lines and Cultures.....	60
5.3.1.4.4. Histone H3 and $\alpha$ -Tubulin Acetylation in U937 Cells.....	61
5.3.1.4.5. Determination of p21WAF1/CIP1 Induction in U937 Cells.....	61
5.3.1.4.6. Cell Cycle Analysis on U937 Cells.....	61
5.3.1.4.7. FACS Analysis of Apoptosis on U937 Cells.....	61
5.3.1.4.8. Proliferation Assay on U937 Cells.....	61
5.3.1.4.9. Granulocytic Differentiation on U937 Cells.....	62
5.3.1.4.10. Granulocytic Differentiation on U937 Cells: Nitroblue Tetrazolium (NBT) assay.....	62
6. Study of 1,4-Dihydropyridine Structural Scaffold: Discovery of Novel Sirtuin Activators and Inhibitors.....	62

6.1. Chemistry .....	63
6.2. Results and Discussion.....	65
6.2.1. SIRT1, -2, and -3 Modulator Activity: Enzyme and Functional Assays. ....	65
6.2.2. Cell Cycle Analysis, Apoptosis Induction, Granulocytic differentiation in U937 cell line .....	68
6.2.3. Involvement in mitochondrial biogenesis. ....	68
6.3. Sirtuins: Possible direct function in mitochondrial biogenesis.....	72
6.4. Sirtuins and Calorie restriction.....	75
6.5. Experimental Section .....	76
6.5.1. Chemistry .....	76
6.5.1.1. <i>General Procedure for the Synthesis of 1-aryl-(or arylalkyl, or cycloalkyl)-diethyl-4-phenyl-1,4-dihydropyridine-3,5-dicarboxylate. Example: synthesis of 1-cyclopropyl-diethyl-4-phenyl-1,4-dihydropyridine-3,5-dicarboxylate (MC 2733).</i> .....	77
6.5.1.2. <i>General Procedure for the Synthesis of 1-Aryl-(or arylalkyl, or cycloalkyl)-4-phenyl-1,4-dihydropyridine-3,5-dicarboxylic Acids (2a-d). Example: 1-Phenethyl-4-phenyl-1,4-dihydropyridine-3,5-dicarboxylic acid (2d).</i> .....	77
6.5.1.3. <i>General Procedure for the Synthesis of 1-aryl-(or arylalkyl, or cycloalkyl)-4-phenyl-1,4-dihydropyridine-3,5-dicarboxamides. Example: synthesis of 1-phenyl-4-phenyl-1,4-dihydropyridine-3,5-dicarboxamide (MC 2744).</i> .....	78
6.5.2. Biological assays .....	78
6.5.2.1. SIRT Assay .....	78
6.5.2.2. Determination of $\alpha$ -Tubulin Specific Acetylation.....	80
6.5.2.3. Cell Cycle Analysis on U937 Cells.....	80
6.5.2.4. FACS Analysis of Apoptosis on U937 Cells.....	80
6.5.2.5. Granulocytic Differentiation on U937 Cells .....	80
6.5.2.6. $\beta$ -Galactosidase Assay.....	80
6.5.2.7. Mitochondrial Density in Murine C2C12 Myoblasts .....	81
6.5.2.8. Transcriptional Activity of mTFA-Promoter in Murine C2C12 Myoblasts .....	81
6.5.2.9. Nitric Oxide synthase activation assay.....	82
7. Biochemical, Structural, and Biological Evaluation of Tranylcypromine Derivatives as Inhibitors of Histone Demethylases LSD1 and LSD2.....	82
7.1. Chemistry .....	83

7.2. Preparation and absolute configuration assignment of the enantiomers of Br-cPCPA HCl .....	84
7.3. Preparation and absolute configuration assignment of the enantiomers of cPCPA HCl .....	86
7.4. Preparation and absolute configuration assignment of the enantiomers of Br-tPCPA HCl.....	88
7.5. Preparation and absolute configuration assignment of the enantiomers of tPCPA HCl.....	89
7.6. Experimental HPLC enantioseparation .....	91
7.7. Small molecule X-ray structural analysis.....	92
7.8. Synthesis of further tranlycypromine derivatives.....	95
7.9. Results and discussion.....	96
7.9.1. Cis versus Trans Diastereoselectivity of Inhibition.....	97
7.9.2. Toward Selective Inhibitors .....	97
7.9.3. Biological Evaluation of the compound MC2580 .....	101
7.10. Material and methods .....	105
7.10.1. <i>General Procedure for the Synthesis of trans and cis Ethyl 2-Phenylcyclopropylcarboxylates (2a-c and 3a-c). Example: trans and cis Ethyl 2-(4-Nitrophenyl) cyclopropylcarboxylates (2c and 3c)</i> .....	105
7.10.2. <i>General Procedure for the Synthesis of trans and cis 2-Phenylcyclopropylcarboxylic Acids (4a-c and 5a-c). Example: trans 2-(4-Nitrophenyl)cyclopropylcarboxylic Acid (4c)</i> .....	106
7.10.3. <i>General Procedure for the Synthesis of trans and cis tert-Butyl 2-(4-Nitrophenyl)cyclopropyl Carbamates (6a-c and 7a-c). Example: trans tert-Butyl 2-(4-Nitrophenyl)cyclopropyl Carbamate (6c)</i> .....	106
7.10.4. <i>General Procedure for the Synthesis of trans and cis tert-Butyl 2-(4-Aminophenyl)cyclopropyl Carbamates (8 and 9) and of tert-Butyl 1-(4-Aminophenyl)propan-2-yl Carbamate (16). Example: trans tert-Butyl 2-(4-Aminophenyl)cyclopropyl Carbamate (8) and tert-Butyl 1-(4-Aminophenyl)propan-2-yl Carbamate (16)</i> .....	107
7.10.5. <i>General Procedure for the Synthesis of trans tert-butyl 2-(4-aryloyl (or arylacetyl or benzyloxycarbonyl)aminophenyl)cyclopropyl carbamates (10a-h). Example: trans tert-butyl 2-(4-benzoylamino phenyl)cyclopropyl carbamate (10b)</i> .....	108
7.10.6. <i>General Procedure for the Synthesis of trans tert-butyl 2-[4-(N-benzyloxycarbonyl aminoacyl)aminophenyl]cyclopropyl</i>	

carbamates (11a-m, 17, and 19) and of <i>cis tert-butyl 2-[4-(N-benzyloxycarbonylphenylalanyl)aminophenyl]cyclopropyl carbamate (12)</i> . Example: <i>trans tert-butyl 2-[4-(N-benzyloxycarbonylphenylalanyl) phenyl]cyclopropyl carbamate (11e)</i> .....	108
7.10.7. General Procedure for the Synthesis of ( $\pm$ )- <i>tPCPA</i> , ( $\pm$ )- <i>cPCPA</i> , ( $\pm$ )- <i>Br-tPCPA</i> , and ( $\pm$ )- <i>Br-cPCPA</i> hydrochlorides, of the <i>trans 2-(4-aryloyl (or arylacetyl or benzyloxycarbonyl)aminophenyl)cyclopropylamines hydrochlorides (13a-h)</i> , of the <i>trans 4-(N-benzyloxycarbonylaminoacyl)aminophenyl)cyclopropylamines hydrochlorides (14a-m, 18, and 20)</i> , and of <i>cis tert-butyl 2-[4-(N-benzyloxycarbonylphenylalanyl) aminophenyl]cyclopropylamine hydrochloride (15)</i> . Example: <i>trans 2-[4-(N-benzyloxycarbonyltryptophanyl)aminophenyl]cyclopropylamine hydrochloride (14l)</i> .....	109
7.10.8. Synthesis of methyl 8-(4-(2- <i>tert-butoxycarbonylamino</i> cyclopropyl)phenylamino)-8-oxooctanoate (21) .....	110
7.10.9. Synthesis of 8-(4-(2- <i>tert-butoxycarbonylamino</i> cyclopropyl)phenylamino)-8-oxooctanoic acid (22) .....	111
7.10.10. Synthesis of <i>N<sup>1</sup>-(4-(2-aminocyclopropyl)phenyl)-N<sup>8</sup>-hydroxyoctanediamide hydrochloride (23)</i> .....	111
7.11. Design and synthesis of new SNAG-like peptide as LSD1 inhibitors .....	117
7.11.1. Materials and methods .....	120
7.11.1.1. Peptide synthesis .....	120
8. Rufomucin B, an old peptide for a new epigenetic challenge .....	123
8.1. Materials and methods .....	123
8.1.1 Chemistry .....	124
8.1.1.1. Procedure for the synthesis of Fmoc-L- <i>N</i> -methyl-leucine .....	124
8.1.1.2. Procedure for the synthesis of Fmoc-L-3-nitrotyrosine.....	126
8.1.1.3. Procedure for the synthesis of Fmoc- L-2-amino-4-hexenoic acid ....	127
8.1.1.4. Procedure for the synthesis of Fmoc-L- <i>N</i> -(2-methyl-3-buten-2-yl)-tryptophan .....	133
8.1.1.5. Procedure for the synthesis of Rufomycin B.....	136
9. Future perspective .....	138
10. Acknowledge.....	138

References ..... 140



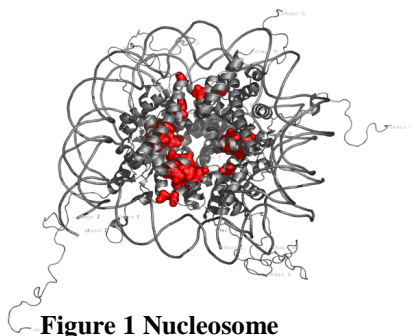
“Der Mensch ist was er isst”

“The man is what he eats”

Probably Ludwig Feuerbach didn't know how much right was when in 1862 he wrote this.

The Epigenetics is a rapidly growing research field that investigates heritable alterations in gene expression caused by mechanisms other than changes in DNA sequence. Many scientists are working on it in order to find a good definition, at the moment the proposed one reads: “an epigenetic trait is a stably inherited phenotype resulting from changes in a chromosome without alterations in the DNA sequence.” At the present we know that DNA isn't everything, environmental factors can alter the way our genes are expressed. These changes can make even identical twins different, and are sometimes passed on to the offspring. Once nurture seemed clearly distinct from nature. Now it appears that our diets and lifestyles can change the expression of our genes influencing a network of chemical switches within our cells collectively known as the epigenome. This new understanding may lead us to potent new medical therapies <sup>1</sup>.

## Introduction



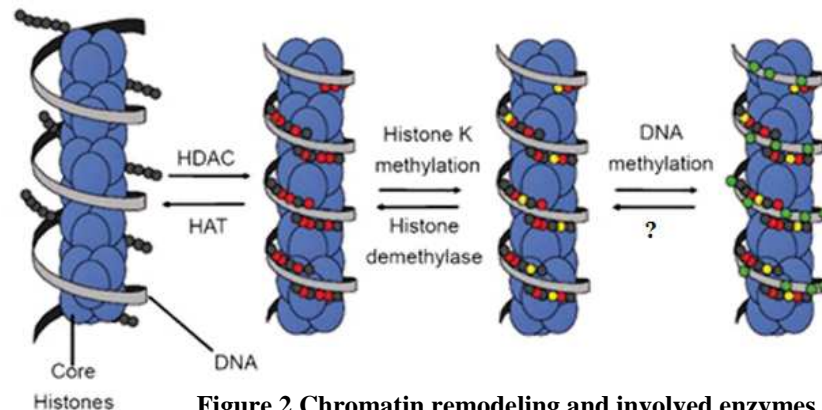
**Figure 1 Nucleosome**

The chromatin remodeling is one of the most important epigenetic regulation of gene expression. Chromatin is an extremely complex structure that compacts eukaryotic DNA in the nucleus. It consists of repeating spherical particles termed nucleosomes. Nucleosomes are formed by the wrapping of 147 bp of DNA in 1.7 left-handed superhelical turns around a highly basic, evolutionary conserved histonic

octamer, consisting of 2 copies each of the proteins named histones H2A, H2B, H3, and H4<sup>2</sup>. Nucleosomes are connected by short stretches of linker DNA resulting in a fiber with a diameter of ~10 nm that has a beads-on-a-string-like appearance. Chromatin organization is regulated on various levels and by a multitude of diverse proteins that can act on both the DNA and histones.

The H3 and H4 histones have long tails protruding from the nucleosome that can be modified post-translationally by acetylation, phosphorylation, ubiquitination, and methylation, affecting their charge and function. Acetylation of the  $\epsilon$ -amino groups of specific histone lysines is catalyzed by histone acetyltransferases (HATs) and correlates with an open chromatin structure and gene activation. Histone deacetylases (HDACs) catalyze the hydrolytic removal of acetyl groups from histone lysine residues and correlates with chromatin condensation and transcriptional repression. Methylation is made by histone-lysine N-methyltransferase and histone-arginine N-methyltransferase (HMTs) that catalyze the transfer of one to three methyl groups from the cofactor S-Adenosyl methionine to lysine and arginine residue of histone proteins. Levels of lysine methylation are known to change during processes such as transcriptional regulation. At the present we know that two different enzymatic

mechanism of lysine demethylation are possible, amine oxidation by LSD1 and LSD2<sup>3</sup> and hydroxylation by JmjC-domain containing proteins<sup>4</sup> (HDMs). In most cases, these histone-



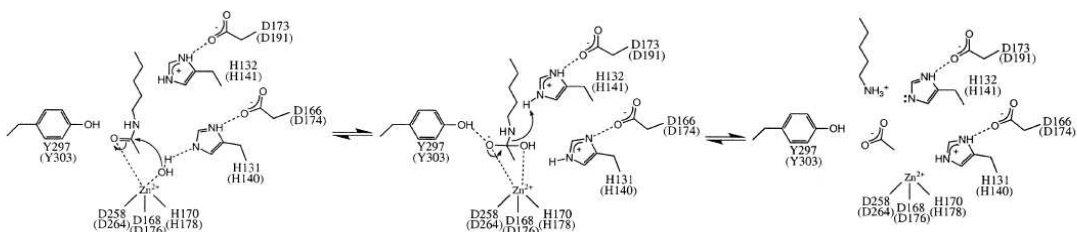
**Figure 2 Chromatin remodeling and involved enzymes**

modifying enzymes are present in multisubunit protein complexes, in which the other components are thought to regulate enzyme activities, modulate substrate recognition, recruit other cofactors, or carry out other undefined functions <sup>5</sup>.

## 1. HDACs, the big family

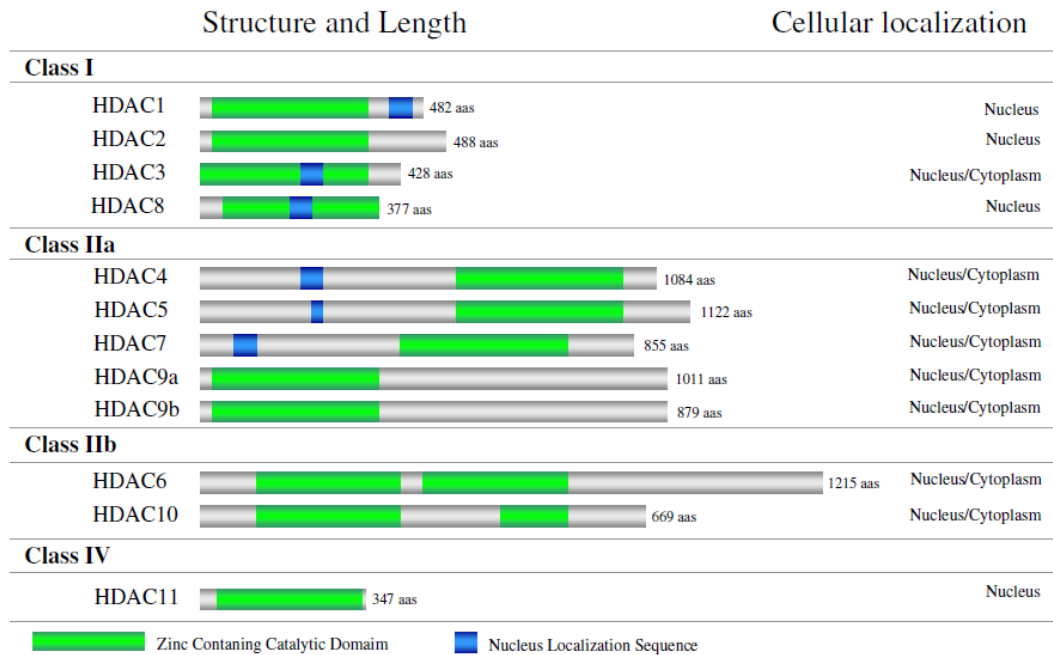
Histone deacetylases (HDACs) are enzymes involved in remodelling of chromatin by deacetylating the histonic lysine residues, and in the regulation of mRNA stability, protein localization and degradation, and protein–protein and protein–DNA interactions by post-translational modifications of non-histone proteins <sup>6</sup>. An aberrant activity of HDACs has been documented in several types of disorders as cancer <sup>7, 8</sup>, immune and inflammatory diseases <sup>9</sup>, neurological <sup>10</sup> and metabolic disorders <sup>11</sup> and many others. Because of this, HDACs have emerged as an attractive therapeutic target.

Nineteen HDAC enzymes have been identified in humans and are categorized into four classes, based on sequence similarity and homology to yeast deacetylases. Class I enzymes, HDAC1, HDAC2,



**Figure 3** The proposed catalytic mechanism for the deacetylation of acetylated lysine. HDLP active-site residues and their proposed HDAC1 counterparts (in parenthesis) are labelled

HDAC3, and HDAC8, are highly homologous to the yeast HDAC RPD3<sup>12</sup> protein, while class II enzymes, HDAC4, HDAC5, HDAC7, HDAC9a, HDAC9b (class IIa) and HDAC6 and HDAC10



**Figure 4.** Classification of classes I, II, and IV HDACs by structure and cellular localization. *BMC Cancer* 2008, 8:243

(class IIb), are homologous to the yeast HDA1 protein<sup>13</sup>. HDAC11 is phylogenetically different from both class I and class II enzymes and is therefore classified separately as class IV.

Class III enzymes, SIRT1-7, are an evolutionarily distinct family dependent on nicotinamide adenine dinucleotide (NAD<sup>+</sup>) for function and are referred to as ‘sirtuins’<sup>14</sup>.

Classes I, II, and IV members are well-conserved zinc-dependent enzymes. Notably, class I and II enzymes differ in their tissue expression profiles, with class I members ubiquitously expressed, while class II enzymes are differentially expressed, with increased levels detectable in the heart, brain, lung, thymus, muscle, liver, spleen, and kidney. Differences in tissue distribution suggest differing cellular

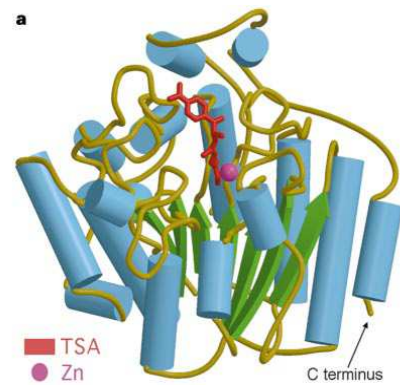
roles for the twelve zinc-dependent HDACs; although their exact functions are not yet elucidated, they are likely to demonstrate considerable overlap. Analysis of available data suggests that class I HDACs regulate cell cycle progression<sup>15</sup>, while class II HDACs are involved in differentiation, development, and osteogenesis<sup>16</sup>. Recent work has now linked the only class IV HDAC (HDAC11) to a role in immune function regulation<sup>17</sup>. HDAC6 is unique among the eleven Zn dependent HDACs in having two catalytic sites and an ubiquitin binding site. Specific substrates of HDAC6 have been identified, including  $\alpha$ -tubulin, cortacin, transmembrane proteins, such as, IFN $\alpha$ R, HSP90 and other chaperone proteins and peroxiredoxins. The ubiquitin site toward the c-terminal end of HDAC6 plays a critical role in aggresome formation in the pathway of proteolysis of misfolded proteins<sup>18</sup>.

### 1.1. HDAC inhibitors

The HDAC inhibitors (HDACi) are a group of new therapeutic agents which have a potential role in regulation of gene expression and induction of cell death, cell cycle arrest, and differentiation by altering the acetylation status of histone and non-histone proteins<sup>19</sup>. In clinical trials, HDAC inhibitors have demonstrated promising antitumour activity as monotherapy in cutaneous T-cell lymphoma<sup>20</sup> and other haematological malignancies<sup>21</sup>. In solid tumours, several HDAC inhibitors have been shown to be efficacious as single agents<sup>22, 23, 24</sup>; however, results of most clinical trials were in favour of using HDAC inhibitors either prior to the initiation of chemotherapy or in combination with other treatments<sup>25, 26, 27</sup>. Two pan-HDAC inhibitors (HDACi's), Vorinostat (SAHA) and Istodax (romidepsin) approved as drugs for cutaneous T-cell lymphoma (CTCL) while several HDACIs are currently under clinical investigation.

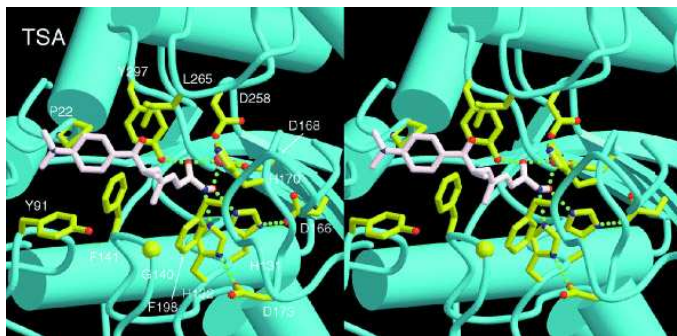
## 1.2. A long lasting story

In 1999 M.S.Finning *et al.* got the crystal structures of HDLP, the *A. aeolicus* histone deacetylase-like protein (HDLP) with 35.2% identity to human HDAC1, of the HDLP+Zn<sup>2+</sup>+TSA and HDLP + Zn<sup>2+</sup> SAHA complexes. In this way they provided a framework for understanding the catalytic activity and inhibition of the histone deacetylase family, and forming a basis for the further development of HDAC inhibitors as antitumour agents core. The X-ray structure, together with the resolution of HDLP/TSA and HDLP/SAHA complexes, have revealed the active site of the enzyme but have also elucidated the mechanism of HDAC inhibition by hydroxamic-acid based inhibitors <sup>28</sup> HDLP has a single domain structure related to the open  $\alpha/\beta$  class of folds. It



**Figure 5** HDLP±Zn<sup>2+</sup>±TSA complex. Figure prepared with the programs MOLSCRIPT and RASTER3D

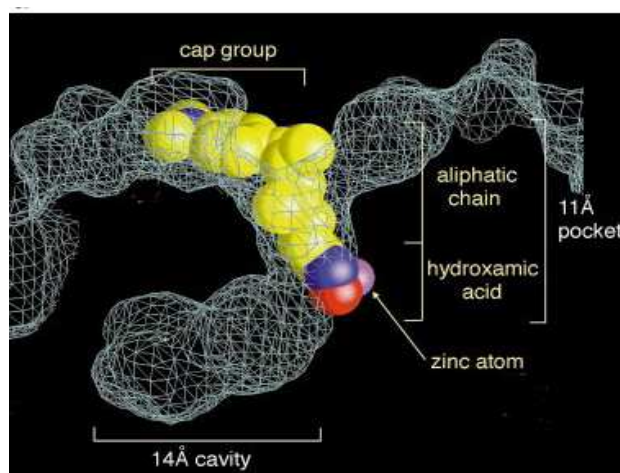
contains a central eight-stranded parallel  $\beta$  sheet, with four  $\alpha$  helices packed on either face. Eight additional  $\alpha$  helices and large loops in the  $\beta$  sheet further extend the structure and result in the



**Figure 6** HDLP residues that interact with TSA in the tubular pocket.

formation of a deep, narrow pocket with an adjacent internal cavity. Concisely, the catalytic core has an  $\alpha/\beta$  motif and the active site consists of a tubular pocket with a zinc-binding site and two Asp-His charge-relay systems (His 131/Asp

166 and His132/Asp173) that facilitate the acetyl cleavage of substrate by weakening the amide bond. The zinc cation required for the enzymatic activity is positioned near the bottom of the pocket and is coordinated by several histidine and aspartate residues too. Hydrophobic residues surround the channel leading to the bottom of the pocket, which is presumably where the aliphatic chain of the acetyl-lysine residue is nestled. TSA and SAHA act as substrate mimics; the aliphatic chain and hydroxamic acid of each inhibitor are analogous to the lysine side chain and acetyl group of the substrate, respectively. These inhibitors bind inside the pocket by inserting the aliphatic chain into the tube, making contact with the residues at the rim, walls and at the bottom of the pocket. Specifically, TSA contains a cap group, an aliphatic chain and a terminal hydroxamic acid functional group. The hydroxamic acid coordinates the zinc cation in a bidentate fashion (through CO and OH groups) and also contacts active-site residues (forming two hydrogen-bonds between its NH and OH groups and the two charge-relay systems His131/Asp166 and His132/Asp173, and another one between its CO and the Tyr297 hydroxyl group). Moreover, hydroxamic acid function replaces the zinc-bound water molecule of the active structure with its OH group<sup>29</sup>. Fitting snugly into the channel, the aliphatic chain makes several Van der Waals contacts with the channel residues. The dimethylaminophenyl group acts as a

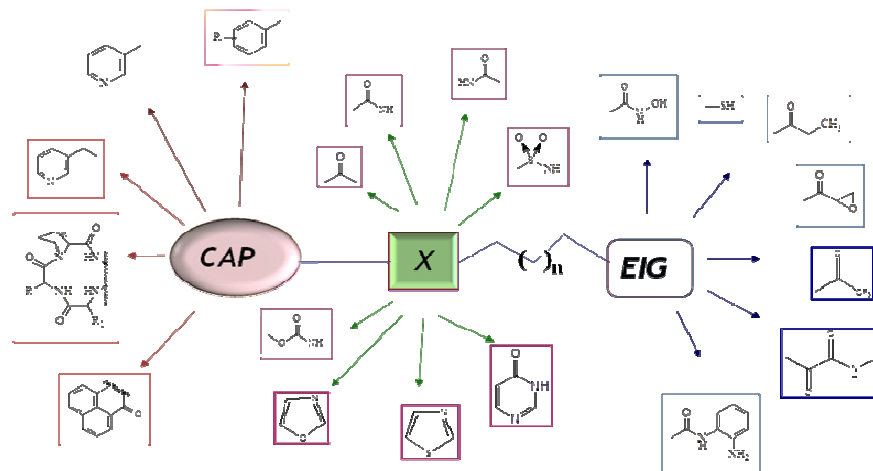


**Figure 7** Space-filling representation of TSA in the active-site pocket. The hydroxamic acid group, most of the aliphatic chain and part of the dimethylamino-phenyl group of TSA are buried (60% of TSA's surface area). The internal cavity has a volume of  $144 \text{ \AA}^3$ .

cap to pack the inhibitor at the rim of the tubular pocket-like active site. Indeed, this cap group contacts the residues of Pro22 and Tyr91 on the rim of the pocket and possibly mimics the amino acids adjacent to the acetylated lysine residue in the histone. The binding of TSA causes a conformational change in a tyrosine residue on this rim (Tyr91) and thereby allows tighter packing of the cap group. It has been postulated that this insertion and binding in the catalytic site blocks substrate access to the active zinc ion and, thereby, inhibits the deacetylase activity. Conservation of the amino acid sequences of the loops that form the active site pocket among HDLP and class I and II mammalian HDACs strongly suggests that the catalytic reaction and mechanism of inhibition by TSA and SAHA are the same in HDACs as HDLP<sup>29</sup>.

The catalytic domains of the known class I and II human HDACs are very well conserved, but there are certain

differences that may allow for the production of specific inhibitors. Most of the residues that are seen in the HDLP structure to interact directly with

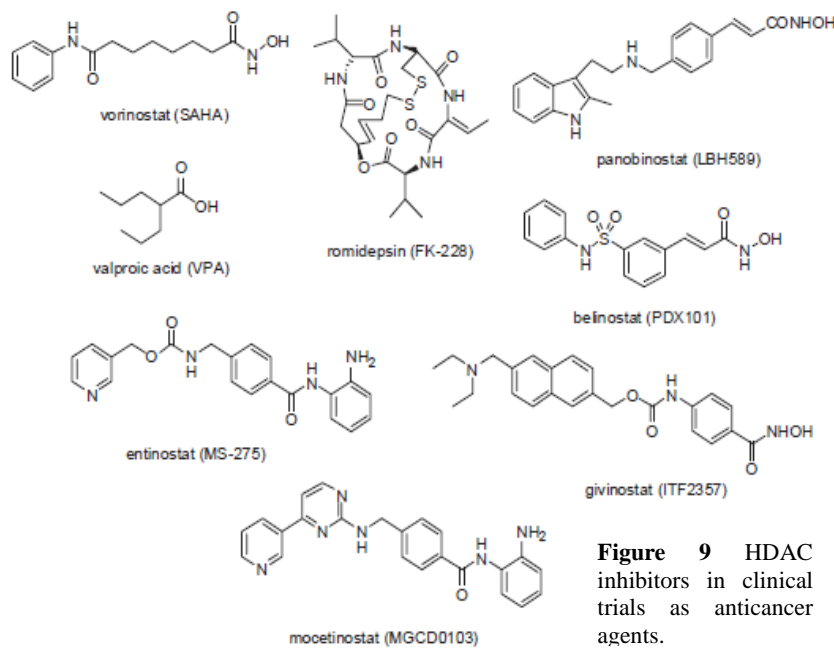


**Figure 8** Known pharmacophoric model for HDAC inhibitors. EIG is the Zn binding group, the most useful groups are hydroxamic acid, trifluoromethyl ketone and 2-aminoanilides. X stays for electronegative group able to do H bonding, between X and EIG it needs to have a CU, a hydrophobic unit of connection. CAP must be a large hydrophobic group, such as substituted benzene rings, pyridine, pyridylmethyl groups.



TSA are completely conserved among all of the HDACs, but there is less conservation in the surrounding residues, with significant differences apparent between the class I and class II HDACs<sup>30</sup>. Notably, there is a striking divergence in the region of Tyr91 of HDLP, and this tyrosine residue itself is very poorly conserved among the human HDACs. This is particularly interesting in that Tyr91 is positioned on the rim of the channel and interacts directly with the cap group of TSA, and it is the only residue that shifts its conformation upon TSA binding<sup>29</sup>. Thus, the considerably diversity in the region of the protein suggests that it would be possible to develop more potent and/or specific inhibitors by altering the structure of this cap group.

From the TSA/HDLP complex data, it has been possible to elaborate a structural model (common



pharmacophore) for class I/II HDAC inhibition.

This pharmacophore (figure 8) consists of a metal binding domain, which interacts with the active site, a linker domain, which occupies the channel, and

**Figure 9** HDAC inhibitors in clinical trials as anticancer agents.

a surface recognition domain, which interacts with residues on the rim of the active site.

In all known natural or synthetic inhibitors it is possible to see an extremely variable cap group. This moiety contacts residues on the rim of the catalytic pocket and is generally connected to an electronegative group (connection unit, CU) that is able to interact by hydrogen bond with other residues. Such CU portion is bound to an hydrocarbon linker interacting with the channel residues of the active site of the enzyme and finishing with the enzyme inhibiting group (EIG), that in many cases chelate the zinc cation near the bottom of the catalytic pocket. The cap groups can be, for example, represented by substituted benzene rings, pyridine, pyridylmethyl groups, a portion of tricyclic systems or of cyclic tetrapeptides. The electronegative group is generally a ketone, an amide, a reverse amide, a carbamate, or a sulfonamide. The linker is a saturated or unsaturated aliphatic chain, which mimics that of the lysine substrate, with an optimal length of 4-6 carbon residues. In some cases, it is possible to find an aromatic or heteroaromatic ring inserted into the hydrocarbon chain.

To date, the most useful EIG is the hydroxamic acid moiety but also ethyl ketone, trifluoromethyl ketone,  $\alpha$ -ketoamide, 2-aminoanilide, thiol and its acetyl derivative (which *in vivo* is rapidly hydrolyzed) are effectively able to chelate the zinc ion.

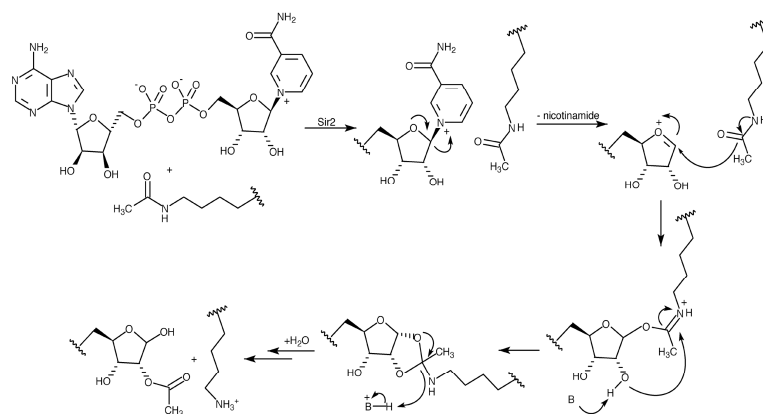
The epoxyketone and epoxy groups of some natural inhibitors seem to react irreversibly with some nucleophilic residues of the catalytic pocket of the HDAC enzymes, but the ketone group can also interact in its hydrate form as ligand with the metal ion. In the last ten years, a number of HDAC inhibitors have been reported as useful tools for the study of function of chromatin acetylation and deacetylation, and gene expression. These compounds can be natural or synthetic.

Since the discovery that the antileukemia properties of trichostatin A (TSA) are due to inhibition of HDAC enzymes, a large number of structurally different HDACi have been reported as novel antiproliferative and cytodifferentiating agents. In addition to vorinostat and romidepsin, valproic

acid (VPA), panobinostat (LBH589), belinostat (PDX101), givinostat (ITF2357), entinostat (MS-275), and mocetinostat (MGCD0103) (Figure 9) are into Phase II/III clinical trials for the therapy of hematological disorders as well as solid tumors<sup>31</sup>.

## 2. SIRTUINS, the “energy road”

Sirtuins (SIRT1–7) are the mammalian homologues of the silent information regulator 2 (Sir2) first



**Figure 10.** Proposed mechanism for sirtuin deacetylation

discovered in *Saccharomyces cerevisiae* as an NAD<sup>+</sup>-dependent histone deacetylase (HDAC). They are classified as class III HDACs: they require NAD<sup>+</sup> as a cofactor to exert their biological function. They contain an evolutionarily conserved core domain,

which is essential for their activity as NAD<sup>+</sup>-dependent deacetylases or ADP-ribosyltransferases<sup>32, 33</sup>. Sirtuin biology is complex, and sirtuins are widely expressed in normal tissues<sup>34</sup>. They are involved in a myriad of cellular and tissue functions, such as regulating oxidative stress, repairing DNA, increasing genomic stability, and affecting cell survival, apoptosis, development, metabolism, aging and longevity<sup>35, 36</sup>. Some sirtuins are located in different cellular compartments. Those in the same compartment, such as the mitochondrial SIRT3, 4, and 5, have different sequences and thus

unique and diverse cellular functions and can interact with different targets <sup>36</sup>.

Sirtuins have gained considerable attention for their impact on mammalian physiology, since they may provide novel targets for treating of many diseases.

## 2.1. SIRT1, a busy target

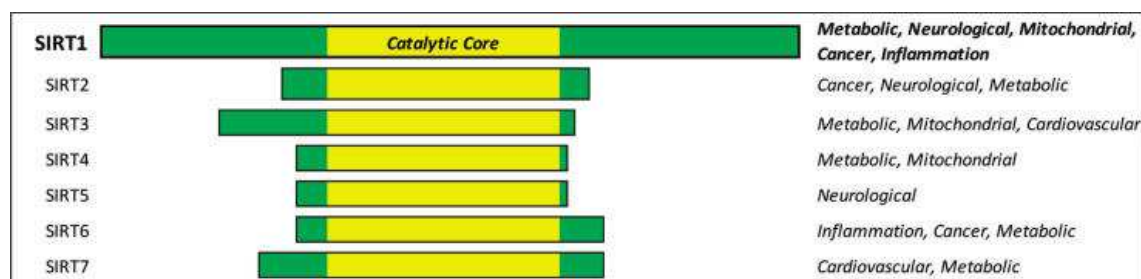
Human SIRT1 is implicated to play a role in a number of age-related human diseases and biological functions including cell survival, apoptosis, stress resistance, fat storage, insulin production, glucose homeostasis, and lipid homeostasis through direct deacetylation or regulation of its many known *in vivo* targets including p53, Ku70/Bax, FOXO, PPAR $\gamma$ , PGC1 $\alpha$ , UCP2, LXR, and NF $\kappa$ B <sup>37,38</sup>.

As an NAD<sup>+</sup>-dependent enzyme, SIRT1 regulates gene expression programs in response to cellular metabolic status, thereby coordinating metabolic adaptation of the whole organism. Several important

**Table 1.** Diversity of mammalian sirtuins

Sirtuin	Activity	Location	Interactions	Biology
SIRT1	Deacetylase	Nucleus	FOXO, PGC-1 $\alpha$	Cell survival/metabolism
SIRT2	Deacetylase	Cytosol	Tubulin, H4	Cell cycle
SIRT3	Deacetylase	Mitochondria	AceCS2	Thermogenesis/metabolism
SIRT4	ADP-ribosyl-transferase	Mitochondria	GDH	Insulin secretion/metabolism
SIRT5	Deacetylase	Mitochondria	?	?
SIRT6	ADP-ribosyl-transferase	Nucleus	DNA Pol $\beta$	DNA repair
SIRT7	?	Nucleolus	Pol I	rDNA transcription

Genes Dev. 2006 20: 2913-2921 1



Journal of Medicinal Chemistry, 2011, Vol. 54, No. 2

mechanisms have emerged for SIRT1-dependent regulation of transcription<sup>39</sup>.

SIRT1 has recently been shown to attenuate amyloidogenic processing of amyloid- $\beta$  protein precursor (APP) in cell culture studies in vitro and in transgenic mouse models of Alzheimer's disease by increasing  $\alpha$ -secretase production and activity through activation of the  $\alpha$ -secretase gene ADAM10. Because  $\alpha$ -secretase is the enzyme responsible for the non-amyloidogenic cleavage of APP, upregulation of  $\alpha$ -secretase shifts APP processing to reduce the pathological accumulation of the presumptive toxic A $\beta$  species that results from  $\beta$ -secretase and  $\gamma$ -secretase activity. Therapeutic upregulation of SIRT1 might provide opportunities for the amelioration of Alzheimer's-disease-type neuropathology through inhibition of amyloidogenesis<sup>40</sup>.

In vasculature of rodent models, SIRT1 mediates vasodilatation via eNOS-derived nitric oxide (NO) and scavenging reactive oxygen species (ROS). Recent studies demonstrated further protective roles of SIRT1 in vascular biology and atherosclerosis.

In endothelial cells and macrophages, SIRT1 has anti-inflammatory functions by downregulating the expression of various pro-inflammatory cytokines by interfering with the NF- $\kappa$ B signaling pathway<sup>41</sup>.

## 2.2. The “handy-enzyme” SIRT2 and the emergent SIRT3

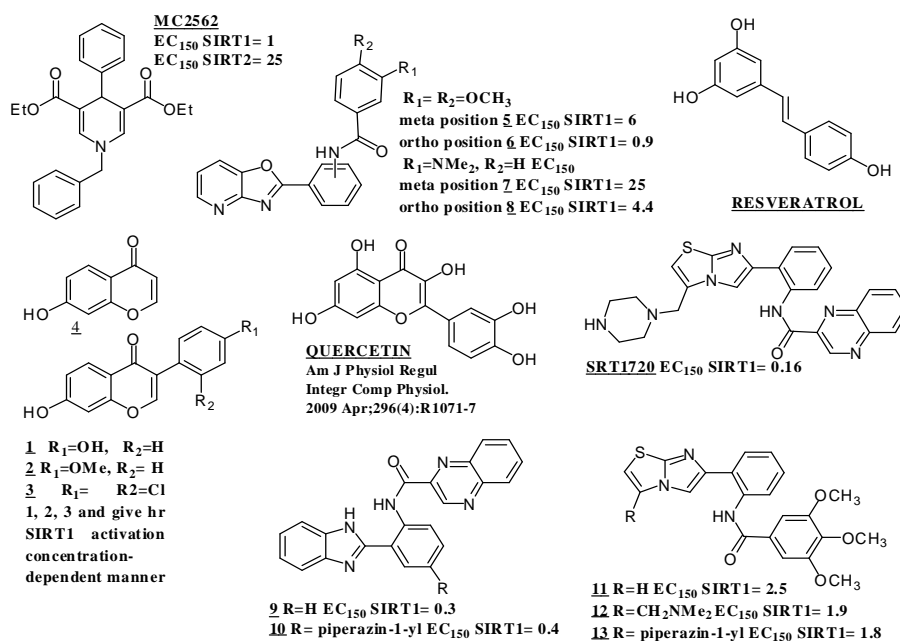
SIRT2 is involved in multiple biological functions, including affecting cell mitosis, cell motility and oligodendrocyte differentiation<sup>42, 43, 44, 45</sup>. There are also studies suggesting that SIRT2 may play either detrimental or beneficial roles on cell survival. Several studies have suggested that SIRT2 activation can reduce cell survival under certain conditions. For example, SIRT2 activation induces increased expression of Bid thus leading to apoptosis<sup>46</sup>; and SIRT2 inhibition reduces  $\alpha$ -Synuclein-induced neurotoxicity in cellular and *Drosophila* models of Parkinson's disease<sup>47</sup>. However, SIRT2 may play beneficial roles under certain conditions.

The effect of SIRT2 on FOXO3a could produce cytoprotective effects by inducing increased expression of antioxidant enzymes such as Mn-SOD<sup>46</sup>, and SIRT2 reductions have been shown to induce cell apoptosis by affecting the levels of p53<sup>48</sup>. SIRT2 has also been shown to be severely reduced in a number of human brain tumor cell lines, which implicates that the absence of SIRT2 may mediate cellular transformation and development of cellular malignancy<sup>49,50</sup>.

SIRT3 was identified as a stress responsive deacetylase recently shown to play a role in protecting cells under stress conditions<sup>51</sup>.

### 2.3. SIRT modulators

Several groups have published on SIRT's inhibitors and activators. Such agents could offer important



clues to the specific role of each isoform in biological and disease mechanisms. While the preponderance of genetic data indicates that increasing SIRT's levels

Figure 11. Known SIRT activators *J. Med. Chem.* 2011, 54, 417–432

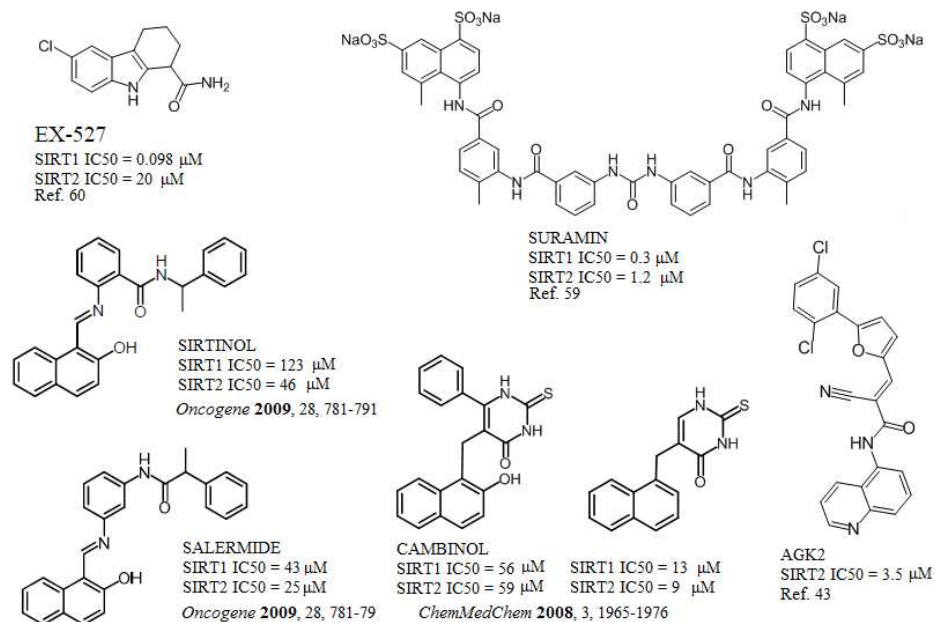
or their activity has beneficial physiological effects, reports are sometimes conflicting.

### 2.3.1 SIRT activators

Resveratrol is a natural compound studied in 2003<sup>52</sup> as first sirtuin activator. In the last years other sirtuin activators are been reported<sup>53, 54, 55</sup>.

### 2.3.2 SIRT inhibitors

Sirtuins may play a critical role in tumor initiation, progression, and drug resistance as well, by



**Figure 12.** Known SIRT inhibitors

blocking  
senescence and  
apoptosis,  
and promoting  
cell growth  
and angiogenesis.  
SIRT inhibitors  
have been shown  
promising

g anticancer effects in animal models of cancer <sup>56</sup>.

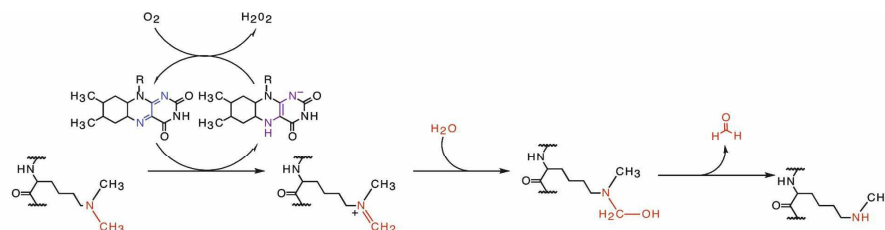
A large number of them have been identified such as sirtinol <sup>57</sup>, splitomycin <sup>58</sup>, cambinol <sup>59</sup>, tenovin <sup>60</sup>, Ro-318220 <sup>61</sup>, surfactin <sup>62</sup>, suramin <sup>63</sup>, the potent SIRT1 inhibitor indole EX527 <sup>64</sup> analogs and the SIRT2 inhibitor AGK2 <sup>47</sup>.

### 3. HDMs, the histone demethylases

Histone methylation plays a very special role in specifying the various chromatin states. The recent discovery of histone demethylases, which represent a large family of enzymes often containing histone modification binding modules, sheds new light on cross-talk mechanisms involving methylated residues. Studies exploring the histone demethylases JmjC (Jumonji C domain)-containing proteins <sup>65</sup>, and histone lysine demethylases FAD dependent LSD1-2 <sup>66, 67</sup>, primarily identified their enzymatic activity at the promoters of specific target genes and in general increased the knowledge about the several pathways where they are involved <sup>68, 69, 70</sup>.

#### 3.1 LSD1 and LSD2

LSD1 acts on mono- and dimethylated H3K4 through a flavin-dependent mechanism (Figure 13) according to the following reaction:



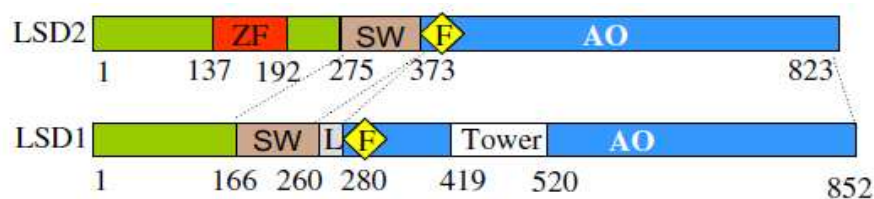
**Figure 13.** LSD1-2 enzymatic mechanism (Genes Dev. 2008 22: 1115-1140)



H3K4 methylation is a gene activation marker<sup>71</sup>, and LSD1 was originally identified as a component of transcriptional repressor complexes<sup>72, 73</sup>. LSD1 is typically associated with a transcriptional corepressor protein (CoREST) and histone deacetylase (HDAC) 1 or 2, forming a stable core subcomplex recruited by many chromatin remodeling multiprotein complexes<sup>72, 74</sup>. However, LSD1 is also involved in some gene activation processes, thus highlighting its multifaceted function in chromatin regulation<sup>75, 76</sup>. It participates in several growth-promoting pathways, and its levels are upregulated in certain high-risk tumors<sup>77, 78</sup>. The potential link between cancer and LSD1 activity is underpinned by the fact that loss of H3K4 methylation and enrichment of H3K9 methylation are associated with several types of tumors<sup>79</sup>.

Recently Mattevi *et al.* reported the discovering of a second mammalian flavin-dependent histone demethylase, named LSD2<sup>67</sup>. The new demethylase is strictly specific for mono- and dimethylated Lys4 of histone H3, recognizes a long stretch of the H3 N-terminal tail, senses the presence of additional epigenetic marks on the histone substrate, and is covalently inhibited by tranylcypromine. As opposed to LSD1, LSD2 does not form a biochemically stable complex with the C-terminal domain of the corepressor protein CoREST. Furthermore, LSD2 contains a CW-type zinc finger motif with potential zinc-binding sites that are not present in LSD1.

The functions and mechanisms of several LSD1/KDM1a family histone demethylases have been



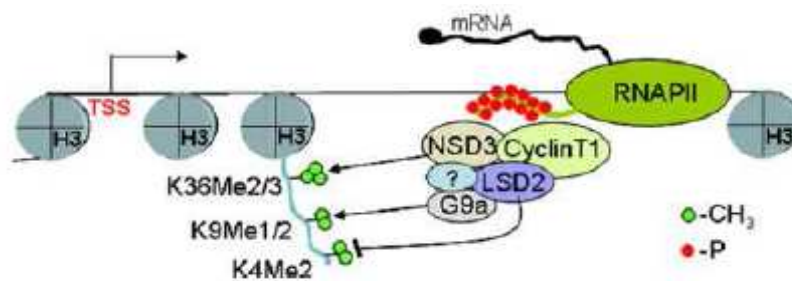
**Figure 14.** Schematic representations of LSD2 and LSD1. ZF, zinc finger domain; SW, SWIRM domain; AO, amine oxidase domain; F, FAD-binding motif; L, linker<sup>80</sup>.

intensively  
studied in  
multiple  
model  
organisms,  
including  
human,

mouse, *Drosophila*, *C. elegans*, and *S. pombe*. Yet our knowledge of the precise roles of LSD1 family members remains mostly limited to promoter association and regulation. Specifically, one key function of LSD1 is balancing promoter H3K4/H3K9 methylation for activation or repression of LSD1 target genes.

LSD2/KDM1b/AOF1, the only mammalian homolog of LSD1, specifically associates with the coding region of its target genes. LSD2 shares similar substrate specificity with LSD1 and demethylates mono- and dimethylated H3K4. Instead of functioning as a corepressor, LSD2 is important for optimal gene transcription. LSD2 is unique in associating specifically with the gene bodies of actively transcribed genes, but not at promoters. A specific function of LSD2 is to maintain low levels of H3K4 methylation within elongation regions. Furthermore, LSD2 forms complexes with H3K9 and H3K36 methyltransferases. These enzymes together orchestrate appropriate histone modifications in order to maintain a repressive chromatin structure at elongation regions, which may be important for optimal transcription elongation<sup>80</sup>.

What until recently seemed to be a puzzle with a few pieces, day by day is becoming more complex



**Figure 15.** Model of gene transcription regulation by LSD2 complex. LSD2 localizes to the 3' end of actively transcribed genes, where it can interact with phosphorylated RNA Pol II and elongation factors. The LSD2 complex coordinates intragenic H3K4me2 and H3K9 methylation and potentially H3K36me2 levels via its own intrinsic demethylase activity and through interaction with histone methyltransferases G9a and NSD3<sup>80</sup>.

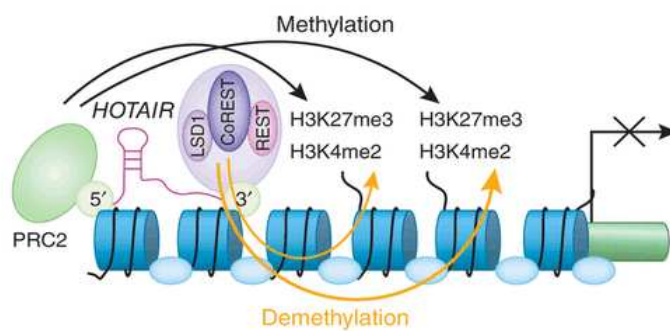
and complete.

While increasing the information about functions and targets of all these epigenetic enzymes, new elegant and exiting cellular epigenetic

mechanisms are discovering.

### 3.1.1 Biological role of LSD1: HOTAIR interaction.

Long intergenic noncoding RNAs (lincRNAs) regulate chromatin states and epigenetic inheritance. The lincRNA HOTAIR serves as a scaffold for at least two distinct histone modification complexes. A 5' domain of HOTAIR binds Polycomb Repressive Complex 2 (PRC2) while a 3' domain of HOTAIR binds the LSD1/CoREST/REST complex. The ability to tether two distinct complexes enables RNA-mediated assembly of PRC2 and LSD1, and coordinates targeting of PRC2 and LSD1 to chromatin for coupled histone H3 lysine 27 methylation and lysine 4 demethylation. The results of recent study made by R.A. Miao-Chih Tsai *et Al.*, suggest that lincRNAs may serve as scaffolds by providing binding surfaces to assemble select histone modification enzymes, and thereby specify the pattern of histone modifications on target genes. The lincRNA termed HOTAIR is increased in expression in primary breast tumours and metastases, and HOTAIR expression level in primary tumours is a powerful predictor of eventual metastasis and death. Using a series of HOTAIR deletion mutants, they showed that HOTAIR is a modular



**Figure 16.** HOTAIR interaction with LSD1, Nat Biotechnol. 2010 Sep;28(9):931-2

bifunctional RNA that has distinct binding domains for PRC2 and LSD1 complexes. HOTAIR-mediated bridging of PRC2 and LSD1 complexes also

enables their coordinate binding to target genes on chromatin. These findings indicate that this lincRNA has active roles in modulating the cancer epigenome by working with LSD1, the important consequence is that both of them may be important targets for cancer diagnosis and therapy<sup>81</sup>.

### **3.1.2 Biological role of LSD1: BLIMP-1 interaction.**

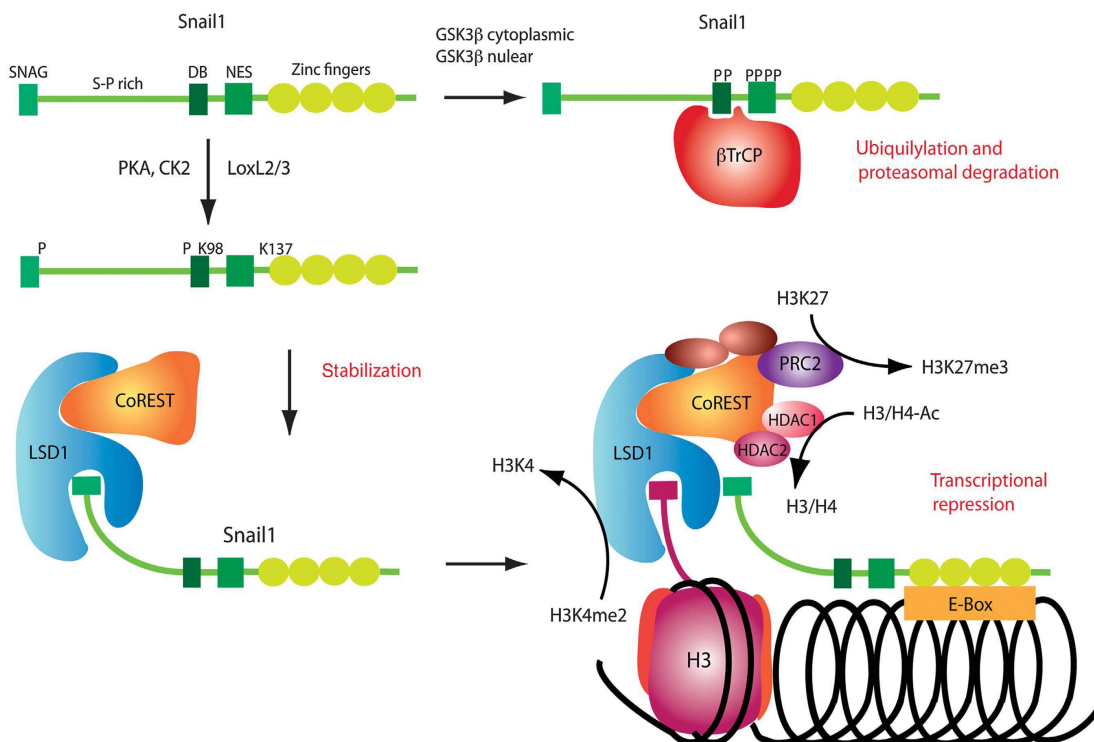
Plasma cell differentiation is orchestrated by the transcriptional repressor B lymphocyte-induced maturation protein-1 (Blimp-1), which silences the gene expression program of mature B cells. The molecular mechanism underlying Blimp-1 suppression of mature B-cell gene expression is not fully understood but it is known that the mechanism underlying Blimp-1-mediated gene suppression, at least partially, includes interaction with several proteins, including HDAC1/2<sup>82</sup>, Groucho family proteins<sup>83</sup>, and G9a histone methyltransferase<sup>84</sup>. Blimp-1 also interacts with the histone arginine methyltransferase, Prmt-5, during germ cell development<sup>85</sup> and with LSD1 for the repression of the mature B-cell gene expression program. Recently Shin-Tang Su *et al.*, report that a proline-rich domain in Blimp-1 directly interacts with LSD1. Both LSD1 knockdown and expression of Blimp-1 lacking the proline-rich domain derepressed the activities of Blimp-1-dependent luciferase reporters. Disruption of the Blimp-1 interaction with LSD1 or reduced LSD1 expression attenuated antibody production, demonstrating the biological significance of this interaction. Finally, using chromatin immunoprecipitation, they showed that Blimp-1 binding to its target sites is accompanied by LSD1 binding to those same sites and that LSD1 binding correlates with histone modifications of accessible chromatin<sup>86</sup>. This new finding is a very useful information to understand better the LSD1 dependent pathways and clarify all the mechanism involved.

### **3.1.3 Biological role of LSD1: SNAIL-1 interaction**

Epithelial–mesenchymal transition (EMT) is a transdifferentiation programs that is required for tissue

morphogenesis during embryonic development. The EMT process can be regulated by a diverse array of cytokines and growth factors, such as transforming growth factor (TGF)- $\beta$ , whose activities are dysregulated during malignant tumor progression. Thus, EMT induction in cancer cells results in the acquisition of invasive and metastatic properties. The mechanism underlying the epigenetic regulation of EMT remains unclear.

At the present, we know that a hallmark of EMT is the loss of E-cadherin, expression, which is often inversely correlated with tumour grade and stage. E-cadherin is a single-span transmembrane



**Figure 17.** Model of the regulatory mechanisms modulating Snail1 stability and activity.  
The EMBO Journal (2010) 29, 1787–1789

glycoprotein that maintains intercellular contacts and cellular polarity in epithelial tissues, its loss is associated with tumor invasiveness, metastatic dissemination, and poor prognosis in several solid tumors<sup>87, 88</sup>. Down-regulation of E-cadherin is believed to induce epithelial-mesenchymal transition (EMT)<sup>89</sup> characterized by dedifferentiation of neoplastic epithelial cells to a more motile mesenchymal phenotype. Several transcription factors, such as Snail-1, Twist and ZEB1, have been implicated in the transcriptional repression of E-cadherin, in the induction of EMT and consequently in the cancer metastasis. In 2009 J. Von Burstin *et al.*'s work demonstrated that E-Cadherin is suppressed by a SNAIL/HDAC1/HDAC2 Repressor Complex linking the epigenetic HDAC machinery to EMT and metastasis<sup>90</sup>.

In 2011 Y. Lin *et al.* showed that Snail-1, known clearly involved in EMT and correlated with high tumour grade and nodal metastasis, interacted with histone lysine-specific demethylase 1 (LSD1)<sup>91</sup>. They demonstrated that LSD1 is able to interact with the Snail-1 amino terminal sequence, named SNAG, using the amine oxidase domain. Interestingly, the sequence of the SNAG domain is similar to that of the histone H3 tail, and the interaction of Snail1 with LSD1 can be blocked by LSD1 enzymatic inhibitors and a histone H3 peptide. So apparently, the SNAG domain of Snail1 resembles a histone H3-like structure, functions as a molecular hook for recruiting LSD1 to its target gene promoters, and resulted in suppression of cell migration and invasion<sup>92</sup>.

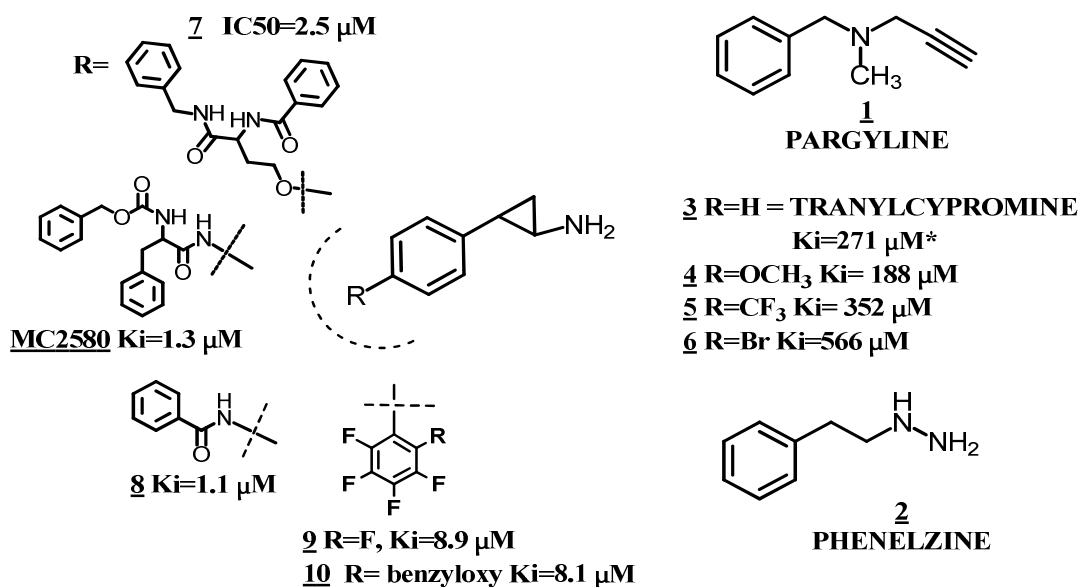
The knowledge about this kind of epigenetic control on tumor grade becomes at the present a new exiting information to use with the objective to find a real able method for checking and blocking the tumor progression and the metastases onset.

### 3.2 LSD1-2 inhibitors

Within the framework of the so-called epigenetic therapies, there is a growing interest in these enzymes as a potential drug target.

Since LSD1 and MAO-A/B share a common mechanism for the oxidative cleavage of the unactivated

nitrogen-carbon bonds of their substrates, many of the known MAO inhibitors have been tested as LSD1 inhibitors<sup>93</sup>, Tranylcypromine displayed the best activity with an IC<sub>50</sub> of less than 2 μM. Since this first study a lot of groups started to work on design and synthesis of new LSD1 inhibitors as tranylcypromine derivatives getting in some cases very nice results<sup>94, 95, 96, 97, 98</sup> (Figure 18).



**Figure 18.** Known LSD1 inhibitors

\*tranylcypromine showed different  $K_i$  value in different reported studies.

*Genes & Cancer* **2011**, (6) 663–679.

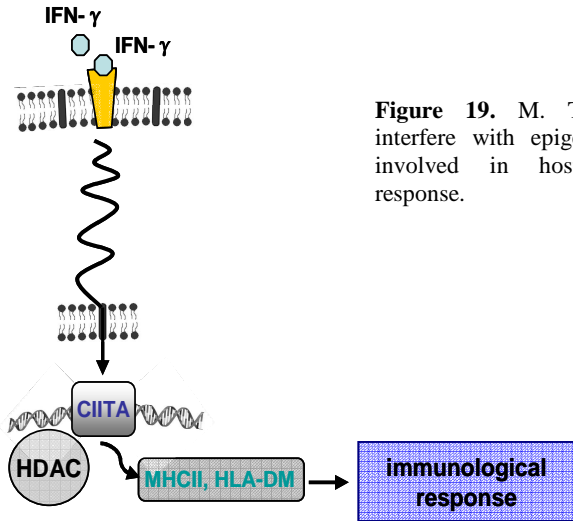
The AO domain of LSD1 shares 20% sequence similarity with those of the FAD-dependent MAO and PAO (polyamine oxidases such as spermine oxidase [SMO] and N1-acetylpolyamine oxidase), with the catalytic domains of LSD1 and SMO showing 60% similarity in amino acid sequences. As compounds bearing guanidine groups were shown to inhibit both SMO and other polyamine

oxidases, a pioneer series of (bis)guanidines and (bis)biguanides were tested as inhibitors of LSD1<sup>99</sup>. Afterwards newer and more powerful polyamine analogues designed showing the importance of this different molecular scaffold in design LSD1 inhibitors<sup>100, 101</sup>.

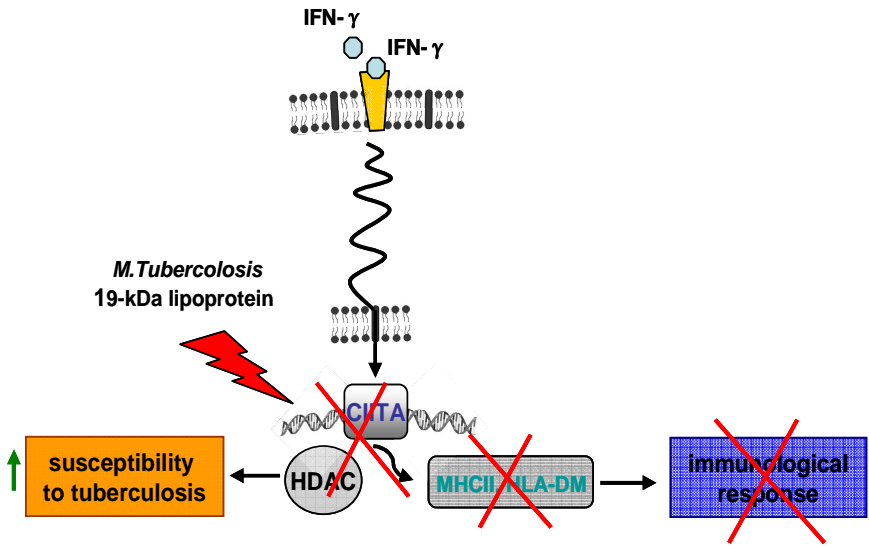
#### 4. New frontiers in Epigenetics

As I have underlined above, the chromatin remodeling is an important epigenetic control of gene expression. Many studies reported the existence of syndromes of disordered “chromatin remodeling” as general deregulation of DNA transcription caused by mutations in genes encoding enzymes which mediate changes in chromatin structure. These mutations result in a loss of proper regulation of chromatin structure, which in turn causes deregulation of gene transcription and inappropriate protein expression. Some of the genetic diseases that arise because of disordered chromatin remodeling include: Alpha-Thalassemia/Mental Retardation Syndrome, ATR-X (ATM/Rad3-related); Rett Syndrome (RS); ICF (Immunodeficiency-Centromeric Instability-Facial Anomalies Syndrome); RSTS (Rubinstein-Taybi Syndrome), and CLS (Coffin-Lowry Syndrome)<sup>102</sup>. Recently M.E. Pennini *et al.* demonstrate the ability of the *Mycobacterium tuberculosis* (Mtb) 19-kDa lipoprotein, a TLR2 agonist expressed by virulent Mtb, to inhibit IFN- $\gamma$ -induced histone acetylation at one locus (*MHC2TA*), but not another (*NOS2*). However, the mechanism for targeted inhibition of a subset of IFN- $\gamma$ -dependent genes is still uncertain, but the proposed mechanism implicates the regulation of chromatin remodeling as a mechanism for Mtb-mediated inhibition of CIITA expression. The causative bacterium in humans is *Mycobacterium tuberculosis*, although infection is necessary, it is not sufficient to cause tuberculosis in most people, human factors governing whether the infected individual will progress to active tuberculosis disease or not are usually assumed to be those governing the immunological state of the host, which are generally determined by the host's genetic make-up. Even the effects of stress and nutrition on the immune response can be influenced by





**Figure 19.** *M. Tuberculosis* may interfere with epigenetic mechanism involved in host immunological response.



genetics and epigenetic mechanisms of gene regulation<sup>103</sup>.

Epigenetic mechanisms, such as aberrant DNA methylation and histone acetylation, regulate the transcription rate and/or tissue-specific expression of certain genes without altering the primary nucleotide sequence of the DNA. DNA methylation plays an important role in the arrangement of some key biological activities such as imprinting and silencing of chromosomal domains<sup>104,105</sup>. It occurs at the cytosine residue in the context of a CpG dinucleotide and in the promoter regions, where it can act as an important modifier of transcription. The relationship between the methylation of the CpG islands and gene expression is very complex and some reports suggest that the change of methylation intensity of the promoter CpG islands is negatively correlated with gene expression levels<sup>106, 107</sup>. Histone acetylation is crucial for gene transcription. Histone acetylation sites and histone acetyltransferases are required for chromatin folding and gene activity, as opening of the chromatin conformation allows binding of transcription factors. Similarly, histone deacetylation plays an important role in transcription<sup>108</sup>. It was found that signalling by *M. tuberculosis*, or its 19-kDa lipoprotein, inhibited IFN- $\gamma$ -induced class II transactivator (CIITA) expression and this process was linked to histone deacetylation at the CIITA gene<sup>109</sup>. Acetylation may therefore contribute to tuberculosis susceptibility. It has been shown that *M. tuberculosis* may interfere with epigenetic regulation; therefore, it is possible that these epigenetic mechanisms may be found to play a role in host susceptibility to tuberculosis.

#### 4.1. Introduction and biological activity of Rufomycin B

The rufomycin B (figure 20) is an antibiotic isolated from *Streptomyces atratus* in 1962 by Higashide et al., it is neutral, lipophylic polypeptide antibiotic composed of seven L-amino acids; L-alanine, L-N-methyl-leucine (2 moles), L-3-nitrotyrosine, L-leucine, L-2-amino-4-hexenoic acid and L-N-(2-methyl-3-buten-2-yl)- tryptophan as shown in figure 20. Biological tests showed that Rufomycin B is inactive against Gram positive and negative bacteria, fungi, and yeast examined, though it has a high

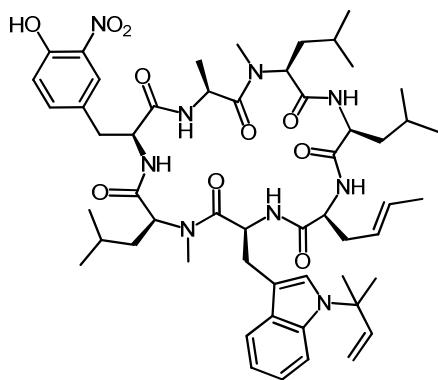


Figure 20: Rufomycin B

antibiotic activity against acid-fast bacteria, especially *Mycobacterium tuberculosis H37Rv* which have been rendered resistant to one or two of the following substances: streptomycin, neomycin, kanamycin and isonicotinic acid hydrazide (table 2)<sup>110</sup>. Tuberculosis is one of the most influential diseases in the history of mankind due to its devastating effect on health and its high mortality rate throughout the world. The World Health Organization (WHO) has estimated that 2 billion

people  
have  
latent TB  
and that  
globally,  
in 2009,  
the  
disease  
killed 1.7  
million  
people  
<sup>111</sup>. New  
TB  
treatment  
s are

Test organism	MIC γ/ml	Test organism	MIC γ/ml
<i>Escherichia coli</i>	>100	<i>Mycobact. Avium (NM-resistant)</i>	5.0
<i>Proteus vulharis</i>	>100	<i>Mycobact. smegmatis</i>	0.5
<i>Pseudomonas aeruginosa</i>	>100	<i>Mycobact. Phlei</i>	5.0
<i>Serratia marcescens</i>	>100	<i>Mycobact. Tuber. H37Rv</i>	1~5.0
<i>Staphylococcus aureus</i>	>100	<i>Mycobact. Tuber. H37Rv (SM-resistant)</i>	2.0
<i>Bacillus subtilis</i>	>100	<i>Mycobact. Tuber. H37Rv (KM- resistan)</i>	2.0
<i>Bacillus brevis</i>	>100	<i>Mycobact. Tuber. H37Rv (SM-KM resistant)</i>	2.0
<i>Sarcina lutea</i>	>100	<i>Mycobact. Tuber. H37Rv (INHA-resistant)</i>	1.0
<i>Mycobact.607</i>	5.0	<i>Sacc. cerevisiae</i>	>100
<i>Mycobact. avium</i>	5.0	<i>Pen. crysogenum</i>	>100
<i>Mycobact. Avium (SM-resistant)</i>	5.0	<i>Candida albicans</i>	>100

being developed<sup>112</sup>, and new TB vaccines are under investigation<sup>113</sup>.

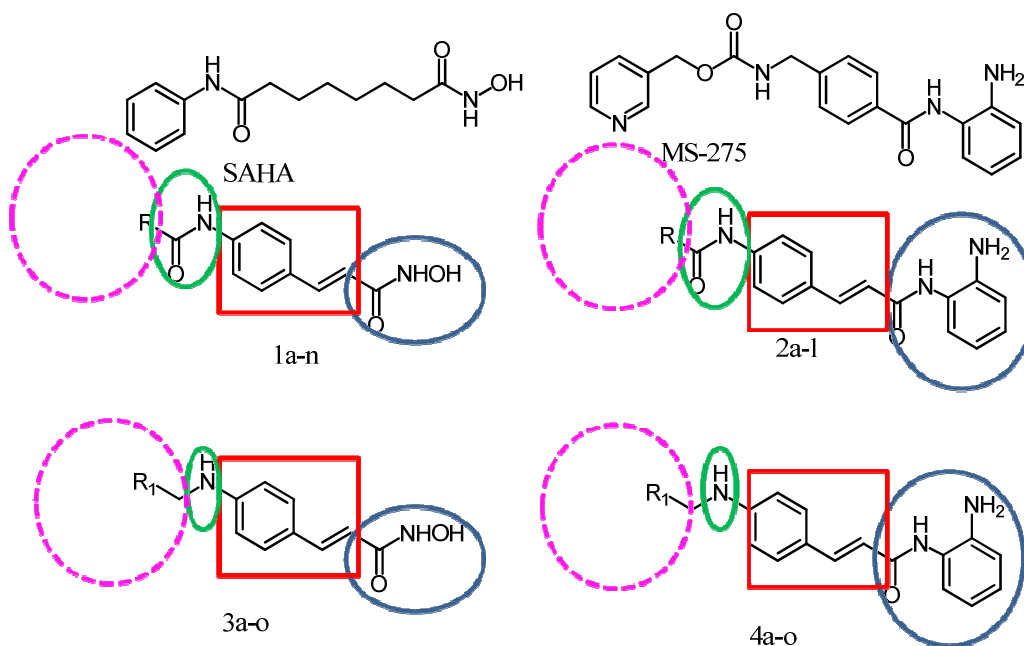
Although TB rates are decreasing in the United States, the disease is becoming more common in many parts of the world. In addition, the prevalence of drug-resistant TB is also increasing worldwide. Co-infection with the human immunodeficiency virus (HIV) has been an important factor in the emergence and spread of resistance. Since its discovery, no one total synthesis of Rufomycin B has been reported in literature. Since many years, the Ely Lilly company is studying this peptidic scaffold in order to get new compounds which are useful as antibiotics, reporting a fermentative synthesis<sup>114</sup>.

## 5. New cinnammil containing HDAC inhibitors

As I told before, the pharmacophore model for HDACi includes a cap group (CAP) that interacts with the rim of the catalytic tunnel of the enzyme, a polar connection unit (CU) linked to a hydrophobic spacer (HS) which allows the molecule to lie into the tunnel, and a Zn-binding group (ZBG) able to complex the Zn<sup>+2</sup> at the bottom of the cavity<sup>114, 115</sup>. Besides TSA and SAHA, the two prototypes of natural and synthetic HDACi, which present an aliphatic chain as HS, a number of HDACi carrying the cinnamyl moiety as HS has been described so far, starting from the SAHA related hybrid polar compound cinnamyl bishydroxamic acid (CBHA)<sup>116-123</sup>. Among them, HDAC42<sup>124</sup> was described as a novel phenylbutyrate-based HDACi highly active in prostate cancer, in hepatocellular carcinoma, in ovarian cancer, and able to sensitize prostate cancer cells to DNA-damaging agents through Ku70 acetylation<sup>125-129</sup>. Moreover, the cited belinostat and panobinostat (Figure 21) are two examples of cinnamyl-containing HDACi at the present in clinical trials for the treatment of many forms of tumors<sup>130, 131</sup>. Mai *et al.*, worked on design, synthesis, and biological evaluation of HDACi with some aroyl-pyrrolylhydroxamates (APHAs), characterized by an aroyl portion as CAP+CU, a pyrrolylacrylic moiety as HS, and the hydroxamate group as ZBG<sup>132-137</sup>. Afterwards, by replacing the

pyrrole nucleus with the benzene ring, they have been reported two different series of cinnamyl hydroxamates, the *N*-hydroxy-3-(2-, 3-, and 4-arylamino)phenyl)acrylamides<sup>138</sup> and the *N*-hydroxy-3-(4-(3-oxo-3-phenylprop-1-enyl)phenyl)acrylamides<sup>139, 140</sup>, acting as anticancer agents through HDAC inhibition. Following these searches on cinnamyl compounds, I worked on the synthesis and enzyme and in-cell evaluation of new arylacetyl-amino- and arylmethyl-amino-cinnamyl hydroxamates and 2-aminoanilides (**1-4**), tested as HDACi and pro-apoptotic, antiproliferative, and/or cytodifferentiating agents.

In particular, choosing a cinnamyl moiety as a HS, I inserted some arylacetyl-amino portions carrying



**Figure 21.** Cinnamyl-containing HDACi

an alkyl/aryl/arylalkyl substituent at the methylene group (compounds **1** and **2**), or alternatively a wide range of (hetero)arylmethylamino groups (compounds **3** and **4**) (CAP+CU groups). All the arylacetamino- and arylmethylaminocinnamyl compounds were prepared both as hydroxamates (**1** and **3**) and 2-aminoanilides (**2** and **4**) (ZBGs: -CONHOH or - CONH(2-NH<sub>2</sub>)Ph). In order to get the biological evaluations, all the new compounds were screened against human HDAC1 and maize HD1-B (class I HDACs), and human HDAC4 and maize HD1-A (class IIa HDACs), to assess their inhibitory activities and selectivity, and in human leukemia U937 cells in order to:

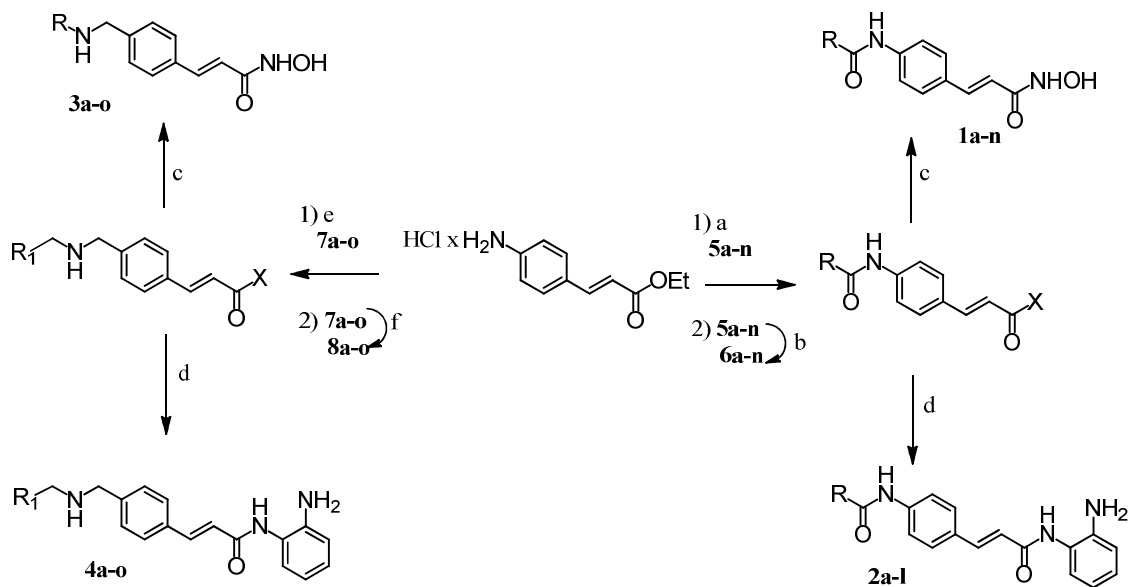
- verify their capability to increase the acetylation levels of histone H3 and  $\alpha$ -tubulin,
- induce the tumor suppressor protein p21WAF1/CIP1.
- test the effects on cycle cell, the induction of apoptosis, the inhibition of proliferation, and the granulocytic differentiation

SAHA, MS-275, and HDAC42 were prepared and included in the assays as reference drugs.

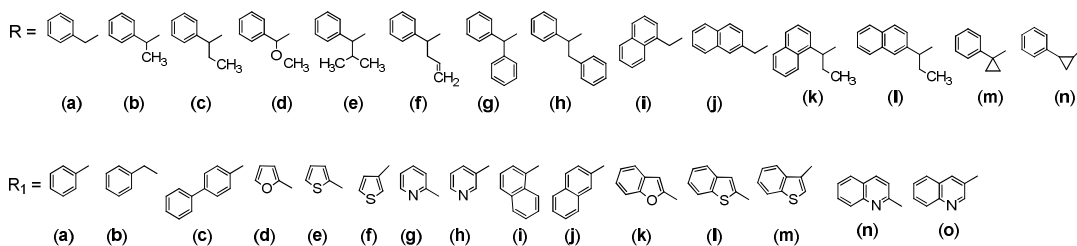
## 5.1. Chemistry

The title compounds were prepared starting from the key intermediate ethyl 4-aminocinnamate hydrochloride<sup>138</sup>, that was treated with the properly substituted arylacetyl chlorides in the presence of triethylamine to afford the ethyl 3-(4-(2- arylacetamido)phenyl)acrylates **5a-n**. Alternatively, the ethyl 4-aminocinnamate hydrochloride was condensed with the appropriate aldehydes to obtain the aldimine intermediates that were reduced to the ethyl 3-(4-(arylmethylamino)phenyl)acrylates **7a-o** with sodium cyanoborohydride. The ethyl esters **5** and **7** were hydrolyzed in basic medium to the related acrylic acids **6** and **8**, respectively. Further reaction of these 3-(4-(2- arylacetamido)- or 3-(4-(arylmethylamino)phenyl)acrylic acids (**6a-n** or **8a-o**, respectively) with i) ethyl chloroformate and triethylamine, ii) *O*-(2-methoxy-2- propyl)hydroxylamine<sup>141</sup>, and iii) Amberlyst 15 ion-exchange resin in methanol furnished the hydroxamates **1a-n** (from **6**) or **3a-o** (from **8**). Alternative treatment

of **6a-l** or **8a-o** with benzotriazole-1-yloxytris(dimethylamino)phosphonium hexafluorophosphate



**Scheme 1** : a)  $\text{RCOCl}$ ,  $\text{Et}_3\text{N}$ , dry  $\text{CH}_2\text{Cl}_2$ ,  $0\text{ }^\circ\text{C}$  to rt; b)  $\text{LiOH}$ ,  $\text{THF}/\text{H}_2\text{O}$ , rt; c) 1)  $\text{ClCOOEt}$ ,  $\text{Et}_3\text{N}$ , dry  $\text{THF}$ ,  $0\text{ }^\circ\text{C}$ ; 2)  $\text{CH}_3\text{OC}(\text{CH}_3)_2\text{ONH}_2$ , dry  $\text{THF}$ ,  $0\text{ }^\circ\text{C}$ ; 3) Amberlyst 15,  $\text{MeOH}$ , rt; d) 1)  $\text{Et}_3\text{N}$ , BOP reagent, dry  $\text{DMF}$ ,  $\text{N}_2$ ; 2) 1,2-phenyldiamine, dry  $\text{DMF}$ ,  $\text{N}_2$ ; e) 1)  $\text{R}_1\text{CHO}$ ,  $\text{CH}_3\text{COOH}$ ,  $\text{MeOH}$ , rt; 2)  $\text{NaCNBH}_3$ ,  $\text{MeOH}$ , rt. f)  $2\text{ N KOH}$ ,  $\text{EtOH}$ , rt.



**Scheme 2.** R and R1 substituents used as acyl chloride (R) and aromatic aldehyde (R1)

(BOP-reagent), triethylamine and 1,2-phenyldiamine afforded the corresponding 2-aminoanilides **2a-l** or **4a-o**, respectively (Scheme 1).

**Table 3.** Chemical and Physical Data for Compounds **1-4**<sup>[a]</sup>

cpd	mp, °C	recryst solvent <sup>[b]</sup>	yield, %	cpd	mp, °C	recryst solvent <sup>[b]</sup>	yield, %
<b>1b</b>	133-135	A	67.3	<b>3d</b>	216-218	C	88.7
<b>1c</b>	128-130	A	59.8	<b>3e</b>	152-154	B	78.5
<b>1d</b>	146-148	B	68.4	<b>3f</b>	162-164	B	58.3
<b>1e</b>	146-148	B	54.9	<b>3g</b>	196-198	C	76.8
<b>1f</b>	110-112	A	67.6	<b>3h</b>	150-152	B	79.1
<b>1g</b>	238-240	E	58.3	<b>3i</b>	216-218	C	68.4
<b>1h</b>	182-184	B	61.3	<b>3j</b>	198-200	C	61.3
<b>1i</b>	216-218	C	59.2	<b>3k</b>	226-228	C	76.4
<b>1j</b>	108-110	A	65.7	<b>3l</b>	>250	E	75.6
<b>1k</b>	160-162	B	75.6	<b>3m</b>	216-218	D	67.6
<b>1l</b>	160-162	B	77.8	<b>3n</b>	170-172	B	75.9
<b>1m</b>	130-132	A	75.9	<b>3o</b>	135-137	A	80.9
<b>1n</b>	103-105	A	76.8	<b>4a</b>	172-174	B	87.0
<b>2a</b>	>250	E	55.2	<b>4b</b>	170-172	B	78.5
<b>2b</b>	228-230	C	87.0	<b>4c</b>	248-250	E	75.7
<b>2c</b>	200-202	C	78.5	<b>4d</b>	186-188	B	77.5
<b>2d</b>	180-182	B	75.7	<b>4e</b>	178-180	B	59.2
<b>2e</b>	239-241	E	74.6	<b>4f</b>	190-192	B	72.8
<b>2f</b>	240-242	E	72.8	<b>4g</b>	156-158	B	73.9
<b>2g</b>	>250	E	77.4	<b>4h</b>	180-182	A	67.9
<b>2h</b>	244-246	E	78.5	<b>4i</b>	180-182	B	65.7
<b>2i</b>	248-250	E	76.4	<b>4j</b>	198-200	C	77.4
<b>2j</b>	>250	E	78.9	<b>4k</b>	208-210	C	78.9
<b>2k</b>	206-208	E	80.9	<b>4l</b>	222-224	E	77.8
<b>2l</b>	206-208	E	81.1	<b>4m</b>	232-234	E	74.6
<b>3a</b>	184-186	D	67.3	<b>4n</b>	210-212	C	76.8
<b>3b</b>	148-150	B	59.8	<b>4o</b>	192-194	C	81.1



<b>3c</b>	>250	E	54.9				
-----------	------	---	------	--	--	--	--

[a] Analytic results were within  $\pm 0.40\%$  of the theoretical values. [b] A, benzene; B, benzene/acetonitrile; C, acetonitrile/methanol; D, acetonitrile; E, methanol.

Chemical and physical data of the tested compounds **1-4** (except **1a**) and the intermediates **5-8** (except **5a** and **6a**) are reported in Table 3 and 4.

**Table 4.** Chemical and Physical Data for Compounds **5-8**<sup>[a]</sup>

cpd	mp, °C	recryst solvent <sup>[b]</sup>	yield, %	cpd	mp, °C	recryst solvent <sup>[b]</sup>	yield, %
<b>5b</b>	114-116	A	87.3	<b>7c</b>	118-120	B	63.1
<b>5c</b>	109-111	A	88.2	<b>7d</b>	130-132	B	90.0
<b>5d</b>	133-135	B	78.4	<b>7e</b>	118-120	B	73.8
<b>5e</b>	95-97	A	78.7	<b>7f</b>	114-116	B	67.8
<b>5f</b>	114-116	A	83.6	<b>7g</b>	66-68	A	58.4
<b>5g</b>	151-153	C	77.5	<b>7h</b>	96-98	A	63.5
<b>5h</b>	143-145	B	73.4	<b>7i</b>	134-136	B	74.6
<b>5i</b>	144-146	B	83.4	<b>7j</b>	111-112	B	77.3
<b>5j</b>	200-202	C	85.0	<b>7k</b>	102-104	A	79.6
<b>5k</b>	135-137	B	81.1	<b>7l</b>	138-140	B	68.9
<b>5l</b>	125-127	B	79.0	<b>7m</b>	204-206	C	81.3
<b>5m</b>	105-107	A	82.2	<b>7n</b>	102-104	A	55.3
<b>5n</b>	144-146	C	82.2	<b>7o</b>	106-108	A	61.7
<b>6b</b>	224-226	D	94.5	<b>8a</b>	180-182	F	88.6
<b>6c</b>	202-204	D	88.6	<b>8b</b>	148-150	C	85.4
<b>6d</b>	198-200	C	95.7	<b>8c</b>	>250	E	95.3
<b>6e</b>	162-164	C	85.7	<b>8d</b>	156-158	C	95.3
<b>6f</b>	171-173	C	89.0	<b>8e</b>	186-188	F	85.6
<b>6g</b>	>250	E	82.3	<b>8f</b>	184-186	F	89.8
<b>6h</b>	168-170	C	81.0	<b>8g</b>	158-160	C	91.6
<b>6i</b>	>250	E	83.4	<b>8h</b>	190-192	F	92.2
<b>6j</b>	>250	E	86.7	<b>8i</b>	198-200	F	91.9
<b>6k</b>	186-188	C	85.3	<b>8j</b>	>250	E	87.1

<b>6l</b>	187-189	C	84.0	<b>8k</b>	>250	E	95.2
<b>6m</b>	>250	E	86.5	<b>8l</b>	>250	E	92.8
<b>6n</b>	>250	E	82.3	<b>8m</b>	204-206	D	85.8
<b>7a</b>	110-115	B	70.3	<b>8n</b>	216-218	D	88.1
<b>7b</b>	80-82	A	66.7	<b>8o</b>	212-214	D	89.3

[a] Analytic results were within  $\pm 0.40\%$  of the theoretical values. [b] A, cyclohexane; B, cyclohexane/benzene; C, benzene/acetonitrile; D, acetonitrile/methanol; E, methanol; F, acetonitrile..

**Table 5.** Maize HD1-B and HD1-A Inhibitory Activity of Hydroxamate Compounds **1** and **3**

compd	IC <sub>50</sub> $\pm$ SD ( $\mu$ M)	
	HD1-B	HD1-A
<b>1a</b>	0.092 $\pm$ 0.003	0.072 $\pm$ 0.004
<b>1b</b>	0.072 $\pm$ 0.003	0.080 $\pm$ 0.003
<b>1c</b>	0.089 $\pm$ 0.004	0.064 $\pm$ 0.002
<b>1d</b>	0.083 $\pm$ 0.003	0.140 $\pm$ 0.007
<b>1e</b>	0.187 $\pm$ 0.006	0.057 $\pm$ 0.002
<b>1f</b>	0.126 $\pm$ 0.005	0.057 $\pm$ 0.003
<b>1g</b>	0.162 $\pm$ 0.006	0.055 $\pm$ 0.003
<b>1h</b>	0.133 $\pm$ 0.004	0.074 $\pm$ 0.003
<b>1i</b>	0.011 $\pm$ 0.0005	0.015 $\pm$ 0.001
<b>1j</b>	0.032 $\pm$ 0.001	0.056 $\pm$ 0.003
<b>1k</b>	0.058 $\pm$ 0.002	0.042 $\pm$ 0.001
<b>1l</b>	0.062 $\pm$ 0.002	0.069 $\pm$ 0.003
<b>1m</b>	0.065 $\pm$ 0.002	0.196 $\pm$ 0.010
<b>1n</b>	0.064 $\pm$ 0.003	0.132 $\pm$ 0.005
<b>3a</b>	0.020 $\pm$ 0.001	0.102 $\pm$ 0.003
<b>3b</b>	0.058 $\pm$ 0.002	0.154 $\pm$ 0.005
<b>3c</b>	0.690 $\pm$ 0.021	0.160 $\pm$ 0.005
<b>3d</b>	0.150 $\pm$ 0.007	0.112 $\pm$ 0.003
<b>3e</b>	0.025 $\pm$ 0.001	0.059 $\pm$ 0.002
<b>3f</b>	0.027 $\pm$ 0.001	0.072 $\pm$ 0.004
<b>3g</b>	0.124 $\pm$ 0.005	0.045 $\pm$ 0.002
<b>3h</b>	0.102 $\pm$ 0.005	0.098 $\pm$ 0.004
<b>3i</b>	0.046 $\pm$ 0.002	0.022 $\pm$ 0.001
<b>3j</b>	0.026 $\pm$ 0.002	0.020 $\pm$ 0.001

<b>3k</b>	0.031 ± 0.001	0.020 ± 0.001
<b>3l</b>	0.700 ± 0.035	0.900 ± 0.054
<b>3m</b>	0.042 ± 0.001	0.037 ± 0.002
<b>3n</b>	0.118 ± 0.006	0.069 ± 0.003
<b>3o</b>	0.127 ± 0.005	0.070 ± 0.004
SAHA	0.028 ± 0.001	0.180 ± 0.009
HDAC42	0.009 ± 0.0005	0.006 ± 0.0003

[a] Data represent mean values of at least three separate experiments.

## 5.2. Results and Discussion

### 5.2.1. Enzyme Inhibitory Assays. Maize HD1-B and HD1-A

#### Enzymes.

Compounds **1-4** were tested against partially purified maize HD1- B and HD1-A, two homologs of class I and class II HDACs, respectively. The maize enzymes are not sensitive to non hydroxamate HDACi up to 250  $\mu\text{M}$ , so just compounds **1** and **3** are tested. The best results are obtained for the compounds with a small alkyl group (methyl, ethyl, cyclopropyl), or its isoster (methoxy), at the methylene of the phenylacetyl portion, whereas the derivatives with bigger substituents at such a position (i.e., *iso*-propyl, allyl, phenyl, benzyl) were less active. Differently, in the case of HD1-A all used substituents furnished inhibitory effects to the derivatives, with the exception of the methoxy and the cyclopropyl (1,1- as well as 1,2-disubstituted) groups, that caused a drop of the HD1- A inhibitory activity of the corresponding derivatives **1d**, **1m**, and **1n**. In regard to the arylmethylamino-cinnamyl hydroxamates **3**, the first member of the series (the 3-(4 (benzylamino)phenyl)-Nhydroxyacrylamide **3a** displayed high and 5-fold lower potency against HD1-A ( $\text{IC}_{50}$  HD1-B = 0.020  $\mu\text{M}$ ;  $\text{IC}_{50}$  HD1-A = 0.102  $\mu\text{M}$ ). inhibitory activity against HD1-B. Among the (hetero)mono- and bicyclic rings replacing the benzene at the R1 position in **3a** only the 2- thienyl, 3-thienyl,

**Table 6.** Human Recombinant HDAC1 and HDAC4 Inhibitory Activity of Compounds **1** and **2**<sup>[a]</sup>

compd	% of inhibition at 5 $\mu$ M	
	hrHDAC1	hrHDAC4
<b>1a</b>	59.8	28.9
<b>1b</b>	54.6	45.0
<b>1c</b>	44.5	42.4
<b>1d</b>	66.6	72.4
<b>1e</b>	37.5	41.6
<b>1f</b>	41.2	11.9
<b>1g</b>	55.3	15.3
<b>1h</b>	54.7	14.9
<b>1i</b>	76.2	14.0
<b>1j</b>	72.7	55.3
<b>1k</b>	75.4	38.9
<b>1l</b>	66.9	42.4
<b>2a</b>	28.6	25.5
<b>2b</b>	71.3	0
<b>2c</b>	56.2	47.6
<b>2d</b>	72.0	38.0
<b>2e</b>	73.2	16.2
<b>2f</b>	56.3	60.4
<b>2g</b>	25.8	70.0
<b>2h</b>	42.9	50.4
<b>2i</b>	59.2	25.3
<b>2j</b>	58.3	6.2
<b>2k</b>	76.7	23.4
<b>2l</b>	72.7	25.2
HDAC42	94.0	27.2
SAHA	93.1	63.2
MS-275	83.4	14.6

[a] Data represent mean values of at least three separate experiments.

2-naphthyl, and 2-benzofuryl rings assured a comparable inhibiting potency against HD1-B, the other being detrimental for enzyme inhibition to various extent. In the anti- HD1-A assay, in addition to the chemical replacements that were important for the HD1-B inhibition, the substitution of the **3a** benzene ring with the 2-pyridyl, 1-naphthyl, 3-benzothienyl, 2- and 3-quinoliny rings increased up to 5-fold the HD1-A inhibitory activity of the compounds. The trend of structure-activity relationship (SAR) observed with **1** and **3** confirmed some our previous findings, according to which the requirements for a HDACi to inhibit maize HD1-B are more stringent than those to inhibit HD1-A: HD1-A has a larger catalytic tunnel than HD1-B, so it can easier accommodate a wider variety of chemically different compounds.

### 5.2.2. Human Recombinant HDAC1 and HDAC4 Assays.

All the compounds were tested at 5  $\mu$ M against human recombinant (hr) HDAC1 and

HDAC4, using the histone H3 (HDAC1) or the non-histone trifluoroacetyl-lysine<sup>143</sup> (HDAC4) as a substrate, respectively.

**Table 7.** Chromatographic analysis of the 1st (F1) and 2nd (F2) fractions collected in the semipreparative enantioseparation of **1b**, **1c**, and **2c**.

compd	mobile phase	A <sup>a</sup>	F1		F2	
			ee(%) <sup>b</sup>	OR <sup>c</sup>	ee(%) <sup>b</sup>	OR <sup>c</sup>
<b>1b</b>	<i>n</i> -hexane-ethyl acetate-ethanol-trifluoroacetic acid 80/20/10/0.1	5	>99.0	(+)	>99.0	(-)
<b>1c</b>	<i>n</i> -hexane-ethyl acetate-ethanol-trifluoroacetic acid 80/20/10/0.1	5	>99.0	(+)	>99.0	(-)
<b>2c</b>	<i>n</i> -hexane-ethanol 30/70	10	>99.0	(+)	>99.0	(-)

<sup>a</sup>Amount of sample (in mg) resolved in a single semipreparative run. <sup>b</sup>Enantiomeric purity for pooled fractions containing the 1<sup>st</sup> (F1) and 2<sup>nd</sup> (F2) eluted enantiomers. <sup>c</sup>Sign of the optical rotation on-line monitored at 365 nm during elution with the mobile phases reported in table and pure ethanol.

Column: Chiralpak IA (250 10 mm I.D.); flow-rate: 4.0 mL/min; detector: UV at 340 nm; temperature: 25 °C.

From these results, it is been possible to get some interesting information about Structure-Activity Relationship. HDAC1 inhibitory potency is improved when:

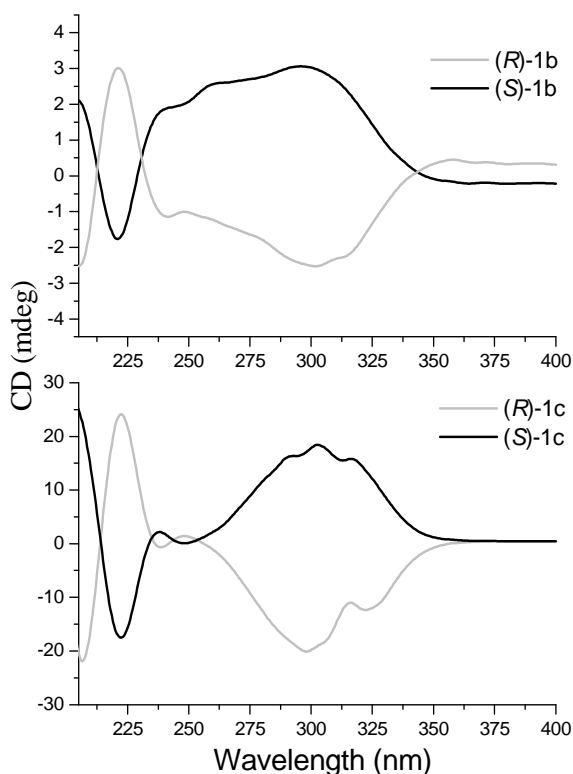
- the phenyl ring at the R position in prototype **1a** and **2a**, is replaced with 1- or 2-naphthyl group (compounds **1i-l**),
- a substituent (particularly a methyl, methoxy, and *iso*-propyl group) is introduced at the phenylacetyl portion the 2-aminoanilide series (compounds **2**), and does not change when:
- some substituents at the methylene portion of the phenylacetyl amino moiety in the hydroxamate prototype **1a** are introduced. With respect to HDAC4 inhibition:
- the introduction of a small (up to the *iso*-propyl) substituent at the methylene connecting the phenyl to the carbonyl group in **1a** improves the potency of the derivatives
- a large unsaturated substituent such as the allyl, phenyl, and benzyl groups (see compounds **2f-h**) in compound **2** increases the activity

- the replacement of the benzene ring of **1a** with the naphthyl moiety (compounds **1i-l**) typically furnishes an increase in the HDAC4 inhibiting potency, with the exception of compound **1i**, that shows lower activity.

Since with the insertion of a substituent at the methylene position of the phenylacetyl moiety of **1a** and **2a** a chiral center was generated, we checked if in these two series of HDACi there is stereoselectivity of action.

Single enantiomers of hydroxamates **1b** and **1c**, as well as the 2-aminoanilide **2c** were obtained by enantioselective HPLC of racemic forms on the amylose-based Chiralpak IA chiral stationary phases (CSP) using normal-phase conditions (Table 7). The absolute configuration

assignment was accomplished by a combined strategy based on chemical correlation/chiral HPLC/circular dichroism (CD) methods. (*R*) and (*S*) enantiomers of 2-phenylbutyric acid were used as chiral synthones to obtain non racemic forms (ee >62%) of **1c** and **2c**. The synthesis occurred in



**Figure 22.** CD spectra of the enantiomers of **1b** and **1c** in ethanol

**Table 8.** Human Recombinant HDAC1 and HDAC4 Inhibitory Activity of Compounds **3** and **4**<sup>[a]</sup>

cpd	% of inhibition at 5 $\mu$ M	
	hr HDAC1	hr HDAC4
<b>3a</b>	55.6	37.5
<b>3b</b>	34.6	29.1
<b>3c</b>	31.9	0
<b>3d</b>	48.1	0
<b>3e</b>	91.5	35.2
<b>3f</b>	91.5	11.1
<b>3g</b>	60.6	0
<b>3h</b>	60.1	30.9
<b>3i</b>	45.5	49.6
<b>3j</b>	94.4	22.3
<b>3k</b>	74.2	0
<b>3l</b>	26.0	0
<b>3m</b>	69.9	0
<b>3n</b>	64.9	0
<b>3o</b>	52.0	0
<b>4a</b>	69.4	0
<b>4b</b>	42.5	0
<b>4c</b>	67.7	31.9
<b>4d</b>	36.7	27.3
<b>4e</b>	38.5	22.9
<b>4f</b>	44.4	32.4
<b>4g</b>	73.2	41.0
<b>4h</b>	52.3	41.9
<b>4i</b>	37.5	0
<b>4j</b>	51.8	0

<b>4k</b>	58.3	0
<b>4l</b>	45.3	0
<b>4m</b>	50.6	20.0
<b>4n</b>	59.0	19.7
<b>4o</b>	74.0	3.5
SAHA	93.1	63.2
MS-275	83.4	14.6

[a] Data represent mean values of at least three separate experiments.

stereoconservative way and the final products maintained the original absolute configuration of starting material. Enantioselective HPLC analysis of racemic samples spiked with the optically active forms of known absolute configuration allowed the stereochemical characterization of **1c** and **2c**. The stereochemistry of **1b** was empirically achieved by comparing its CD spectra with those of the structurally analogue **1c** (Figure 21). The enantiomers of **1b**, **1c** and **2c**, separated on semipreparative scale, were tested against maize HD1-B and HD1-A, as well as against hrHDAC1 and hrHDAC4, in comparison with their corresponding racemates. In general, the (*R*)-enantiomer is slightly more active than the (*S*)-enantiomer. In the case of the two hydroxamates **1b** and **1c**, the inhibition is enantioselective against both maize (HD1-B and HD1-A) and human (HDAC1 and HDAC4) enzymes. In effect, the (*R*)-**1b** enantiomer is 3-fold more potent than (*S*)-**1b** as maize HD1-B inhibitor. In the case of **1c** against maize HD1-A enzyme there is not a large difference of action between the enantiomers. As concerns the 2-aminoanilide **2c**, the (*R*)-enantiomer shows an appreciable improvement in activity respect to the racemic form only against HDAC1 (table 10). The inhibitory data for the arylmethylaminocinnamylhydroxamates (**3**) and -2-aminoanilides (**4**) against hrHDAC1 and hrHDAC4 are reported in Table 8. In the case of the hydroxamates **3**, the phenylmethylamino prototype **3a** displayed 55.6% of HDAC1 inhibition at 5  $\mu$ M, and the replacement of the phenyl ring with the 2- or 3-thienyl (compounds **3e** or **3f**) as well as 2-naphthyl or 2-benzofuryl moiety (compounds **3j** or **3k**) highly improves this inhibitory action.



**Table 9.** IC<sub>50</sub> values of selected **1-4** derivatives against HDAC1, HDAC4, and HDAC6<sup>[a]</sup>

cpd	IC <sub>50</sub> ± SD (μM)		
	HDAC1	HDAC4	HDAC6
<b>1k</b>	0.07 ± 0.01	4.55 ± 0.27	2.9 ± 0.12
<b>2c</b>	2.0 ± 0.1	54.4 ± 3.6	5.3 ± 0.21
<b>3f</b>	0.08 ± 0.004	78.3 ± 4.7	0.27 ± 0.02
<b>3g</b>	0.31 ± 0.01	48.8 ± 2.44	0.15 ± 0.01
<b>4n</b>	0.59 ± 0.02	86.6 ± 4.33	8.17 ± 0.49
<b>4o</b>	1.38 ± 0.05	71.8 ± 3.6	102.7 ± 5.13

[a] Data represent mean values of at least three separate experiments.

In the corresponding 2-aminoanilide series (compounds **4**), the phenyl → thienyl replacement led to less potent compounds (see **4e** and **4f** vs **4a**).

However, in this 2-aminoanilide series this activity is promptly restored by replacing the thienyl ring (R1 position) with the 2-pyridyl (compound **4g**) and 3-quinolinyl

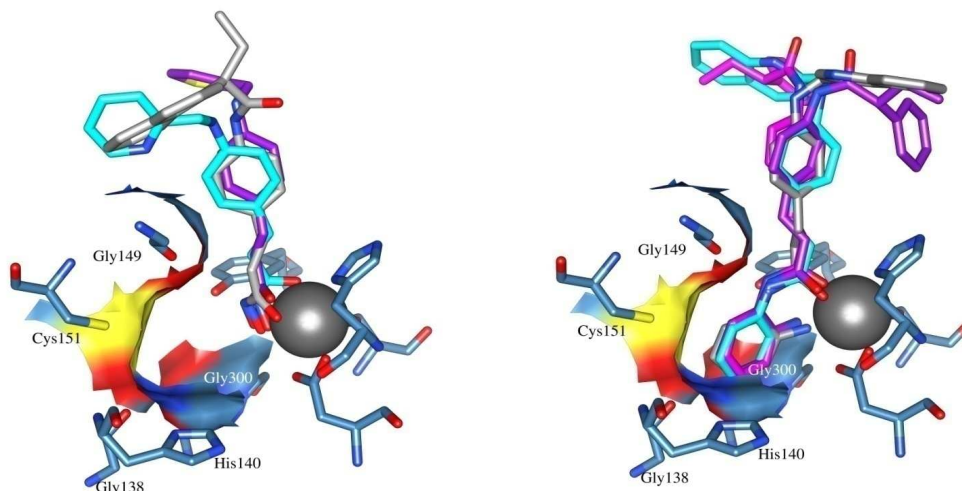
(compound **4o**), and to a lesser extent with other related mono- or bicyclic rings (see for example **4h**, **4n**, and **4k**).

**Table 10.** Anti-HDAC Activity of **1b**, **1c**, and **2c** Pure Enantiomers<sup>[a]</sup>

cpd	IC <sub>50</sub> ± SD (μM)		% of inhibition at 5 μM	
	HD1-B	HD1-A	hr HDAC1	hr HDAC4
<b>1b</b>	0.072 ± 0.003	0.080 ± 0.003	54.6	45.0
<b>(S)-1b</b>	0.170 ± 0.007	0.125 ± 0.006	45.2	33.3
<b>(R)-1b</b>	0.056 ± 0.002	0.073 ± 0.004	59.0	51.1
<b>1c</b>	0.089 ± 0.004	0.064 ± 0.002	44.5	42.4
<b>(S)-1c</b>	0.101 ± 0.003	0.063 ± 0.003	29.5	39.2
<b>(R)-1c</b>	0.040 ± 0.002	0.070 ± 0.003	49.8	49.2
<b>2c</b>			56.2	47.6
<b>(S)-2c</b>			52.6	26.7
<b>(R)-2c</b>			78.9	48.3

[a] Data represent mean values of at least three separate experiments.

Against HDAC, the majority of the tested **3** and **4** compounds displayed low or no inhibiting activity.



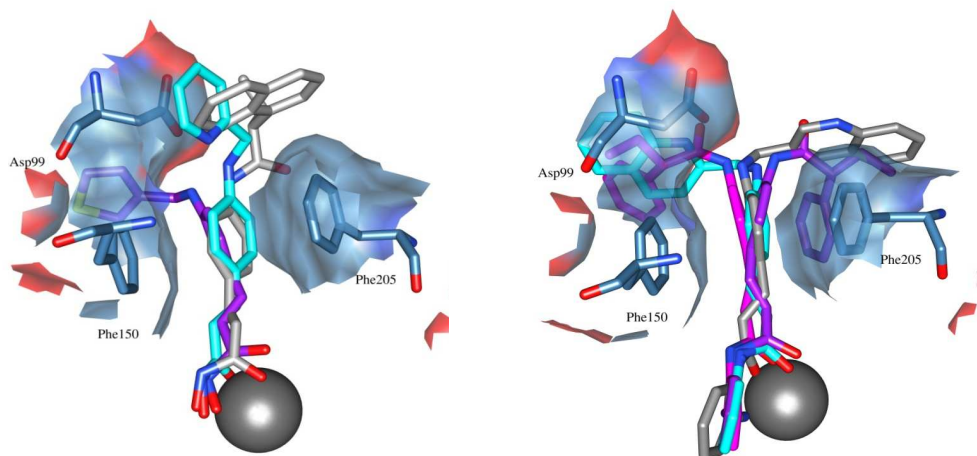
**Figure 23.** Ligands/HDAC1 interactions around the catalytic Zinc ion. In turquoise are displayed all the residues within 3.5 Å from either the hydroxamate or the benzamide groups. In the left side are reported the hydroxamates (**1k** in gray, **3f** in purple and **3g** in cyan) and in the right window are depicted the 2-aminoanilides ((*S*)-**2c** in magenta, (*R*)-**2c** in purple, **4n** in cyan and **4o** in gray). The surface pocket for the 2-aminoanilide moiety is highlighted in atom type coloring. Residue enumeration was taken by the Q13547 accession from UniProtKB protein

For selected 1-4 derivatives, IC<sub>50</sub> values against HDAC1, HDAC4, and HDAC6 were determined (Table 9). Among them, **1k** is 65- and 41-fold more potent to inhibit HDAC1 than HDAC4 and HDAC6, respectively, whereas **3f** and **3g**, as well as the HDAC4. Finally, the anilides **4o** and, to a lesser extent, **4n** show privileged HDAC1 inhibition.

### 5.2.3. Molecular Modeling and Docking Studies.

All the representing compounds of the titled derivatives **1-4** are able to inhibit HDAC1 with an

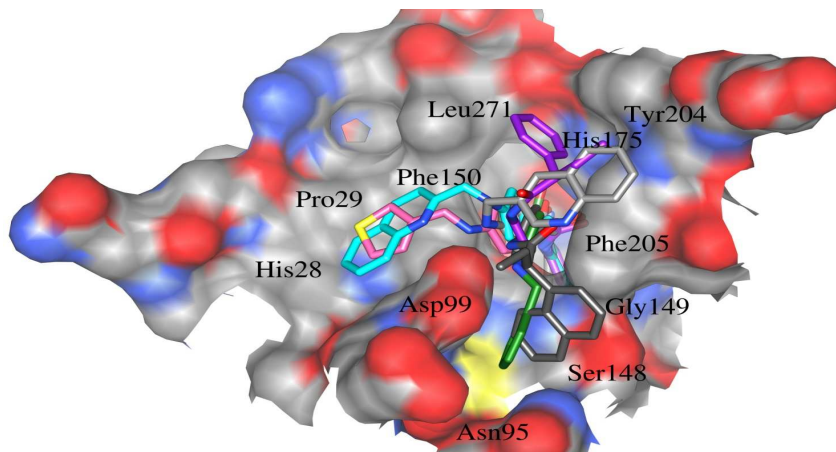
activity from 30 to 1000 times stronger than against HDAC4. In order to get some insights on the HDAC1 selectivity, the **1k**, **2c**, **3f**, **3g**, **4n**, and **4o** binding modes were analyzed in both human HDAC1 (modeled from HDAC2 co-crystallized with *N*-(4-aminobiphenyl-3-yl)benzamide<sup>142</sup>, pdb entry code 3max) and human HDAC4<sup>143</sup>, (pdb entry codes: 2vqj and 2vqm) by the means o



**Figure 24.** Ligands/HDAC1 interactions along the enzyme channel. In turquoise are displayed the residues within 3.5 Å from anilide/aniline (CU+connected Ph) groups. In the left side are reported the hydroxamates (**1k** in gray, **3f** in purple and **3g** in cyan) and in the right window are depicted the 2-aminoanilides ((*S*)-**2c** in magenta, (*R*)-**2c** in purple, **4n** in cyan and **4o** in gray). The surface for  $\pi$ - $\pi$  stacking is highlighted in atom type coloring. Residue enumeration was taken by the Q13547 accession from UniProtKB protein sequence database, (<http://www.uniprot.org>) The gray sphere represents the catalytic zinc ion

Autodock 4.2. Into the modelled HDAC1 both the hydroxamate (**1k**, **3f** and **3g**) and 2- aminoanilide (**2c** [both enantiomers], **4n** and **4o**) representative derivatives showed interactions and binding conformations similar to those of the reference experimental bound compounds (TSA, taken from the HDAC8 co-complex, pdb code 1t64, and *N*-(4-aminobiphenyl- 3-yl)benzamide from the HDAC2 co-complex, pdb code 3max; Figure 23). Among the ligand/enzyme interactions, for hydroxamates (**1k**,

**3f** and **3g**) the zinc ion chelation is the inhibition driving force, while for the weaker zinc chelating 2-aminoanilides (**2c**,



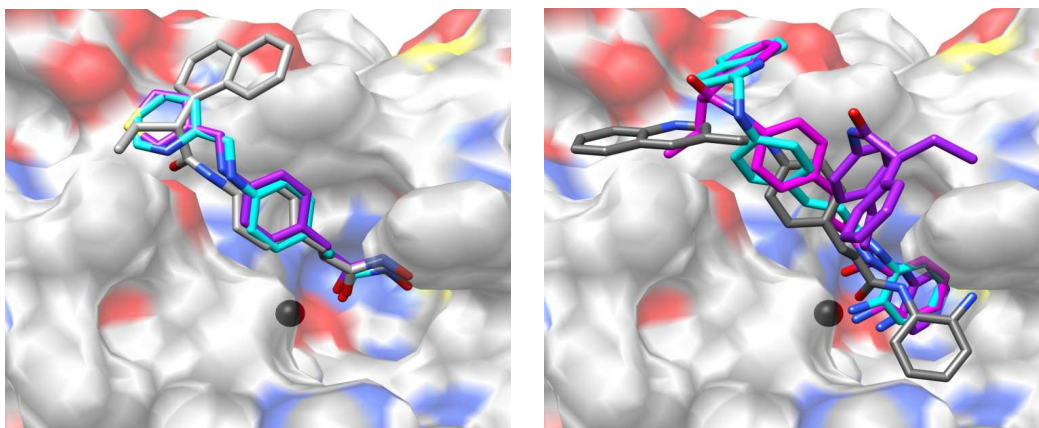
**Figure 25.** Ligands/HDAC1 interactions around the rim of the HDAC1 substrate entrance. In turquoise are displayed all the residues within 3.5 Å from the inhibitor CAP groups. In the figure are reported both the hydroxamates (1k in dark gray, 3f in pink and 3g in green) and the 2-aminoanilides (*R*)-2c in purple, 4n in cyan and 4o in light gray). The surface of HDAC1 is in atom type coloring. Residue enumeration was taken by the Q13547 accession from UniProtKB protein sequence database, (<http://www.uniprot.org>).

**4n** and **4o**) further interactions are visible in a pocket formed by His140, Gly149, Cys151 and Gly300 (Figure 24), at the beginning of the 14 Å acetate escape tunnel<sup>144</sup>.

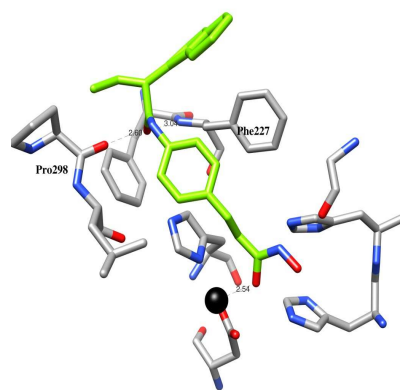
Nevertheless, others moieties play some roles in the inhibition potency, and in

particular all the anilide/aniline (CU+connected phenyl group) moieties establish  $\pi$ - $\pi$  interactions with the HDAC1's Phe150 and Phe205, while electrostatic interactions are placed between HDAC1-Asp99 and the anilide/aniline nitrogen atom (Figure. 24). Regarding the CAP groups, although no interaction seems to be relevant for the inhibition potency, at a deeper interaction modes: a TSA-like mode, shared by **3f** and **4n**, where the dimethylaminophenyl (TSA), inspection the most active derivatives (**1k**, **3f**, **3g** and **4n**) show that there are two preferred CAP the 3-thienyl (**3f**) and the 2-quinoliny (**4n**) groups fit into a large cleft paved mainly by main and side chains of His28, Pro29,

**Figure 26.** HDAC4 Autodock proposed binding modes for the representative hydroxamates (left: **1k** in gray, **3f** in purple and **3g** in cyan) and 2-aminoanilides (right: (*S*)-**2c** in magenta, (*R*)-**2c** in purple, **4n** in cyan and **4o** in gray). The gray sphere represents the catalytic zinc ion.



Asp99 and Phe150 residues, and a narrow canyon delimited by Asn95, Asp99, Ser148, Gly149 and Phe205 where the **1k** naphthylethylmethyl and the **3g** pyridylmethyl groups fulfill the available space. On the other hand less active compounds, such as **2c** and **4o**, although structurally related, were docked by Autodock with a different mode, in which the phenylethylmethyl (**2c**) and the 3-quinoliny (**4o**) moieties are lying on a wide opened area described by His175, Tyr204 and Leu271 (Figure 26). Differently from HDAC1, HDAC4 shows a wider substrate binding channel partially deprived of the acetate escape tunnel<sup>145</sup>, at the side of the zinc ion. This lack prevents the 2-aminoanilide derivatives to reach effective chelating distances thus lowering the activity against HDAC4 (Figure 25). The open wide



**Figure 27.** Binding mode of derivative **1k** (green) into HDAC4

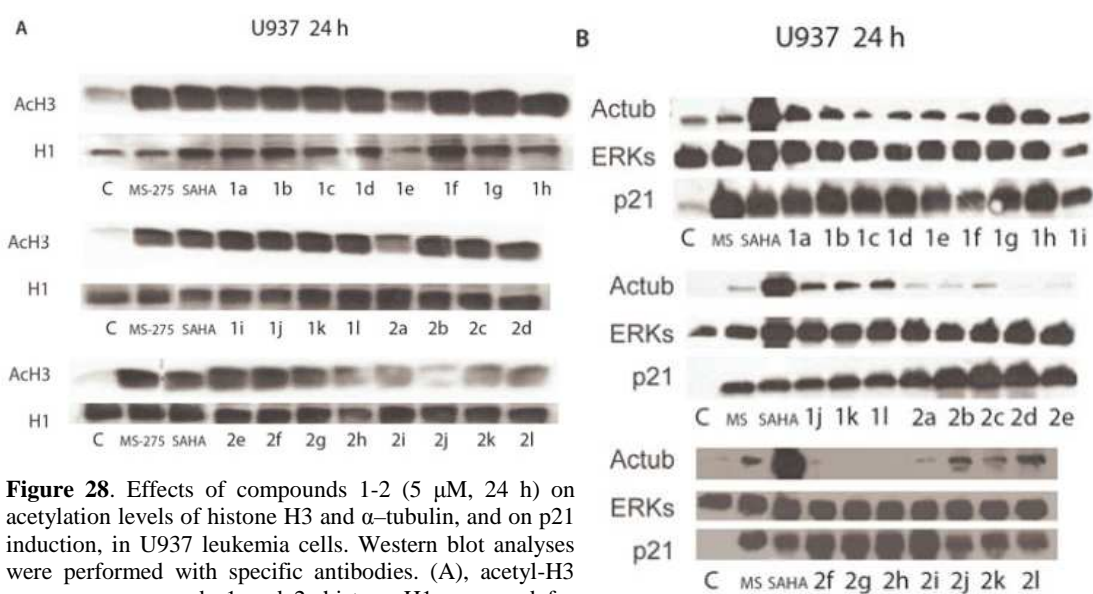
shape of the HDAC4 catalytic tunnel also has some negative influence for the hydroxamate series. The missing  $\pi$ - $\pi$  sandwich, observed for HDAC1, prevents the inhibitors to be anchored to the tunnel, and the hydroxamate functions to properly chelate the zinc ion. Similarly as reported for the cocrystal structure 2vqm, only the hydroxamate carbonyl groups showed the needed distances to make electrostatic type interactions with the zinc ion, whereas the hydroxyl groups are on the average 5 Å away from the metal ion. Interestingly, among the tested derivatives in Table 9, **1k** displayed the highest activity. A deeper inspection of **1k** Autodock binding mode revealed that the central amide makes two strong hydrogen bonds with Phe227 and Pro298 (Figure 27), that in some way compensates the lack of a full zinc ion chelation.

#### **5.2.4. Effects on Acetylation Level of Histone (Histone H3) and Non-Histone ( $\alpha$ -Tubulin) Substrates. p21 Induction.**

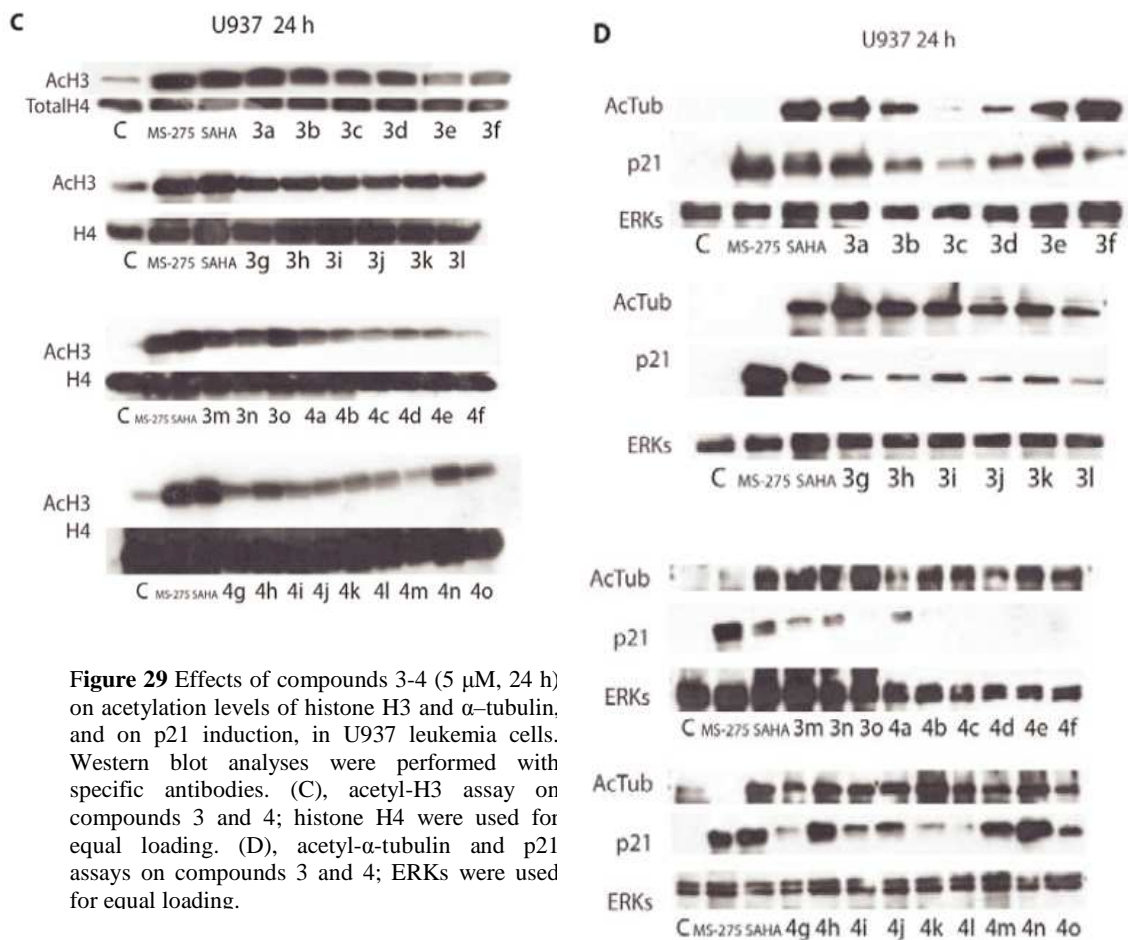
In order to determine the effects on the acetylation levels of histone H3 and  $\alpha$ -tubulin for compounds **1-4**, all of them were tested at 5  $\mu$ M for 24 h on human leukemia U937 cells and western blot analyses were performed with specific antibodies using SAHA and MS-275 as reference drugs. In the above conditions, the acylamino hydroxamates **1** as well as most of the related 2-aminoanilides **2** (see compounds **2a-g,k,l**) were able to increase the acetylation levels of histone H3, having fair correlation with their HDAC1 inhibition activities (Figure 28 A). Only few hydroxamates from the **1** series (**1a**, **1g**, and **1h**) and none 2-aminoanilide from the **2** series were able to induce high acetylation of  $\alpha$ -tubulin (Figure 28 B), suggesting a general low or no inhibitory activity of the above derivatives against HDAC6. Differently, among the arylmethylamino cinnamyl compounds **3** and **4**, in general all of them gave an increase of both the acetyl-histone H3 and acetyl- $\alpha$ -tubulin levels, with no difference of the substrate used (Figures 29 C and 29 D). In particular, **3f-i**, **3m-o**, and **4k** were been able to give an increase of  $\alpha$ -tubulin acetylation higher than SAHA. p21 is a cell cycle inhibitor.

Typically the increase of expression of p21 is an effect reported mainly for I HDAC inhibitors<sup>146, 147</sup>. So in order to get some insights on the HDAC1 selectivity, western blot was performed.

Figure 28 B shows that, in general, both the hydroxamates **1** and the 2- aminoanilides **2** gave a high induction of p21, compounds **2** being in many cases (**2b-i**) more efficient than MS-275 and SAHA in the tested conditions. Conversely, the arylmethylaminocinnamyl hydroxamates **3** showed weak p21 induction, lower than SAHA and MS-275, with the exception of **3a** and **3e**, that gave a high signal. The arylmethylaminocinnamyl anilides **4** were, in general, unable to induce p21 in these conditions, with the remarkable exception of **4h**, **4m**, and **4n**, that showed a p21 induction level higher than (**4h** and **4n**) or similar as (**4m**) those obtained with MS-275 and SAHA (Figure 29 D).



**Figure 28.** Effects of compounds 1-2 (5  $\mu$ M, 24 h) on acetylation levels of histone H3 and  $\alpha$ -tubulin, and on p21 induction, in U937 leukemia cells. Western blot analyses were performed with specific antibodies. (A), acetyl-H3 assay on compounds 1 and 2; histone H1 was used for equal loading. (B), acetyl- $\alpha$ - tubulin and p21 assays on compounds 1 and 2; ERKs were used for equal loading.

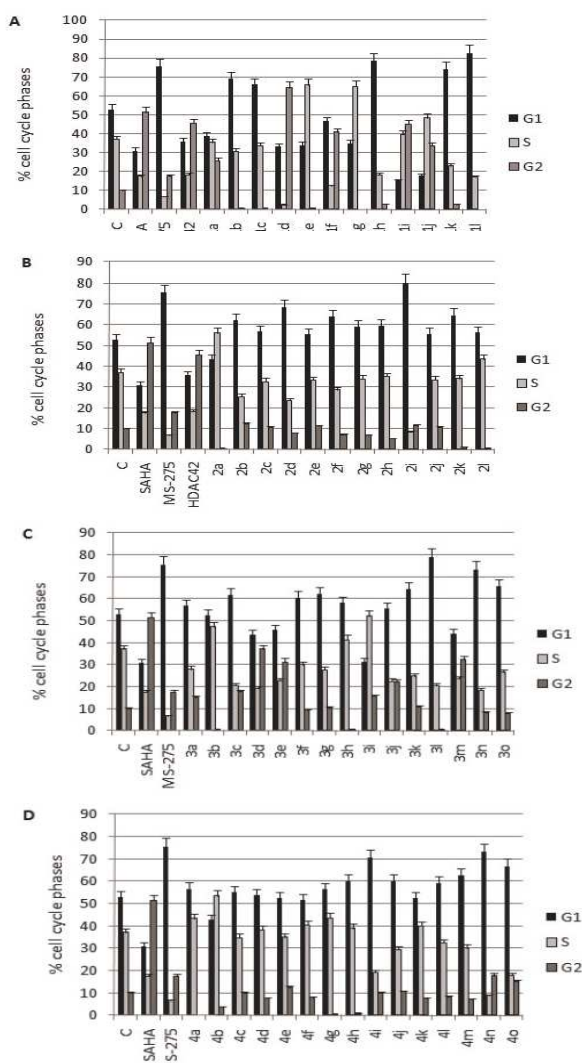


**Figure 29** Effects of compounds 3-4 (5  $\mu$ M, 24 h) on acetylation levels of histone H3 and  $\alpha$ -tubulin, and on p21 induction, in U937 leukemia cells. Western blot analyses were performed with specific antibodies. (C), acetyl-H3 assay on compounds 3 and 4; histone H4 were used for equal loading. (D), acetyl- $\alpha$ -tubulin and p21 assays on compounds 3 and 4; ERKs were used for equal loading.

### 5.2.5. Cell Cycle Analysis, Apoptosis Induction, Granulocytic

All the compounds **1-4** were tested in the human U937 leukemia cell line in order to determine their





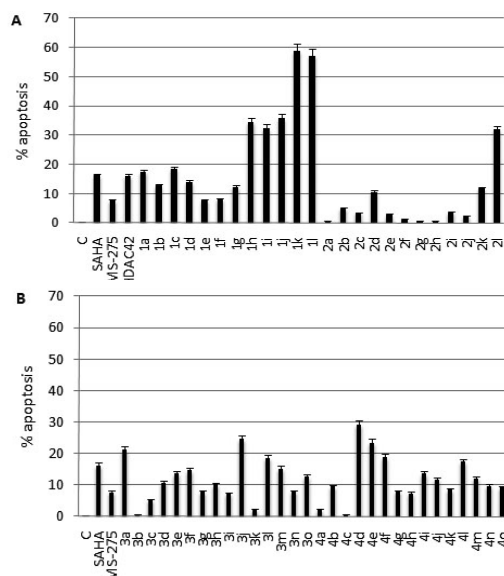
**Figure 30.** Cell cycle analysis on U937 leukemia cells treated with compounds **1-4** at 5  $\mu$ M for 30 h.

effects on cell cycle, apoptosis induction, granulocytic differentiation, and antiproliferative activity. SAHA, MS-275, and/or HDAC42 were used as reference drugs. All the compounds were tested at 5  $\mu$ M for 30 h.

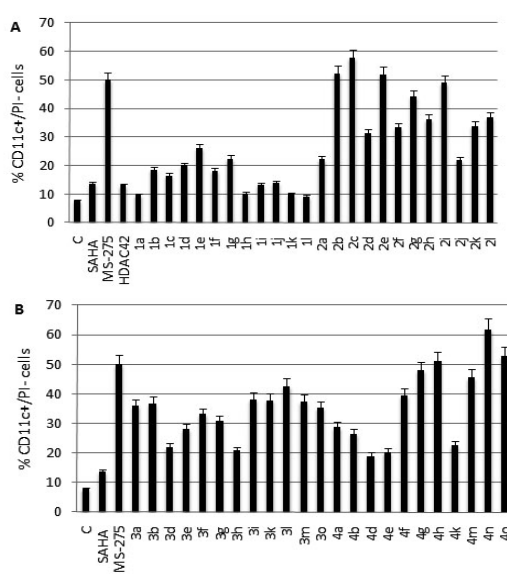
In general all the compounds showed an arrest of the cell cycle of U937 cells either at G2/M or G1/S phase, according to a general behaviour shown by the treatment of cancer cells with HDACi (Figure 30)<sup>148, 149</sup>. In particular, some of the tested hydroxamates gave a block at the G2/M phase (including SAHA and HDAC42), others showed a cell cycle arrest at the G1/S phase. Differently, the 2-aminoanilide derivatives **2** and **4**, as well as MS-275, when altered the cell cycle, they always provided a block at the G1/S phase

The induction of apoptosis was evaluated by caspase 3-7 activation (Figure 31). After treatment of U937 cells with **1-4** at 5  $\mu$ M for 30 h, some hydroxamates

belonging to the **1** series (**1h-l**) furnished the highest percent of apoptosis, higher than those obtained with SAHA and HDAC42 in this assay. In particular, **1k** and **1l** carrying as a CAP+CU group the 2-(1- and 2- naphthyl)butyrylamino moieties, induced high, dose-dependent apoptosis more efficiently



**Figure 31.** Apoptosis induction on U937 leukemia cells by compounds 1-4, tested at 5 μM for 30 h.



**Figure 32.** Cytodifferentiation activity (evaluated as % of CD11c positive/PI negative cells) given by compounds 1-4 (5 μM, 30 h) on U937 leukemia cells.

than SAHA, used as reference drug (Figure 34).

The percent of apoptosis obtained with the other compounds active in this test was higher than (see, for example, **2l** and **4d**) or similar as that observed with SAHA (**1a**, **1c**, **3a**, **3j**, **3l**, **3m**, **4e**, **4f**, and **4l**). The benzamide MS-275 showed a modest apoptosis induction (7.7%) in this setting. The hydroxamates **1k** and **1l** as well as the 2-aminoanilides **2c** and **4n** were tested at 5 μM in U937 cells to evaluate their effects on cell proliferation (Figure 33) using SAHA (5 μM) as reference drug. The

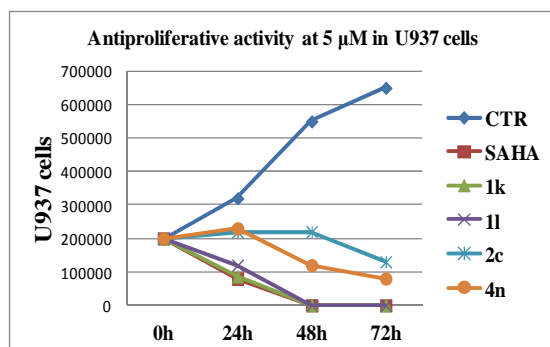


Figure 33. Antiproliferative activity at 5 μM in u937 cells

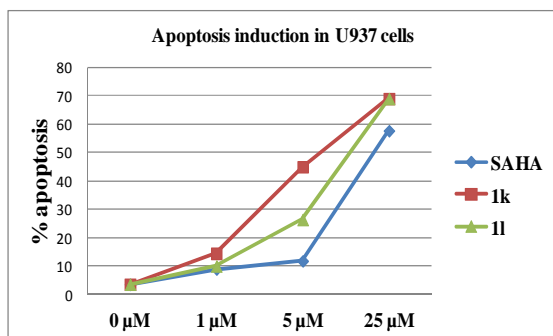


Figure 34 Dose dependent apoptosis induction in U937

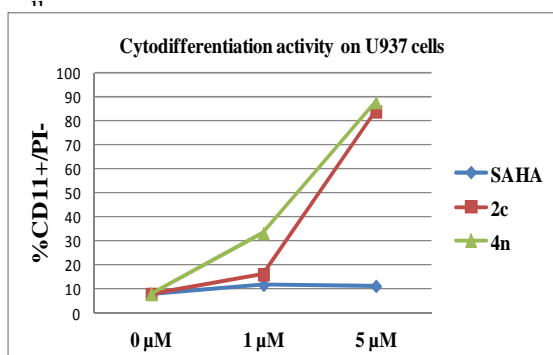
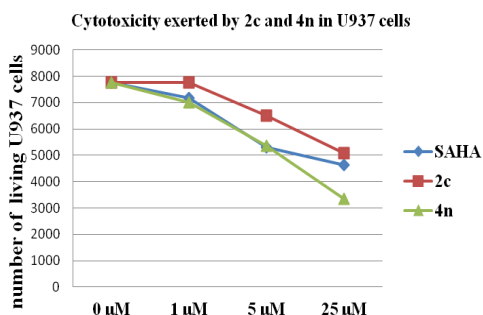


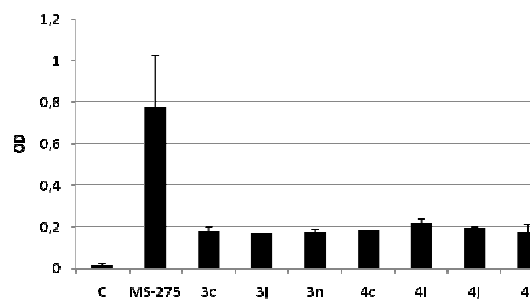
Figure 35. Cytodifferentiation activity on U937 cells

cells were counted with Trypan Blue dye every 24 h for 3 days. **1k** and **1l** and, to a lesser extent, **4n** and **2c** showed to give a dose dependent arrest of the cell proliferation stronger than SAHA.

The increased expression of the surface antigen CD11c was used as a marker of granulocytic differentiation in U937 leukemia cells. The cells were treated with compounds **1-4** at 5 μM for 30 h, and then the percent values of CD11c positive/propidium iodide (PI) negative cells were determined (Figure 32). In these conditions, the majority of the 2-aminoanilide derivatives (series 28 and 4) showed interesting (around 50% of CD11c+/PI- cells) cytodifferentiation properties, similarly as that observed with MS- 275. In particular, **2b**, **2c**, **2e**, and **2i** (bearing as a CAP+CU a methyl-, ethyl-, and *iso*-propyl substitution at the phenylacetyl amino moiety, or a 1-naphthylacetyl amino group, respectively), as well as **4g**, **4h**, **4n**, and **4o** (showing the



**Figure 36.** Cytotoxicity exerted by 2c and 4n in U937 cells



**Figure 37.** NBT test performed on selected 3 and 4 derivatives.

2- and 3-pyridyl or the 2- or 3-quinolinyl ring as a CAP, respectively), furnished values of CD11c+/PI- cells similar as or higher than that of MS-275. Dose-response curves were generated for the top scoring compounds **2c** and **4n**, obtaining dose-dependence differentiation activity from 1 to 5 μM (Figure 34), while at 25 μM a lesser number of CD11c+/PI- cells was registered, probably due to cytotoxicity problems (Figure 36).

Among the hydroxamates **1** and **3**, the majority of those from the **3** series furnished a differentiating activity ranging from 30 to 40% of CD11c+/PI- cells, whereas those from the **1** series were less active. Due to their intense coloration, some compounds could not be tested in the CD11c assay. Thus, they were tested on U937 cells at 5 μM for 30 h by using the Nitro-tetrazolium Blue (NBT) assay, a general test for differentiation of cells. All the tested compounds (**3c**, **3j**, **3n**, **4c**, **4i**, **4j**, and **4l**) were less efficient than MS-275 in this test to induce cell differentiation (Figure 37).

### 5.3. Materials and methods

Melting points were determined on a Buchi 530 melting point apparatus and are uncorrected. Infrared (IR) spectra (KBr) were recorded on a Perkin-Elmer Spectrum One instrument. <sup>1</sup>H NMR spectra were recorded at 400 MHz on a Bruker AC 400 spectrometer; chemical shifts are reported in δ (ppm)

units relative to the internal reference tetramethylsilane (Me<sub>4</sub>Si). All compounds were routinely checked by TLC and <sup>1</sup>H NMR. TLC was performed on aluminumbacked silica gel plates (Merck DC, Alufolien Kieselgel 60 F254) with 9 spots visualized by UV light. All solvents were reagent grade and, when necessary, were purified and dried by standard methods. Concentration of solutions after reactions and extractions involved the use of a rotary evaporator operating at reduced pressure of ca. 20 Torr. Organic solutions were dried over anhydrous sodium sulphate. Analytical results are within ±0.40% of the theoretical values. A SAHA sample for biological assays was prepared as previously reported<sup>150</sup>. MS-275 and HDAC42 were synthesized according to the literature<sup>151, 124</sup>. All chemicals were purchased from Aldrich Chimica, Milan (Italy), or from Lancaster Synthesis GmbH, Milan (Italy), and were of the highest purity.

### 5.3.1. Experimental section

#### **h**

**5.3.1.1.1. General Procedure for the Synthesis of Ethyl 3-(4- Acylaminophenyl)-2-propenoates (5a-n). Ethyl 3-[4-(2- Phenylbutyryl)aminophenyl]-2-propenoate (5c).** 2-Phenylbutyryl chloride (7.32 mmol, 1.33 g) and triethylamine (15.22 mmol, 2.12 mL) were added to a solution of ethyl 3-(4-aminophenyl)-2-propenoate hydrochloride<sup>[43]</sup> (6.1 mmol, 1.39 g) in dry dichloromethane (20 mL) at 0 °C. After stirring at room temperature for 4 h, the reaction mixture was poured into water (50 mL), the organic layer was separated, and the aqueous one was extracted with chloroform (2 × 50 mL). The combined organic solution was washed with water (100 mL) and brine (100 mL), and was dried and evaporated to dryness. The residual solid was purified by crystallization from cyclohexane to yield the pure 5c. <sup>1</sup>H NMR (CDCl<sub>3</sub>) δ 0.93 (m, 3H, CH<sub>2</sub>CH<sub>3</sub>), δ 1.32 (m, 3H, OCH<sub>2</sub>CH<sub>3</sub>), δ 1.85-2.25 (m, 2H, CH<sub>2</sub>CH<sub>3</sub>), δ 3.40 (m, 3H, PhCHCO), δ 4.25 (OCH<sub>2</sub>CH<sub>3</sub>), δ 6.34

(d, 1H, PhCH=CHCOOEt),  $\delta$  7.26-7.49 (m, 9H, benzene protons),  $\delta$  7.60 (d, 1H, PhCH=CHCOOEt).

**5.3.1.1.2. General Procedure for the Synthesis of 3-(4-Acylaminophenyl)-2-propenoic Acids (6a-n). 3-[4-(2-Phenyl-4-pentenoylamino)phenyl]-2-propenoic Acid (6f):** A mixture of ethyl 3-[4-(2-phenyl-4-pentenoylamino)phenyl]-2-propenoate 5f (0.57 mmol, 0.20 g), lithium hydroxide hydrate (1.14 mmol, 0.048 g), and tetrahydrofuran (15 mL) was stirred at room temperature. After 24 h, 2 N HCl was added to the mixture until the pH was 5, and the obtained solid was filtered and recrystallized to yield pure 6f. <sup>1</sup>H NMR (DMSO-d<sub>6</sub>)  $\delta$  2.48-2.76 (m, 2H, CH<sub>2</sub>CH=CH<sub>2</sub>),  $\delta$  3.50 (m, 1H, PhCHCO),  $\delta$  5.00 (m, 2H, CH<sub>2</sub>CH=CH<sub>2</sub>),  $\delta$  5.72 (m, 1H, CH<sub>2</sub>CH=CH<sub>2</sub>),  $\delta$  6.35 (d, 1H, PhCH=CHCOOEt),  $\delta$  7.31-7.60 (m, 10 H, benzene protons and PhCH=CHCOOEt),  $\delta$  10.30 (s, 1H, CONHPh).

**5.3.1.1.3. General Procedure for the Synthesis of the 3-(4-Acylaminophenyl)-N-hydroxy-2-propenamides (1a-n) and the 3[4-(Arylalkylamino)phenyl]-N-hydroxy-2-propenamides (3a-o). 3-[4-(2,3-Diphenylpropionyl)aminophenyl]-N-hydroxy-2-propenamide (1h):** Ethyl chloroformate (1.26 mmol, 0.12 mL) and triethylamine (1.37 mmol, 0.19 mL) were added to a cooled (0 °C) solution of 3-[4-(2,3-diphenylpropionyl)aminophenyl]-2-propenoic acid 6h (1.05 mmol, 0.39 g) in dry THF (10 mL), and the mixture was stirred for 10 min. The solid was filtered off, and *O*-(2-methoxy-2-propyl)hydroxylamine (3.15 mmol, 0.23 mL) was added to the filtrate. The solution was stirred for 15 min at 0 °C, then was evaporated under reduced pressure, and the residue was diluted in methanol (10 mL). Amberlyst 15 ion-exchange resin (105 mg) was added to the solution of the *O*-protected hydroxamate, and the mixture was stirred at room temperature for 1 h. Afterwards, the reaction was filtered and the filtrate was concentrated in vacuo to give the crude 1h, which was purified by crystallization. <sup>1</sup>H NMR (DMSO-d<sub>6</sub>)  $\delta$  3.05 (m, 1H, PhCH<sub>2</sub>),  $\delta$  3.60 (m, 1H, PhCH<sub>2</sub>),  $\delta$  3.75 (m, 1H, PhCHCO),  $\delta$  6.36 (d, 1H, PhCH=CHCOOEt),  $\delta$  7.15-7.70 (m, 15H, benzene protons and PhCH=CHCOOEt),  $\delta$  9.00 (s, 1H, OH),  $\delta$  10.23 (s, 1H,

CONHPh),  $\delta$  10.85 (s, 1H, NHOH).

**5.3.1.1.4. General Procedure for the Synthesis of the N-(2-Aminophenyl)-3-(4-acylamino)phenyl-2-propenamides (2a-l) and the N-(2-Aminophenyl)-3-[4-(arylamino)phenyl]acrylamide (4a-o).** **N-(2-Aminophenyl)-3-[4-(quinolin-2-ylmethylamino)phenyl]acrylamide (4n):** Triethylamine (1.96 mmol, 0.27 mL) and BOP reagent (0.59 mmol, 261 mg) were added under nitrogen atmosphere to a solution of compound 8n (0.49 mmol, 0.15 mg) in dry DMF (5 mL), and the resulting mixture was stirred for 30 min. After this time, 1,2-phenyldiamine (0.49 mmol, 0.053 mg) was added and the stirring was continued for further 30 min. The reaction was quenched by water (30 mL) and the precipitate was filtered, washed with water (3  $\times$  30 mL) and dried. The solid residue was chromatographed on silica gel eluting with ethyl acetate/chloroform 1/1 to provide the desired compound 4n, that was recrystallized by acetonitrile/methanol. <sup>1</sup>H NMR (DMSO-*d*<sub>6</sub>)  $\delta$  4.56-4.58 (d, 2H, ArCH<sub>2</sub>NH), 4.86 (s, 1H, PhNH<sub>2</sub>), 6.52-6.56 (m, 2H, aniline protons), 6.63-6.65 (d, 2H, benzene protons), 6.68-6.70 (d, 1H, PhCH=CHCONHPh), 6.80 (t, 1H, aniline proton), 7.01 (t, 1H, aniline proton), 7.28-7.35 (m, 4H, benzene protons, PhCH=CHCONHPh and ArCH<sub>2</sub>NH), 7.54-7.73 (m, 2H, quinoline protons), 7.90 (t, 1H, quinoline proton), 7.96 (d, 1H, quinoline proton), 8.29 (d, 1H, quinoline proton), 9.14 (s, 1H, PhNHCO).

**5.3.1.1.5. General Procedure for the Synthesis of Ethyl 3-[4-(Arylmethylamino)phenyl]-2-propenoates (7a-o).** **Ethyl 3-[4-(Benzofuran-2-ylmethylamino)phenyl]-2-propenoate (7k):** Ethyl-4-aminocinnamate (7.52 mmol, 1.44 g) and acetic acid (1 mL) were added to a solution of benzofuran-2-carboxaldehyde (6.84 mmol, 1.0 g) in methanol (10 mL), and the resulting mixture was stirred at room temperature for 1 h. Then the mixture was cooled at 0 °C, and sodium cyanoborohydride (13.68 mmol, 0.80 g) was added. After 30 min, the solvent was removed and the residue was eluted with water (50 mL) and extracted with ethyl

acetate (3 × 30 mL). The organic layers were washed with sodium chloride solution (3 × 30 mL), dried with sodium sulphate and concentrated. The organic residue was chromatographed on silica gel eluting with ethyl acetate/*n*-hexane 1/5, to afford the pure product **7k** as a yellow solid that was recrystallized by cyclohexane. <sup>1</sup>H NMR (CDCl<sub>3</sub>) δ 1.28-1.32 (t, 3H, CH<sub>2</sub>CH<sub>3</sub>), δ 4.19- 4.24 (q, 2H, OCH<sub>2</sub>CH<sub>3</sub>), δ 4.47 (s, 1H, ArCH<sub>2</sub>NH), δ 4.49 (m, 3H, ArCH<sub>2</sub>NH and ArCH<sub>2</sub>NH), δ 6.18-6.22 (d, 1H, PhCH=CHCO), δ 6.59 (s, 1H, benzofuran protons), δ 6.64-6.66 (d, 2H, benzene protons), δ 7.18-7.24 (m, 2H, benzofuran protons), δ 7.35-7.37 (d, 2H, benzene protons), δ 7.41-7.43 (d, 1H, benzofuran protons), δ 7.47-7.49 (d, 1H, benzofuran protons), δ 7.55-7.59 (d, 1H, PhCH=CHCO).

**5.3.1.1.6. General Procedure for the Synthesis of 3-[4- (Arylalkylamino)phenyl]-2-propenoic Acids (8a-o). 3-[4-(3- Pyridylmethylamino)phenyl]-2-propenoic acid (8h):**

A mixture of **7h** (1.42 mmol, 0.4 g), 2 N KOH (5.68 mmol, 0.32 g, 2.84 mL), and ethanol (15 mL) was stirred at room temperature overnight. Afterward, the solution was poured into water (50 mL) and extracted with ethyl acetate (3 × 20 mL). 2 N HCl was added to the aqueous layer to reach pH 5, and the obtained precipitate was filtered and dried to give the pure compound **8h**, which was recrystallized by acetonitrile. <sup>1</sup>H NMR (DMSO-*d*<sub>6</sub>) δ 4.33 (s, 1H, ArCH<sub>2</sub>NH), δ 6.09-6.13 (d, 1H, PhCH=CHCOOH), δ 6.56-6.58 (d, 2H, benzene protons), δ 6.85-6.88 (t, 1H, ArCH<sub>2</sub>NH), δ 7.29-7.40 (m, 4H, benzene protons, PhCH=CHCOOH, pyridine proton), δ 7.68-7.70 (d, 1H, pyridine proton), δ 8.40-8.42 (d, 1H, pyridine proton), δ 8.53-8.54 (s, 1H, pyridine proton), δ 11.9 (s, 1H, COOH).



HPLC enantioseparations were performed by using stainless-steel Chiralpak IA (250 x 4.6 mm I.D. and 250 x 10 mm I.D.) (Daicel, Chemical Industries, Tokyo, Japan) columns. HPLC-grade solvents were supplied by Carlo Erba (Milan, Italy). HPLC apparatus consisted in a Perkin Elmer (Norwalk, CT, USA) 200 lc pump equipped with a Rheodyne (Cotati, CA, USA) injector, a HPLC Dionex (CA,



USA) Model TCC-100 oven and a Jasco (Jasco, Ishikawa-cho, Hachioji City, Tokyo, Japan) Model 2095 Plus UV/CD detector. The sign of optical rotation was on-line monitored by using a Perkin-Elmer polarimeter model 241 equipped with Hg/Na lamps and a 40  $\mu$ l flow-cell. The mobile phases were filtered and degassed by sonication immediately before using. In analytical enantioseparations, standard solutions were prepared by dissolving 1-3 mg of sample, into 10 ml of mobile phase. The injection volume was 10-20  $\mu$ l. In semipreparative enantioseparation a 1 mL sample loop was used. After 10 semipreparative separation, the collected fractions were analyzed by chiral analytical columns to determine their enantiomeric excess (ee). The column hold-up time ( $t_0 = 3.0$  min for the 250 x 4.6 mm i.d. column) was determined from the elution of an unretained marker (toluene), using ethanol as eluent, delivered at a flow-rate of 1.0 mL/min. The mobile phase and the corresponding analytical chromatographic data for each resolved compound are summarized as follows: **1b**: *n*-hexane- ethyl acetate-ethanol-trifluoroacetic acid 80/20/10/0.1 (v/v/v/v),  $k_1 = 1.48$ ,  $\alpha = 1.36$ ,  $R_s = 3.23$ ; **1c**: *n*-hexane-ethyl acetate-ethanoltrifluoroacetic acid 80/20/10/0.1 (v/v/v/v),  $k_1 = 1.26$ ,  $\alpha = 1.61$ ,  $R_s = 4.05$ ; **2c**: *n*-hexane-ethanol 30/70 (v/v),  $k_1 = 0.73$ ,  $\alpha = 1.66$ ,  $R_s = 3.89$ .  $k_1$ : retention factor of the first eluted enantiomer, defined as  $(t_1 - t_0)/t_0$  where  $t_0$  is the void time of the column;  $\alpha$ : enantioselectivity factor defined as  $k_2/k_1$ ;  $R_s$ : resolution factor defined as  $2(t_2-t_1)/(w_1+w_2)$  where  $t_1$  and  $t_2$  are retention times and  $w_1$  and  $w_2$  are band widths at the baseline in time units. Other analytical chromatographic conditions: flow-rate, 1.0 mL/min; temperature, 25 °C; detector: UV at 300 nm. Specific rotations were measured at 589 nm by a Perkin-Elmer polarimeter model 241 equipped with a Na lamp. The volume of the cell was 1 ml and the optical path was 10 cm. The system was at a temperature of 20°C by a Neslab RTE 740 cryostat. The circular dichroism (CD) spectra of the enantiomers of **1b** and **1c**, dissolved in ethanol, in a quartz cell (0.1 cm-path length) at 25°C, were measured by using a Jasco Model J-700 spectropolarimeter. The spectra are average computed over three instrumental scans and the intensities are presented in terms of ellipticity values

(mdeg).



All molecular modeling software run on Beowulf cluster running the operating system is GNU/Linux Debian 5.0-Lenny using MPI (Message Passing Interface) libraries for parallel processes. *HDAC1 model preparation.* HDAC1 structure was prepared using the deposited sequence in the Universal Protein Resource<sup>152</sup>. (UniProt) (entry code Q13547) The homology model was automatically obtained by feeding the The Protein Model Portal (PMP) Server<sup>153</sup> with the above sequences. The PMP returned a HDAC1 model made using the HDAC2/N-(4-aminobiphenyl-3-yl)benzamide complex<sup>138</sup> chain B as template (pdb entry code 3max, 94% sequence identity). The model was then refined by AMBER 8.0 program using the following protocol. First, the experimental bound conformation of N-(4-aminobiphenyl-3-yl)benzamide as found in the template was merged into the HDAC1 structure. AM1-BCC charges was calculated on the ligand employing the antechamber module of Amber 8.0 using the xLeap Amber module, the starting complex was added of the hydrogen atoms and solvated in a octahedral box of TIP3P water with each box side at least 10.0 Å away from the nearest atoms of the complex. Sodium ions were included to neutralize the charge of the system. The ions were placed randomly in the system 10 Å away from the nearest atoms. The hydrogen atoms, counter ions and water molecules were then minimized for 1000 iterations. Finally the whole complex was relaxed for 5000 iterations. *HDAC4 preparation.* HDAC4 structures<sup>144</sup> were retrieved from RCSB PDB (pdb entry codes: 2vqj and 2vqm) co-crystallized with a trifluoromethylketone and a hydroxamic acid inhibitors. The structures were refined by AMBER 8 program using the previous described protocol as used for HDAC1.

*Docking procedure.* The docking studies were performed using Autodock 4.2 . The proteins, prepared

as described above, (HDAC1 and HDAC4) were aligned by means of UCSF Chimera<sup>154</sup> MatchMaker tool. The structure of the inhibitors to be docked were built by the Chemaxon sketch module<sup>155</sup>. AutoDock Tools package 1.5.4 (<http://mgltools.scripps.edu/>) was employed to generate the docking input files and to analyze the docking results; the same procedure as described in the manual was followed. A grid box size of 51 x 58 x 57 points spacing of 0.375 Å were used, centered to the bound co-crystallized inhibitors and covered most of the catalytic channels of the enzymes. Two hundred structures, i.e. 200 runs, were generated using Lamarckian genetic algorithm. A default protocol was applied, with an initial population of 150 randomly placed individuals, a maximum number of  $2.5 \times 10^6$  energy evaluations, and a maximum number of  $2.7 \times 10^4$  generations. A mutation rate of 0.02 and a crossover rate of 0.8 were used. The docking results were clustered using a 2.0 Å tolerance. In all the cases lowest energy docked conformation belonged to the most populated cluster. In the case of HDAC4 100 runs for each structure were generated (cross-Docking<sup>156</sup>) and the results of either dockings were clustered using the Autodock internal clustering algorithm.



**5.3.1.4.1. In Vitro Maize HD1-B and HD1-A Enzyme Inhibition.** Radioactively labeled chicken core histones were used as the enzyme substrate according to established procedures. Purification of maize HD1-A and HD1-B enzymes were performed in part as recently described<sup>157-160</sup>. Briefly, frozen seedlings of maize were ground to powder in a mortar. Chromatin was prepared as described<sup>161</sup> which results in a soluble cytoplasmic fraction that contains HD1-A and a “chromatin fraction” that contains HD1-B. Cytoplasmic and nuclear fractions were further separated by ion exchange chromatography (Q-Sepharose) with subsequent size exclusion chromatography (S200). Resulting protein fractions with HDAC activity were used for inhibition assays. The enzymatic activity liberated tritiated acetic acid from the substrate, which was quantified by scintillation

counting. IC<sub>50</sub> values are results of triple determinations. A 50 µL sample of partially purified endogenous (native) maize enzymes was incubated (30 min, 30 °C) with 10 µL of total [<sup>3</sup>H]acetate-prelabeled chicken reticulocyte histones (2 mg/mL). Reaction was stopped by addition of 36 µL of 1 M HCl/0.4 M acetate and 800 µL of ethyl acetate. After centrifugation (10 000 g, 5 min), an aliquot of 600 µL of the upper phase was counted for radioactivity in 3 mL of liquid scintillation cocktail. The compounds were tested at a starting concentration of 40 µM, and active substances were diluted further. SAHA and HDAC42 were used as the reference compounds, and blank solvents were used as negative controls.

**5.3.1.4.2. Fluorimetric Human Recombinant HDAC1 and HDAC4 Assays.** The HDAC Fluorescent Activity Assay for HDAC1 and HDAC4 is based on the Fluor de Lys Substrate and Developer combination (BioMol), and has been carried out according to supplier's instruction and as previously reported. First, the inhibitors and purified recombinant HDAC1 or HDAC4 enzymes have been pre-incubated at room temperature for 15 minutes before substrate addition, the Fluor de Lys Substrate, which comprises an acetylated lysine side chain. For HDAC4 assay, the HDAC4-selective, non-histone substrate reported by Lahm *et al*<sup>142</sup> has been used. Full length HDAC1 and HDAC4 with C-terminal His tag were expressed using baculovirus systems. Deacetylation sensitizes the substrates that, in the second step, treated with the developer produce a fluorophore. Fluorescence has been quantified with a TECAN Infinite M200 station. IC<sub>50</sub> data were analyzed using GraphPad Prism Software.

**5.3.1.4.3. Cellular Assays. Cell Lines and Cultures.** U937 cell line was cultured in RPMI with 10% fetal calf serum, 100 U/mL penicillin, 100 µg/mL streptomycin and 250 ng/mL amphotericin-B, 10 mM HEPES and 2 mM glutamine. U937 cells were kept at the constant concentration of 200000 cells per millilitre of culture medium.

**Ligands and Materials.** SAHA, MS-275, HDAC42, and the cinnamylbased compounds **1-4** were

dissolved in DMSO and used at 5  $\mu$ M as described <sup>162</sup>.

**5.3.1.4.4. Histone H3 and  $\alpha$ -Tubulin Acetylation in U937 Cells.** For quantification of histone H3 acetylation, 5  $\mu$ g of total histone extracts were separated on a 15% polyacrylamide gel and blotted as described <sup>162</sup>. Western blots were shown for acetylated histone H3 (Upstate), and histone H1 (Abcam) was used to normalise for equal loading. For determination of  $\alpha$ -tubulin acetylation, 25  $\mu$ g of total protein extracts were separated on a 10% polyacrylamide gel and blotted as described <sup>161</sup>. Western blots were shown for acetylated  $\alpha$ -tubulin (Sigma) and total ERKs (Santa Cruz) were used to normalise for equal loading.

**5.3.1.4.5. Determination of p21WAF1/CIP1 Induction in U937 Cells.** 100  $\mu$ g of total protein extracts were separated on a 15% polyacrylamide gel and blotted as previously described <sup>163</sup>, <sup>164</sup>. Western blots were shown for p21 (Transduction Laboratories) and total ERKs (Santa Cruz) were used to normalise for equal loading.

**5.3.1.4.6. Cell Cycle Analysis on U937 Cells.**  $2.5 \times 10^5$  cells were collected and resuspended in 500  $\mu$ L of an hypotonic buffer (0.1% Triton X-100, 0.1% sodium citrate, 50  $\mu$ g/mL propidium iodide (PI), RNase A). Cells were incubated in the dark for 30 min. Samples were acquired on a FACS-Calibur flow cytometer using the Cell Quest software (Becton Dickinson) and analysed with standard procedures using the Cell Quest software (Becton Dickinson) and the ModFit LT version 3 Software (Verity) as previously reported <sup>163</sup>. All the experiments were performed 3 times.

**5.3.1.4.7. FACS Analysis of Apoptosis on U937 Cells.** Apoptosis was measured with the caspase 3-7 detection (B-Bridge) method; samples were analysed by FACS with Cell Quest technology (Becton Dickinson) as previously reported <sup>164</sup>.

**5.3.1.4.8. Proliferation Assay on U937 Cells.** U937 cells have been cultured in 24 multiwells (Corning) at the initial dilution of 200 000 cells/mL with vehicle or with HDAC inhibitors used at the indicated concentrations. Every 24 h, living U937 cells have been counted using the Trypan Blue dye

(Sigma) for dead cells staining. The graph shows data plotted after three days. The experiment has been carried out in triplicate. In parallel, an MTT colorimetric proliferation assay (Promega) has been carried out in duplicate (data not shown) following manufacturer's instructions.

**5.3.1.4.9. Granulocytic Differentiation on U937 Cells.** Granulocytic differentiation was carried out as previously described<sup>164</sup>. Briefly, U937 cells were harvested and resuspended in 10  $\mu$ L phycoerythrineconjugated CD11c (CD11c-PE). Control samples were incubated with 10  $\mu$ L PE conjugated mouse IgG1, incubated for 30 min at 4 °C in the dark, washed in PBS and resuspended in 500  $\mu$ L PBS containing PI (0.25  $\mu$ g/mL). Samples were analysed by FACS with Cell Quest technology (Becton Dickinson). PI positive cells have been excluded from the analysis.

**5.3.1.4.10. Granulocytic Differentiation on U937 Cells: Nitroblue Tetrazolium (NBT) assay.**  $2 \times 10^6$  U937 cells were harvested and washed in 500 microL of PBS/BSA(1mg/mL). 500  $\mu$ L of 0.2% NBT (Sigma) in PBS/BSA 0.1% were added. 200 ng/mL of 12-*O*-tetradecanoylphorbol-13-acetate (TPA, Sigma) were added. After a gentle stirring, samples (**3c**, **3j**, **3n**, **4c**, **4i**, **4j**, **4l**, and MS-275 as reference drug, all at 5  $\mu$ M) were incubated at 37 °C for 30 min. The formazan deposits were dissolved with 500  $\mu$ L of lysis buffer (50% *N,N*-dimethylformamide, 20% SDS, pH 4.7). The optical density (OD) was measured at 570 nm.

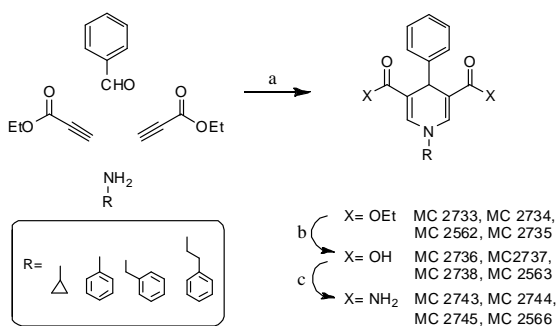
## 6. Study of 1,4-Dihydropyridine Structural Scaffold: Discovery of Novel Sirtuin Activators and Inhibitors

In regard to their roles in physiology and pathology, sirtuins are multifaceted enzymes that regulate a variety of cellular functions, from controlling gene expression and genome maintenance to longevity and metabolism<sup>165-168</sup>. Several diseases are reported being correlated to SIRT activity disfunctions. In order to find some Sirtuin modulating compounds this work, starting from the information that

nicotinamide is a micromolar SIRT inhibitor<sup>169</sup> and that iso-nicotinamide is a SIRT activator<sup>170</sup>, shows the exploration of the known scaffold 1,4-dihydropyridinic ring, obtained for the simpler pyridinic ring. Using a three-component (aliphatic/aromatic amine, ethyl propiolate, and benzaldehyde), one-pot reaction, I prepared some 3,5-dicarbethoxy-, 3,5-dicarboxy-, and 3,5-dicarboxamido-4-phenyl-1,4-dihydropyridines **1a-d**, **2a-d**, and **3a-d**, respectively. All of them were tested against human SIRT1, SIRT2, and SIRT3.




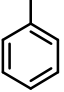
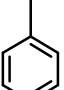
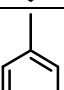
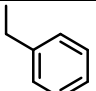
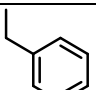
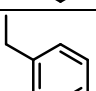
## 6.1. Chemistry

The 3,5-dicarbethoxy-4-phenyl-1,4-dihydropyridines **1a-d** were prepared by cyclocondensation between benzaldehyde, ethyl propiolate and the opportune amine, heated at 80 °C in glacial acetic acid. Furthermore, compounds **1a-d** underwent alkaline hydrolysis at 80 °C in ethanol to furnish the corresponding 3,5-dicarboxy derivatives **2a-d**. Finally, these last compounds reacted with triethylamine, benzotriazole-1-yl-oxytris(dimethylamino)phosphonium hexafluorophosphate (Bop reagent), and 33% aqueous ammonia under N<sub>2</sub> atmosphere to give the 3,5-diamides **3a-d** (Scheme 2). Among the synthesized derivatives, compounds **1b**, **1c**, and their corresponding acids **2b** and **2c** are known in the literature (**1b** and **2b**<sup>171</sup>, **1c**,<sup>172</sup> **2c**<sup>173</sup>). Chemical and physical data for compounds **1-3** are reported in Table 11.

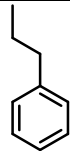
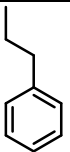
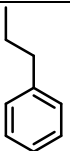


**Scheme 2.** a: CH<sub>3</sub>COOH, 80°C; b: 5N KOH, EtOH, 80°C; c: 1) Et<sub>3</sub>N, Bop Reagent, dry DMF, r.t., 30 min., N<sub>2</sub> atmosphere, 2) 33% aqueous NH<sub>3</sub>, dry DMF, r.t., 30 min., N<sub>2</sub> atmosphere.

**Table 11.** Chemical and physical data for compounds 1-3

Compounds	R	X	M. P. (°C)	Recrystallization solvent	Yield (%)
MC 2733		OEt	100-102	cyclohexane	75
MC 2736		OH	220-222	methanol	87
MC 2743		NH <sub>2</sub>	>250	methanol	72
MC 2734		OEt	143-145	Cyclohexane/benzene	60
MC2737		OH	240-242	methanol	83
MC 2744		NH <sub>2</sub>	194-196	Acetonitrile/methanol	69
MC 2562		OEt	139-141	Cyclohexane/benzene	78
MC 2563		OH	191-193	Acetonitrile/methanol	86
MC 2566		NH <sub>2</sub>	>250	methanol	74



MC 2735		OEt	91-93	cyclohexane	68
MC 2738		OH	218-220	Acetonitrile/methanol	85
MC 2745		NH <sub>2</sub>	>250	methanol	70

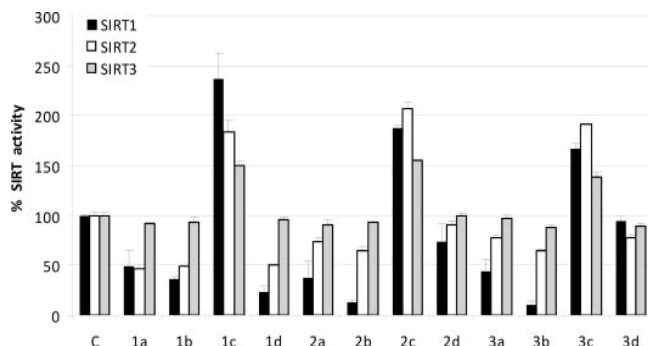
## 6.2. Results and Discussion

### 6.2.1. SIRT1, -2, and -3 Modulator Activity: Enzyme and Functional Assays

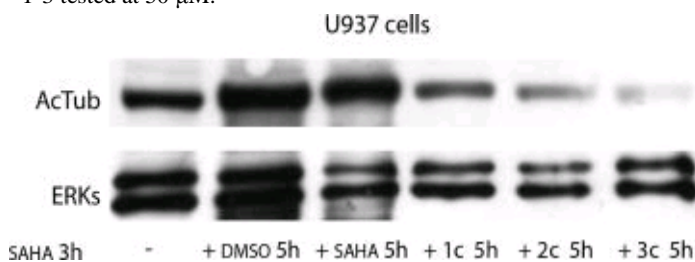
All the prepared compounds were tested against human SIRT1, SIRT2, and SIRT3 at 50  $\mu$ M, using the Fluor de Lys fluorescent biochemical assay (BioMol) (Figure 38). The results showed that the new 1,4-dihydropyridine (DHP) derivatives have different activities for different substituent at the N1 and/or at the 3,5 position of the DHP ring. In particular, a cyclopropyl, a phenyl, or a phenylethyl group at N1 make the compound SIRT1-2 inhibitor.

The highest SIRT1 inhibition activities were seen with the N1- phenyl analogues bearing a carboxy or a carboxamido group at the 3,5 positions (**2b** and **3b**, 86.6% and 89.1% of SIRT1 inhibition at 50  $\mu$ M), followed by the 1-phenethyl- and 1- phenyl-3,5-dicarbethoxy derivatives **1d** and **1b** (76.6% and 63.6% of inhibition, respectively).

Against SIRT2, the diester compounds **1a**, **1b**, and **1d** showed the highest inhibition activity, with comparable potency (1a: 53.7%; 1b: 51.3%; 1d: 49.6% of SIRT2 inhibiting activity at 50  $\mu$ M). Surprisingly, the DHPs bearing a benzyl group at the N1 position, regardless of their substitution at the 3,5 positions (either a carbethoxy (**1c**), carboxy (**2c**), or carboxamido (**3c**) moiety), did not inhibit the tested sirtuins but behaved as potent, dose-dependent SIRT1, -2, and -3 activators (Figure 40). The most potent compounds are **1c** and **2c** that showed the strongest SIRT1 activation with a EC150 (effective concentration able to increase the enzyme activity of 150%) around 1  $\mu$ M, while the 3,5-dicarboxamide **3c** was less effective (EC150=36  $\mu$ M). In SIRT2 assay the dicarboxy derivative **2c**



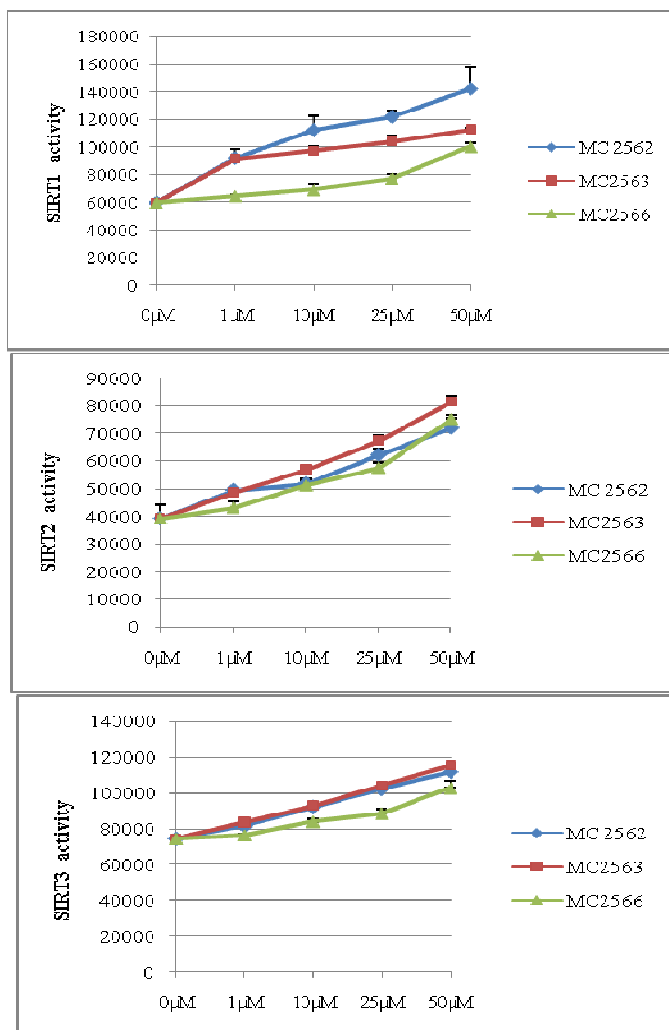
**Figure 38.** SIRT1, -2, and -3 modulating activities of compounds 1-3 tested at 50  $\mu$ M.



**Figure 39.** Effects of SIRT activators MC2562, MC2563, and MC2566 (50  $\mu$ M) on  $\alpha$ -tubulin acetylation in SAHA-pretreated U937 cells

displayed the highest activating potency (EC150=15  $\mu$ M), followed by the dicarboxy compound **1c** (EC150=25  $\mu$ M), while **3c** was less efficient. Against SIRT3 assay, although being less effective than in SIRT1 and -2 assays, **1c** and **2c** exhibited higher activation activity than **3c** (EC150 values: **1c** and **2c**, around 50  $\mu$ M; **3c**, >50  $\mu$ M).  $\alpha$ -tubulin is a known substrate for SIRT2.

In order to determine their effect on acetylation level of this substrate, the new SIRT



**Figure 40.** Dose-dependent SIRT1, -2, and -3 activation by the N-benzyl DHPs **1c**, **2c**, and **3c**.

activators **1c**, **2c**, and **3c** were tested in functional assay. Western blot analysis was performed on the human leukemia U937 cell line. Because U937 cells typically show weak basal acetylation levels for  $\alpha$ -tubulin<sup>174, 175</sup>, the expected hypoacetylation effect from the SIRT activators may be difficult to appreciate.

Thus in order to amplify the acetylation of  $\alpha$ -tubulin<sup>174, 175</sup>, the cells were pretreated with the well-known HDAC inhibitor SAHA<sup>176</sup> (suberoylanilide hydroxamic acid, 3 h, 5  $\mu$ M). After the wash out at 3 h of SAHA incubation, the effects of **1c**, **2c**, and **3c**, used at 50  $\mu$ M, in comparison with vehicle or SAHA treatment (5  $\mu$ M) on tubulin acetylation levels after 5 h of treatment, have been assessed.

As depicted in Figure 39, the tested N-benzyl-DHP compounds induced

hypoacetylation on  $\alpha$ -tubulin in U937 cells. In SAHA-untreated U937 cells, the SIRT activators showed no effects on tubulin acetylation.

### 6.2.2. Cell Cycle Analysis, Apoptosis Induction, Granulocytic differentiation in U937 cell line

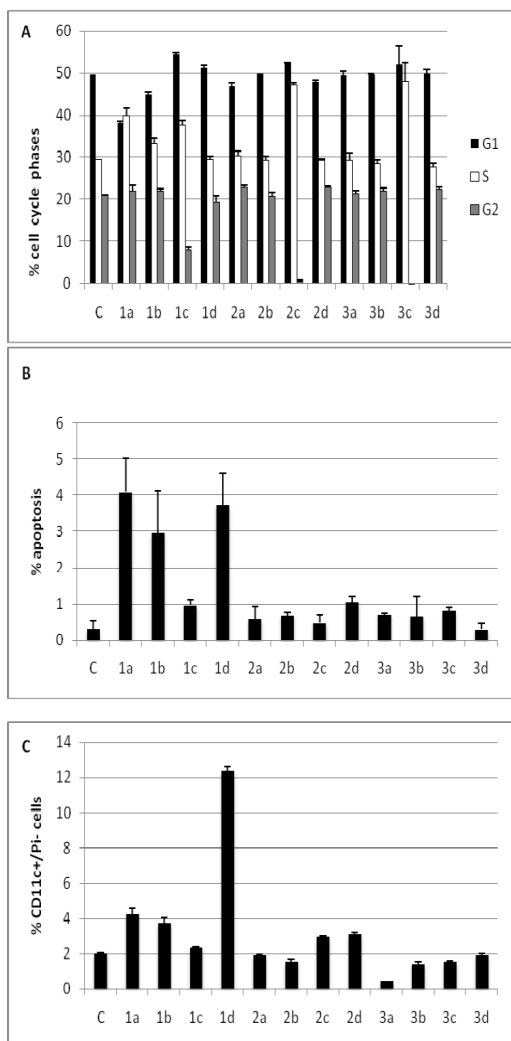
All the synthesized modulators were tested, initially, in the human U937 leukemia and in MCF-7 breast cancer cell lines, to study their effects on cell cycle, apoptosis induction, and granulocytic differentiation<sup>177</sup>. When tested in the MCF-7 breast cancer cell lines, these compounds did not show significant effects. A treatment at 50  $\mu$ M for 30 h on U937 cell line, displayed only marginal effects. (Figure 41). In particular, the three SIRT activators **1c**, **2c**, and **3c** were able to

- arrest the cell cycle at the G1/S phase, with an effect that could be related to p53 deacetylation as well as to effects on multiple targets within the cell,
- induce a slight apoptosis (3-4%), in particular the diester inhibitors **1a**, **1b**, and **1d**
- don't give any granulocytic differentiation, except the diethyl 1-phenethyl-4-phenyl-1,4-dihydropyridine-3,5-dicarboxylate **1d**, that show a significant (12.3%) increase, with an effect that seems not to be related to its SIRT1 and -2 inhibition activity.

### 6.2.3. Involvement in mitochondrial biogenesis

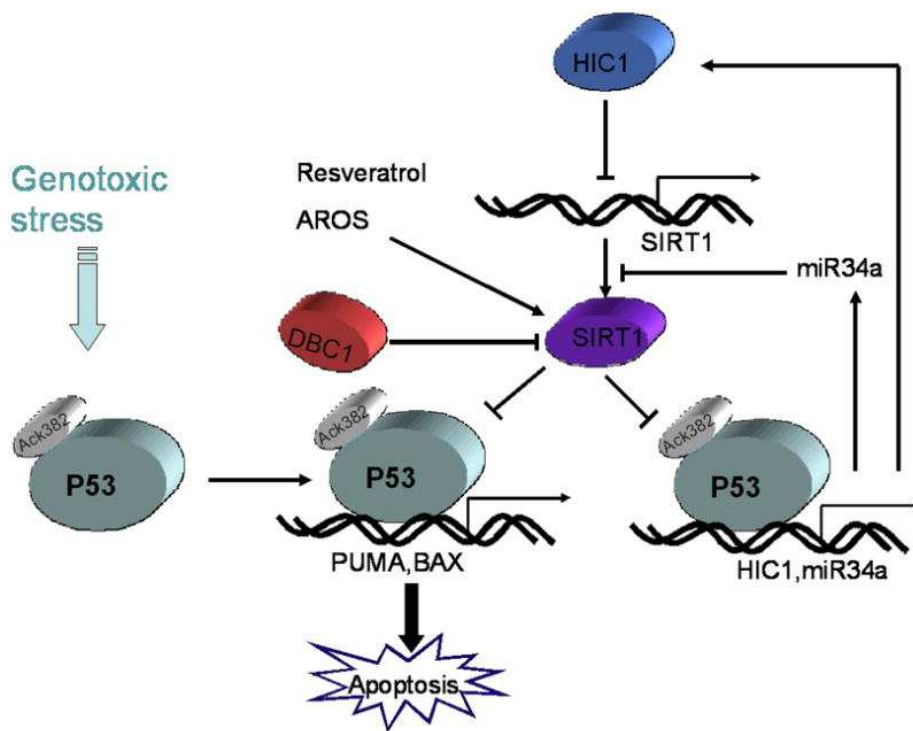
The most studied natural compound for SIRT1 activator is resveratrol although the activation effects of resveratrol on SIRT activity are controversial<sup>178</sup>. Activation of SIRT1 by resveratrol has been claimed to partially mimic caloric restriction and resveratrol delays aging parameters in mice<sup>179</sup>. In spite of the appeal of SIRT1 activation for improving metabolic parameters in mammals, an increased cancer risk is a concern if activation of SIRT1 leads to unhealthy repression of p53 activity. It would

be highly desirable to find an optimal condition or drug that would activate SIRT1 and not increase human cancer risk. Besides inducing cell growth arrest and apoptosis, p53 activation also



**Figure 41.** Effects of 1-3 (50  $\mu$ M, 30 h) on cell cycle, apoptosis induction, and granulocytic differentiation in human U937 leukemia cells. *Sciences, XXIV cycle, Rome, 29th February, 2012*

induces cellular senescence in response to oxidative stress. The promyelocytic leukemia protein (PML) nuclear bodies are discrete nuclear substructures and represent the natural accumulation sites of PML proteins<sup>180</sup>. The size and number of PML nuclear bodies are altered during the cell cycle and in response to various cellular and environmental stresses<sup>181</sup>. There are seven splice variants of PML named PML I–VII in mammalian cells. PML IV interacts with HDACs in the regulation of p53 function and induction of premature senescence<sup>180, 182-184</sup>. Upon PML IV upregulation or oncogenic Ras expression, SIRT1 is recruited to nuclear bodies and interacts directly with PML IV and p53 to repress p53-dependent transactivation by deacetylation of p53<sup>180</sup>. The recruitment of SIRT1 also rescues PML-induced cellular senescence by inhibiting p53 acetylation<sup>180</sup>. This phenomenon of senescence inhibition by SIRT1 also exists in human endothelial

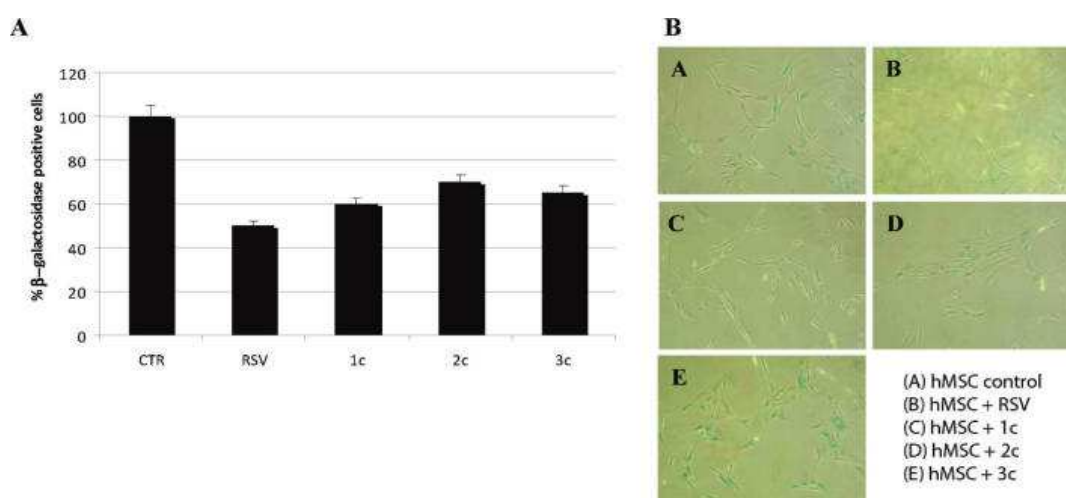


**Figure 42** SIRT1 promotes tumorigenesis. Upon genotoxic stress, p53 is acetylated at K382, which enhanced DNA binding and transactivation activity. HIC1, miR34a, and DBC1 suppress SIRT1 activity. Multilayered inhibition of SIRT1 allows the activation status of p53 for p21, PUMA and BAX genes expression which induced cell cycle arrest, apoptosis, and senescence. Resveratrol and AROS, Along with other SIRT1 activators, enhance SIRT1 deacetylation on p53 and suppress p53 transcription-dependent cell cycle arrest and apoptosis by genotoxic stress (Biochim Biophys Acta. 2010 Aug;1804(8):1684-9)

cells<sup>185</sup>. Endothelial cells with down-regulated SIRT1 exhibit increased acetylation of p53 and premature senescence-like phenotype. Conversely, overexpression of SIRT1 prevents cells from physiological alteration

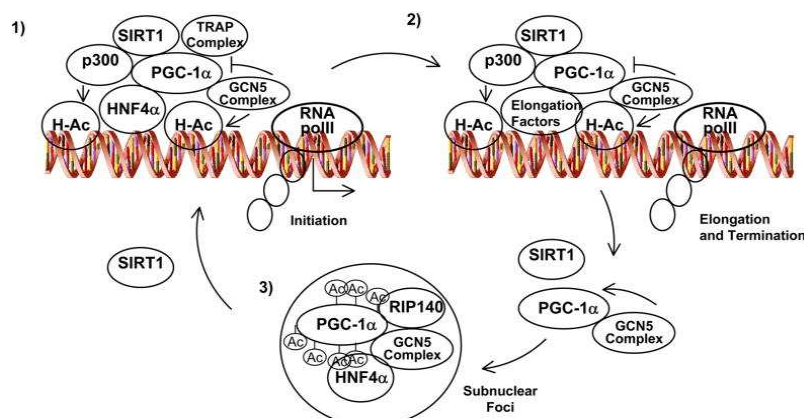
toward senescence<sup>185</sup>. Therefore, SIRT1 seems to exert a protective role against p53-dependent senescence under multiple cellular stresses although it was also reported that SIRT1 could limit replicative life span in response to chronic genotoxic stress. A recent study by Van der Veer and

colleagues<sup>186</sup> demonstrated an extension of human vascular smooth muscle cell (SMC) lifespan by overexpression of Nampt, known to increase cellular NAD<sup>+</sup> and caused increased SIRT1 activity and reduced fraction of p53 bearing acetylation on Lys382. Overexpression of Nampt resulted in deferred senescence and significantly prolonged lifespan, concomitant with enhanced SIRT1 activity. Increased SIRT1 activity represses p53 activity to prevent p53-dependent cellular senescence. Either SIRT1 overexpression or resveratrol increased the SIRT1 activity and inhibited the senescence and increased lifespan in many species including rodents<sup>187</sup>. Primary human mesenchymal stem cells (MSC) have a limited lifespan *in vitro* as any normal, somatic cell. After a certain number of cell divisions, MSC enter senescence, which is morphologically characterized by enlarged and irregular cell shapes and ultimately a stop of proliferation. The most used biomarker for senescent and aging cells is senescence-associated  $\beta$ -galactosidase (SA- $\beta$ -gal), which identifies the senescent cells after cytoplasmatic coloration in blue color<sup>188, 189</sup>.



**Figure 43**  $\beta$ -Galactosidase assay in hMSC. (A) Percent of  $\beta$ -gal positive hMSC treated with RSV, 1c, 2c, or 3c at 50  $\mu$ M for 48 h. (B) Optic microscope images (10X) of treated hMSC

From these data, we tested our SIRT activators **1c**, **2c**, and **3c** (all used at 50  $\mu$ M) in primary human mesenchymal stem cells (hMSC), to determine their potential protection against senescence. RSV (50



**Figure 44** Model for PGC-1 $\alpha$  transcriptional gene expression activity. 1) PGC-1 $\alpha$  is part of multiprotein complexes that contain histone acetyl transferase activity that open and remodels chromatin to allow the transcription factor to bind DNA. In the transcriptional initiation complex SIRT1 would maintain deacetylated PGC-1 $\alpha$ . 2) PGC-1 $\alpha$  and its associated proteins will move with RNA processing, elongation factors and RNA polII to transcribe the mRNA. 3) After the mRNA processing, GCN5 would acetylate PGC-1 $\alpha$  localizing the whole complex to a RIP140 containing subnuclear repressive foci. To initiate another cycle, SIRT1 would deacetylate PGC-1 $\alpha$  freeing it from the repressive foci, allowing it to become incorporated into protein complexes at promoter regions<sup>191</sup>

these conditions, considering the amount of senescent positive cells in the control population as 100%, **1c**, **2c**, and **3c** gave 60%, 70%, and 65% positive cells, respectively, in comparison with 50% positive cells by RSV.

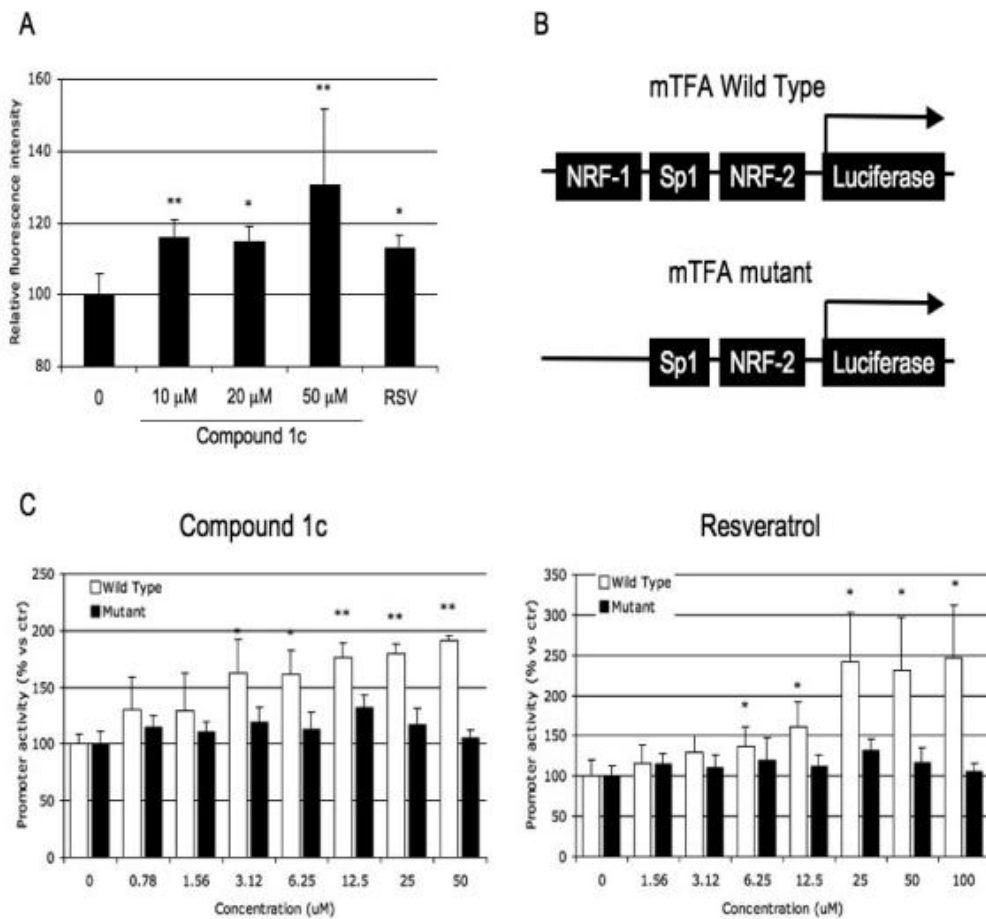
$\mu$ M) has been used as a reference drug.

After 48 h of treatment, the number of  $\beta$ -galactosidase positive cells, used as a marker of senescence, have been counted (Figure 43 A). Optic microscopy images (10X) of the cell cultures have been also obtained (Figure 43 B). In



### **6.3. Sirtuins: Possible direct function in mitochondrial biogenesis**

The transcriptional co-activator PGC-1 $\alpha$  and the NAD<sup>+</sup>-dependent deacetylase SIRT1 are considered



**Figure 45** Mitochondrial function in C2C12 myoblasts. (A) Fluorescence intensity of C2C12 myoblasts treated for 16 h with DMSO (0), or increasing concentrations of 1c, or 50  $\mu$ MRSV, and stained with Mitotracker Green. The data represent the values obtained after subtraction of the mean fluorescence background (unstained cells). (B) Scheme of the constructs carrying the wild type and mutant mTFA promoters. (C) Transcriptional activity of wild type (white bars) and mutant (black bars) mTFA promoter in C2C12 myoblasts treated for 16 h with increasing concentrations of 1c (left panel) and RSV (right panel). \*  $p < 0.05$ , \*\*  $p < 0.01$  versus DMSO (0) treated cells (Student's t-test).

important inducers of mitochondrial biogenesis because in the nucleus they regulate transcription of  
*PhD course in Pasteurian Sciences, XXIV cycle, Rome, 29th February, 2012*

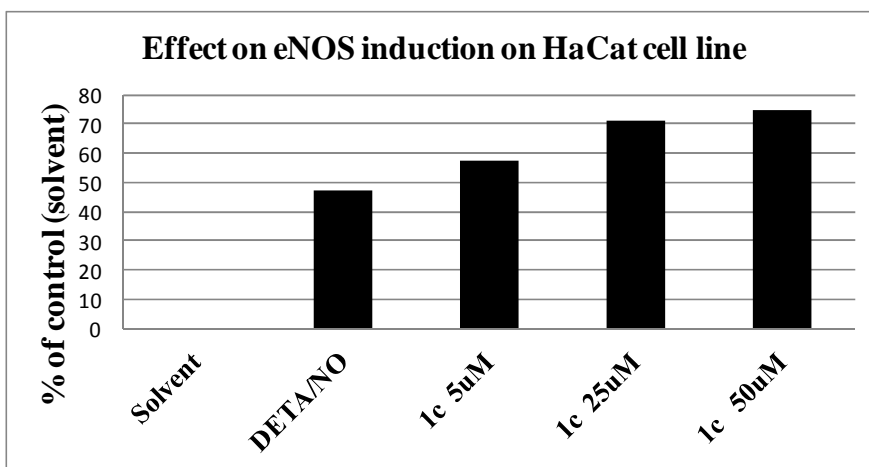
nucleus-encoded mitochondrial genes<sup>190</sup>.

By regulating peroxisome proliferator-activated receptor  $\gamma$  co-activator 1 $\alpha$  (PGC-1 $\alpha$ ), through a functional protein-protein interaction, SIRT1 influences the activity of one of the most versatile metabolic transcriptional co-activators of genes involved in energy metabolism<sup>191, 192</sup>. In particular, PGC-1 $\alpha$  represents an upstream inducer of genes of mitochondrial metabolism by positively affecting the activity of some hormone nuclear receptors (peroxisome proliferator-activated receptor  $\gamma$  and estrogen-related receptor  $\alpha$ ) and nuclear transcription factors (NRF-1, 2)<sup>193</sup>. NRF-1 is a downstream effector of SIRT1/PGC-1 $\alpha$  and activates the expression of OxPhos components, mitochondrial transporters, and ribosomal proteins. Additionally, NRF-1 regulates the activation of the *Tfam*, *Tfb1m*, and *Tfb2m* promoters and indirectly affects the expression of *Cox* genes, *Glut4* and *PGC-1 $\alpha$*  itself<sup>194</sup>. Importantly, the coordination of the two genomes seems to be exclusively achieved by the nucleus-encoded proteins TFAM<sup>195</sup> TFB1M, and TFB2M, among which the mitochondrial transcription factor A seems to play a central role being essential for transcription, replication, and maintenance of mtDNA<sup>196, 197</sup>. RSV was reported to improve mitochondrial function in skeletal muscle, largely due to PGC-1 $\alpha$  activation<sup>198</sup>, we tested the ability of our SIRT activator **1c** to modulate mitochondrial function in murine C2C12 myoblasts. As shown in Figure 45 A, treatment with compound **1c** for 16 h led to a significant increase of fluorescence intensity due to the mitochondrial specific probe Mitotracker Green, indicating increased mitochondrial density. The effect was similar to that observed with 50  $\mu$ M RSV. Mitochondrial transcription factor A (mTFA) is crucial for mitochondrial DNA replication/transcription, and it was described that its expression replication/transcription, and it was described that its expression is controlled by transcription factors belonging to the nuclear respiratory factor (NRF) family and by PGC-1 $\alpha$ <sup>199</sup>. Therefore, it had been interesting to verify if **1c** was able to improve mitochondrial biogenesis using the PGC-1 $\alpha$  pathway. Thus using two different cell population, one with wild type mTFA promoter and the other one with

mutant mTFA promoter, it had been found that both compound **1c** (Figure 45, left panel) and RSV (Figure 45, right panel) stimulated the promoter activity in a dose-dependent manner. The effect of both the SIRT activators is PGC-1 $\alpha$ -dependent as the effect was not seen upon deletion of the NRF1 site.

#### 6.4. Sirtuins and Calorie restriction

Calorie restriction (CR) is a dietary regimen that extends the lifespan of every organism tested to date. SIRT1, may regulate many physiological processes known to be affected during aging and which are altered by CR. A recent study has shown that production of NO, stimulated by caloric restriction, increases SIRT1 expression; this study suggests that eNOS may be involved in regulation



**Figure 46.** 1c eNOS induction in HaCat cell line

of the expression of SIRT1 in murine white adipocytes<sup>200</sup>. Importantly, SIRT1 had been recognized as a key regulator of vascular endothelial homeostasis, controlling angiogenesis, endothelial senescence, dysfunction<sup>201-203</sup>, and increase in mitochondrial biogenesis (Nisoli et al. 2005). Moreover, this mitochondrial induction by CR does not occur in eNOS deficient mice. Interestingly, the SIRT1 gene is activated by NO in vivo and in vitro

(Nisoli et al. 2005), tracing a pathway in which CR induces NO production and activates mitochondrial biogenesis and SIRT1. In previous studies, it had been found that after treatment of human umbilical vein ECs (HUVEC) cell line with either an NO donor (such as DETA-NO or SNAP), expression of SIRT1 protein was markedly higher than that in untreated ones<sup>204</sup> and that treatment with sirtinol or SIRT1siRNA itself promoted endothelial senescence by inhibiting SIRT1. Thus it had been interesting to test the effects on SIRT dependent NO production after treatment of HaCat cell line with SIRT activators. **1c** was tested in a Nitric Oxide synthase activation assay. As the figure 46 shows, in HaCat cell line treated with **1c** it was possible to see a dose-dependent NO production stronger than the NO donor DETA-NO, used as a reference, due to SIRT activation.

## 6.5. Experimental Section

### 6.5.1. Chemistry

Melting points were determined on a Buchi 530 melting point apparatus and are uncorrected. Infrared (IR) spectra (KBr) were recorded on a Perkin-Elmer Spectrum One instrument. <sup>1</sup>H NMR and <sup>13</sup>C NMR spectra were recorded at 400 MHz on a Bruker AC 400 spectrometer; chemical shifts are reported in  $\delta$  (ppm) units relative to the internal reference tetramethylsilane (Me<sub>4</sub>Si). All compounds were routinely checked by TLC and <sup>1</sup>H NMR. TLC was performed on aluminum-backed silica gel plates (Merck DC, Alufolien Kieselgel 60 F<sub>254</sub>) with spots visualized by UV light. All solvents were reagent grade and, when necessary, were purified and dried by standard methods. Concentration of solutions after reactions and extractions involved the use of a rotary evaporator operating at reduced pressure of ca. 20 Torr. Organic solutions were dried over anhydrous sodium sulphate. Analytical results are within  $\pm 0.40\%$  of the theoretical values. All chemicals were purchased from Aldrich Chimica, Milan (Italy), or from Lancaster Synthesis GmbH, Milan (Italy), and were of the highest

purity.

The esters MC 2733, MC 2734, MC 2562 and MC 2735 were prepared by acid catalyzed reaction between benzaldehyde, ethyl propiolate and the opportune amine, afterwards these esters underwent alkaline hydrolysis to furnish the respective acid compounds MC 2736, MC2737, MC 2563 and MC 2738 which reacted with triethylamine, Bop reagent and the appropriate amine to give finally the amides compounds MC 2743, MC 2744, MC 2566, MC 2745.

**6.5.1.1. General Procedure for the Synthesis of 1-aryl-(or arylalkyl, or cycloalkyl)-diethyl-4-phenyl-1,4-dihydropyridine-3,5-dicarboxylate. Example: synthesis of 1-cyclopropyl-diethyl-4-phenyl-1,4-dihydropyridine-3,5-dicarboxylate (MC 2733).** Ethyl propiolate (18.84 mmol, 1.9 mL), benzaldehyde (9.42 mmol, 0.96 mL) and cyclopropylamine (9.42 mmol, 0.65 mL) in glacial acetic acid (0.5 mL) were heated at 80°C for 30 min. After cooling, the mixture was poured into water (20 mL) and stirred for 1 h. The solid product was filtered and washed with Et<sub>2</sub>O (3 x 30 mL) to give pure **MC 2733** that was recrystallized by cyclohexane. <sup>1</sup>H NMR (400 MHz, CDCl<sub>3</sub>) δ 0.83-0.90 (m, 4H, cyclopropane protons), 1.14-1.17 (t, 6H, -OCH<sub>2</sub>CH<sub>3</sub>), 2.94-2.99 (m, 1H, cyclopropane proton), 3.97-4.11 (q, 4H, -OCH<sub>2</sub>CH<sub>3</sub>), 4.83 (s, 1H, PhCH), 7.08-7.23 (m, 5H, benzene protons), 7.31 (s, 2H, dihydropyridine protons) ppm; <sup>13</sup>C NMR (400 MHz, CDCl<sub>3</sub>) δ 6.10 (2C), 14.20 (2C), 38.50, 44.50, 61.70 (2C), 108.0 (2C), 125.80, 128.70 (2C), 129.10 (2C), 142.20, 146.10 (2C), 167.20 (2C) ppm; MS (EI): *m/z*: 341 (*M*)<sup>+</sup>.

**6.5.1.2. General Procedure for the Synthesis of 1-Aryl-(or arylalkyl, or cycloalkyl)-4-phenyl-1,4-dihydropyridine-3,5-dicarboxylic Acids (2a-d). Example: 1-Phenethyl-4-phenyl-1,4-dihydropyridine-3,5-dicarboxylic acid (2d).** A mixture of **1d** (1.23 mmol, 0.5 g) and 5N KOH (6.15 mmol, 0.34 g, 1.23 mL) in ethanol (10 mL) was stirred at 80°C overnight. Afterward, the solvent was evaporated, the residue was eluted with water (30 mL) and the resulting solution acidified with 2N HCl. The obtained precipitate was filtered, washed by water (3 x 30 mL)

and dried to afford pure compound **2d**, that was recrystallized by acetonitrile/methanol.  $^1\text{H}$  NMR (400 MHz, DMSO- $d_6$ )  $\delta$  2.95-2.99 (t, 2H, PhCH<sub>2</sub>CH<sub>2</sub>), 3.61-3.65 (t, 2H, PhCH<sub>2</sub>CH<sub>2</sub>), 4.82 (s, 1H, PhCH), 7.07-7.34 (m, 12H, benzene protons and dihydropyridine protons), 12.00 (bs, 2H, -COOH) ppm;  $^{13}\text{C}$  NMR (400 MHz, DMSO- $d_6$ )  $\delta$  42.00, 43.80, 57.70, 107.30 (2C), 125.70, 125.90, 127.70 (4C), 128.60 (4C), 139.40, 144.40, 148.90 (2C), 171.30 (2C) ppm; MS (EI);  $m/z$ : 349 ( $M$ )<sup>+</sup>.

**6.5.1.3. General Procedure for the Synthesis of 1-aryl-(or arylalkyl, or cycloalkyl)-4-phenyl-1,4-dihydropyridine-3,5-dicarboxamides. Example: synthesis of 1-phenyl-4-phenyl-1,4-dihydropyridine-3,5-dicarboxamide (MC 2744).** Triethylamine (10.38 mmol, 1.44 mL) and BOP reagent (3.12 mmol, 1.38 g) were added under nitrogen atmosphere to a solution of compound **MC 2737** (0.47 mmol, 0.150 g) in dry DMF (5mL), and the resulting mixture was stirred for 30 min at room temperature. After this time 33% aqueous ammonia (4.7 mmol, 0.27 mL) was added and the resulting mixture was stirring for further 30 min. The reaction was quenched by water (30 mL), the precipitate filtered was washed with water (3 x 30 mL) and Et<sub>2</sub>O (3 x 30 mL) to provide **MC 2744** that was recrystallized by acetonitrile/methanol.  $^1\text{H}$  NMR (DMSO- $d_6$ )  $\delta$  5.07 (s, 1H, PhCH), 6.73 (bs, 4H, -CONH<sub>2</sub>), 7.02-7.53 (m, 12H, benzene protons and dihydropyridine protons) ppm;  $^{13}\text{C}$  NMR (400 MHz, DMSO- $d_6$ )  $\delta$  45.10, 110.20 (2C), 116.30 (2C), 118.80, 125.80, 128.70 (2C), 129.60 (2C), 138.10 (2C), 141.30, 142.20, 171.0 (2C) ppm; MS (EI):  $m/z$ : 319 ( $M$ )<sup>+</sup>.

## 6.5.2. Biological assays

**6.5.2.1. SIRT Assay.** Modulation of sirtuin activity by compounds was assessed using the Fluor de Lys fluorescent biochemical assay available through BioMol International, LP in 96-well format. In the first part of a two-step reaction, an acetylated lysine side chain present on the substrate is deacetylated during incubation at 37 °C for an hour with active enzyme (SIRT1, SIRT2, or SIRT3), compounds 1-3, and NAD pin white, 96-well polystyrene luminescence plates (Perkin Elmer-

6005680). The latter half of the reaction produces a fluorophore upon treatment with a developing reagent. The reaction is read by a Perkin-Elmer Victor2V 1420 Multilabel Counter plate reader with filters that excite at 355 nm and detect emitted light at 460 nm with a read time of 0.1s per well. Sirtuin 1 enzyme (BioMol-SE-239) is a 747 amino acid protein with a molecular weight of 82 kDa, while Sirtuin 2 enzyme (BioMol-SE-251) is a 389 amino acid protein with a molecular weight of 43 kDa; both were purified from human cDNA expressed in *Escherichia coli* and stored in 25 mM Tris, pH 7.5, 100 mM NaCl, 5 mM DTT, and 10% glycerol. Sirtuin 3 enzyme (BioMol-SE-270) is inactive prior to removal of its Nterminus, thus this assay only utilizes the catalytically active fragment spanning amino acids 102-299 with a molecular weight of 32.7 kDa. Like sirtuins 1 and 2, the fragment was purified from cDNA expressed in *E. coli* and stored in 25 mM Tris, pH 7.5, 100 mM NaCl, 5 mM DTT, and 10% glycerol. While there is variability in activity among individual lots, each experiment normalizes SIRT1 activity to 1U/reaction well and SIRT2 and SIRT3 activity to 5U/reaction well (where U=1 pmol/min at 37 °C, 250 μM substrate, and 500 μM NAD β). All reagents are diluted on ice in the following reaction buffer: 50 mM Tris/Cl, pH 8.0, 137 mM NaCl, 2.7 mM KCl, 1 mM MgCl<sub>2</sub>, and 1 mg/mL BSA. Thus for each reaction well, the requisite amount of enzyme (as detailed above) is added to 500 μM NADβ (BioMol-KI-282), 250 μM fluorogenic deacetylase substrate (BioMol-KI-177), and the compound of interest at a given concentration in a total reaction volume of 50 μL. After an hour incubation at 37 °C, the reaction is stopped upon addition of 1x Developer (BioMol-KI-176) for a final reaction volume of 100 μL. The reaction is incubated at 37 °C for an additional 15 min and then read on the plate reader. Experimental replicates were done in triplicate with appropriate controls. Positive controls contained only enzyme, substrate, NAD β, and DMSO while background controls contained substrate, NADβ, and DMSO only. Autofluorescent controls were also included for testing of activators and included substrate, NAD β, and the compound at the same concentration as its experimental counterpart. Background signal was



subtracted from positive control well signals, and autofluorescent background was subtracted from experimental well signals at all tested compound doses.

**6.5.2.2. Determination of  $\alpha$ -Tubulin Specific Acetylation.** For  $\alpha$ -tubulin acetylation studies, 50  $\mu\text{g}$  of total protein extracts (U937 cells) were separated on a 10% polyacrylamide gels and blotted. Western blots were shown for acetylated  $\alpha$ -tubulin (Sigma, dilution 1:500) and total ERKs (Santa Cruz) were used to normalize for equal loading

**6.5.2.3. Cell Cycle Analysis on U937 Cells.** First,  $2.5 \times 10^5$  cells were collected and resuspended in 500  $\mu\text{L}$  of a hypotonic buffer (0.1% Triton X-100, 0.1% sodium citrate, 50  $\mu\text{g}/\text{mL}$  propidium iodide (PI), RNase A). Then cells were incubated in the dark for 30 min. Samples were acquired on a FACS-Calibur flow cytometer using the Cell Quest software (Becton Dickinson) and analyzed with standard procedures using the Cell Quest software (Becton Dickinson) and the ModFit LT version 3 Software (Verity) as previously reported<sup>163</sup>. All experiments were completed in triplicate.

**6.5.2.4. FACS Analysis of Apoptosis on U937 Cells.** Apoptosis was measured with the caspase 3-7 detection (B-Bridge) method; samples were analyzed by FACS with Cell Quest technology (Becton Dickinson) as previously reported<sup>164</sup>.

**6.5.2.5. Granulocytic Differentiation on U937 Cells.** Granulocytic differentiation was carried out as previously described<sup>164</sup>. U937 cells were harvested and resuspended in 10  $\mu\text{L}$  phycoerythrin-conjugated CD11c (CD11c-PE). Control samples were incubated with 10  $\mu\text{L}$  of PE conjugated mouse IgG1, incubated for 30 min at 4°C in the dark, washed in PBS, and resuspended in 500  $\mu\text{L}$  of PBS containing PI (0.25  $\mu\text{g}/\text{mL}$ ). Samples were analyzed by FACS with Cell Quest technology (Becton Dickinson). PI positive cells have been excluded from the analysis.

**6.5.2.6.  $\beta$ -Galactosidase Assay.** For this assay, we used  $3 \times 10^5$  cells/ well. Human primary mesenchymal stem cells have been kept in culture for 30 days (corresponding to the ninth passage) before starting the experiment. Cultured cells were washed in PBS and fixed with 2% (w/v)

formaldehyde and 0.2% (w/v) glutaraldehyde solution. Cells were then washed with PBS and incubated overnight at 37 °C in freshly prepared staining buffer (30 mM citric acid/ phosphate buffer (pH 6), 5 mM  $K_4Fe(CN)_6$ , 5 mM  $K_3Fe(CN)_6$ , 150mMNaCl, 2 mM  $MgCl_2$ , 1 mg/mL X-Gal). At the end of incubation, cells were washed with PBS and examined under the microscope. The percent of senescent cells was calculated by counting the number of blue cells (positive cells) out of total cells<sup>188</sup>.

**6.5.2.7. Mitochondrial Density in Murine C2C12 Myoblasts.** Murine C2C12 myoblasts were plated in 96-well clusters (3000 cells/ well) and treated overnight with the compounds under investigation. Mitochondria were stained with the Mito-Tracker Green FM dye (200 nM) from Molecular Probes (Invitrogen, Milan, Italy). Fluorescence intensities were measured using the EnVision multilabel reader platform (PerkinElmer, Italia Spa, Monza, Italy). The data shown represent the values obtained after subtraction of the mean fluorescence background measured in wells with unstained cells.

**6.5.2.8. Transcriptional Activity of mTFA-Promoter in Murine C2C12 Myoblasts.** Murine C2C12 myoblasts (CRL-1772, ATCC, Teddington, UK) were grown in Dulbecco's Modified Eagle's Medium supplemented with 10% heat inactivated fetal calf serum. Cells were retrotransfected with the plasmids bearing either the mTFA-promoter or the mutated form lacking the NRF1 binding site<sup>205</sup>, fused to the luciferase gene. Lipofectamine (Invitrogen, Milan, Italy) was used as transfecting reagent (2.5  $\mu$ L/ $\mu$ g DNA). Transfected cells were then plated in 96-well clusters (3000 cells/well) and treated overnight with the compounds under investigation. The luciferase activity was measured using the EnVision multilabel reader platform (PerkinElmer Italia Spa, Monza, Italy). The constructs used in the transfection assays were first validated overexpressing PGC-1 $\alpha$  or SIRT1. In both conditions the wild type promoter was stimulated by 2-3 fold, whereas the mutant promoter lacking the NRF1 binding site did not respond.

**6.5.2.9. Nitric Oxide synthase activation assay.** NO production was measured with the DAF-2 DA detection method. DAF-2 DA is a cell permeable fluorescent probe for NO detection. It was used to load cells, subsequent hydrolysis by cytosolic esterases released DAF-2, which is relatively non-fluorescent at physiological pH, however in the presence of NO DAF-2 is converted to the fluorescent triazole derivative, DAF-2T. After samples were analyzed by FACS.

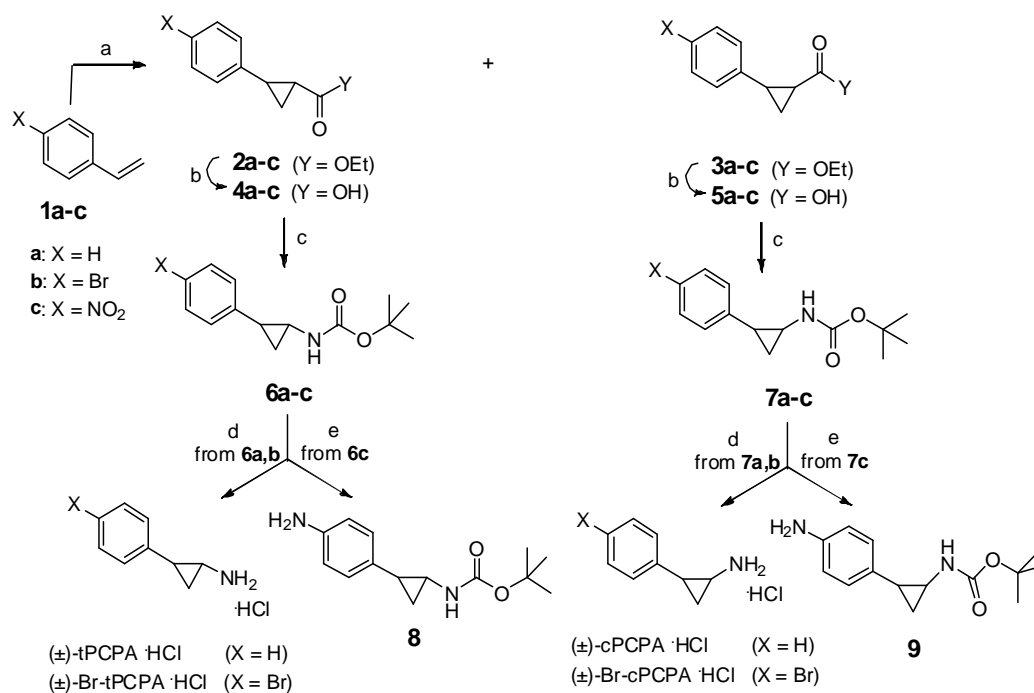
## **7. Biochemical, Structural, and Biological Evaluation of Tranylcpromine Derivatives as Inhibitors of Histone Demethylases LSD1 and LSD2**

LSD1 and LSD2 share a similar catalytic domain (45% sequence identity) that is structurally homologous with the amine oxidases, a class of flavin-dependent enzymes that act on biogenic amines<sup>206, 207</sup>. Among these proteins, human monoamine oxidases (MAOs) A and B have been the subject of more than 50 years of research that has led to the development of a multitude of inhibitors including antidepressive and antiparkinson drugs<sup>208</sup>. Their similarity in the catalytic and structural properties prompted the investigation of antiMAO drugs as potential LSD1 inhibitors<sup>209</sup>. It was found that tranylcpromine, a MAO inhibitor used as antidepressive drug, is able to inhibit LSD1<sup>210-213</sup>. On this basis, it had been interesting to design compounds that would be more selective for demethylases using tranylcpromine as the lead scaffold.

Tranylcpromine is a racemic mixture of ((-)-*trans*-2-phenylcyclopropyl-1-amine · HCl (tPCPA) that covalently inhibits the LSD and MAO enzymes. The aim of this project had been to study the tranylcpromine in order to verify the presence of possible enantio-selective inhibitory activity and, once got this information, to design new compounds tranylcpromine-like in order to improve the first results.

## 7.1. Chemistry

The syntheses of ( $\pm$ )-*trans*-2-phenylcyclopropyl-1-amine (tPCPA), ( $\pm$ )-*cis*-2-phenylcyclopropylamine (cPCPA), ( $\pm$ )-*trans*-2-(4-bromophenyl)cyclopropyl-1-amine (Br-tPCPA), and ( $\pm$ )-*cis*-2-(4-



**Scheme 3.** a) EDA, CuCl, dry CHCl<sub>3</sub>, 60 °C, N<sub>2</sub> atmosphere; b) 2 N KOH, EtOH, rt; c) 1) DPPA, Et<sub>3</sub>N, dry *t*-BuOH, dry benzene, 80 °C, N<sub>2</sub> atmosphere; 2) Boc<sub>2</sub>O, dry benzene, 80 °C, N<sub>2</sub> atmosphere; d) 6 N HCl, THF, rt; e) 2 N K<sub>2</sub>CO<sub>3</sub>, NaH<sub>2</sub>PO<sub>2</sub>, Pd/C, THF, 60 °C, N<sub>2</sub> atmosphere.

bromophenyl)cyclopropylamine (Br-cPCPA) and their hydrochlorides were performed by a variety of methods, but in some cases a confusion occurred between the various diastereoisomers and the mixtures of them (1-9). To follow an unambiguous pathway of synthesis, we prepared the

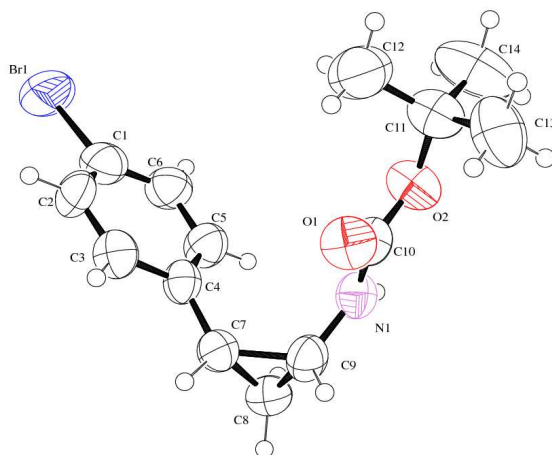
unsubstituted, 4-bromo-, and 4-nitro-2-phenylcyclopropyl-1-amine derivatives according to Scheme 1, following the procedure described by Rosen *et al.* (*J Med Chem* **47**, 5860-5871.). *Trans* and *cis* ethyl 2-phenylcyclopropylcarboxylates (**2a-c** and **3a-c**) were synthesized by treating the appropriate styrene derivatives **1a-c** with ethyl diazoacetate (EDA) in the presence of copper (I) chloride (CuCl) in dry CHCl<sub>3</sub>. Alkaline hydrolysis of **2a-c** and **3a-c** furnished the corresponding carboxylic acids **4a-c** and **5a-c**, which were in turn converted into the related *t*-butoxy carbamates **6a-c** and **7a-c** through reaction with diphenylphosphoryl azide and *t*-butanol in the presence of triethylamine in dry benzene. Acidic hydrolysis (6 N HCl) of **6a, b** and **7a, b** yielded tPCPA·HCl and Br-tPCPA·HCl (from **6a** and **6b**), and cPCPA·HCl and Br-cPCPA·HCl (from **7a** and **7b**). Reduction of the nitro group of **6c** and **7c** with sodium hypophosphite, palladium on carbon, and potassium carbonate afforded the related 4-aminophenyl carbamates **8** and **9** (Scheme 3).

The enantiomers of (±)-tPCPA HCl, (±)-cPCPA HCl, (±)-Br-tPCPA HCl, and (±)-Br-cPCPA HCl were obtained by the following two-step procedure: 1) direct multi-mg enantioseparation of their *N*-*tert*-butoxycarbonyl (Boc)- intermediates **6a,b** and **7a,b** by HPLC on polysaccharide-based chiral stationary phases (CSPs); 2) cleavage of the Boc group of the isolated enantiomers using 6 N HCl.

## 7.2. Preparation and absolute configuration assignment of the enantiomers of Br-cPCPA HCl.

The enantiomers of **7b** were separated on a semipreparative scale by enantioselective HPLC on the Chiralcel OD CSP using the mixture *n*-hexane-ethanol 97:3 (v/v) as eluent. The chromatographic data were:  $k_1 = 1.14$ ;  $k_2 = 1.62$ ;  $\alpha = 1.42$ ; amount of sample resolved in a single semipreparative run = 6 mg; injection volume = 0.4 ml; flow rate = 5.0 ml/min, detector = UV at 260 nm; temperature = 25 °C.  $k_1$ : retention factor of the first eluted enantiomer, defined as  $(t_1 - t_0)/t_0$  where  $t_0$  is the void time of the column;  $\alpha$ : enantioselectivity factor defined as  $k_2/k_1$ . Polarimetric analysis indicated that the first

eluted enantiomer on the OD CSP rotated the polarized light in the negative direction in ethanol solution {  $[\alpha]_D^{20}$  -148 (c: 0.1, ethanol), ee>99% }, whereas the second eluted enantiomer was dextrorotatory {  $[\alpha]_D^{20}$  +146 (c: 0.1, ethanol), ee>99% }. Suitable crystals for X-ray analysis were obtained for the dextrorotatory enantiomer (second eluted on the OD CSP) which allowed the determination of the (1*R*,2*R*) absolute configuration (AC) [(1*R*,2*R*)-(+)-**7b**] (Figure 45). Therefore its levorotatory enantiomer had the (1*S*,2*S*) AC [(1*S*,2*S*)-(-)-**7b**].



**Figure 47.** An ORTEP view of the molecular structure of the (1*R*,2*R*)-(+)-**7b** enantiomer.

The isolated pure enantiomers of **7b** were converted to the corresponding Br-cPCPAs hydrochlorides by treatment with 6 N HCl (see Scheme 3). Thus starting from optically pure of known (1*R*,2*R*) or (1*S*,2*S*) AC, optically pure (enantiomeric excess, ee>99%) forms of (+)- and (-)-Br-cPCPA HCl with the same AC were obtained. The enantiomeric purity was determined by nantioselective HPLC on the Chiralcel OJ CSP using the mixture *n*-hexane-2-propanol-diethylamine 90:10:0.1 (v/v/v) as mobile phase. The chromatographic data were:  $k_1 = 1.44$ ;  $k_2 = 1.76$ ;  $\alpha = 1.22$ ; flow rate = 1.0 ml/min; detector = UV at 254 nm; temperature = 25°C. The single enantiomers of Br-cPCPA HCl were characterized as follows: first eluted enantiomer on the OJ CSP: AC: (1*R*,2*R*),  $[\alpha]_D^{20}$  -57 (c: 0.1, H<sub>2</sub>O), ee>99% {(1*R*,2*R*)-(-)-Br-cPCPA

The isolated pure enantiomers of **7b** were converted to the corresponding Br-cPCPAs hydrochlorides by treatment with 6 N HCl (see Scheme 3). Thus starting from optically pure of known (1*R*,2*R*) or (1*S*,2*S*) AC, optically pure (enantiomeric excess, ee>99%) forms of (+)- and (-)-Br-cPCPA HCl with the same AC were obtained. The enantiomeric purity was determined by nantioselective HPLC on the Chiralcel OJ CSP using the mixture *n*-hexane-2-propanol-diethylamine 90:10:0.1 (v/v/v) as mobile phase. The chromatographic data